Regulation of autophagy in animal models of pulmonary fibrosis.

Inauguraldissertation

zur Erlangung des Grades eines Doktors der Humanbiologie

des Fachbereichs Medizin

der Justus-Liebig-Universität Gießen

vorgelegt von

Saket Ahuja

aus

Indien

Giessen, 2020

Aus dem Zentrum für Innere Medizin

Der Medizinische Klinik II

Der Uniklinikum Gießen und Marburg GmbH

Standort: Gießen

Leiter/Direktor: Prof. Dr. W. Seeger

Gutachter: Prof. Dr. A. Günther

Gutachter: Prof. Dr. R. Tikkanen

Tag der Disputation: 04-12-2020

Table of contents

List of figures:

List of abbreviations:

3-MA	3-methyl adenine
ABCA3	ATP binding cassette subfamily A member 3
AECII	Alveolar epithelial cell type II
AP3B1	Adaptor-related protein complex 3, beta 1 subunit
ATG	Autophagy related protein
BLOC	Biogenesis of lysosome-related organelles complex
CFTR	Cystic fibrosis transmembrane conductance regulator
CHS	Chediak-Higashi syndrome
CMA	Chaperone mediated autophagy
COPD	Chronic obstructive pulmonary disease
CQ	Chloroquine
DPLD	Diffuse parenchymal lung diseases
EBV	Epstein-Barr virus
ELMOD	ELMO containing domain
EMT	Epithelial-mesenchymal transition
ER	Endoplasmic reticulum
FITC	Fluorescein isothiocyanate
FVC	Forced vital capacity
GERD	Gastroesophageal reflux disease
HPS	Hermansky-Pudlak syndrome
HPSIP	HPS associated interstitial pneumonia
HRCT	High resolution computed tomography
hTERT	Telomerase reverse transcriptase in humans

IIP	Idiopathic interstitial pneumonias
ILD	Interstitial lung diseases
IPF	Idiopathic pulmonary fibrosis
LAMP	Lysosome associated membrane protein
LB	Lamellar bodies
LRO	Lysosome related organelles
LSD	Lysosomal storage disorder
MAP1LC3B	Microtubule associated protein-1 light chain 3 beta
MLE12	Mouse lung epithelial cancer cell line
MUC5B	Mucin 5B
NSIP	Non-specific interstitial pneumonia
OCA	Oculocutaneous albinism
PAH	Pulmonary arterial hypertension
RAGE	Receptor of the advanced glycation end products
SP-A	Surfactant protein-A
SLB	Surgical lung biopsy
SP-C	Surfactant protein-C
SQSTM1	Sequestosome-1
TEM	Transmission electron microscopy
TFEB	Transcription factor EB
TGF-β1	Transforming growth factor-β1
UIP	Usual interstitial pneumonia
UPR	Unfolded protein response

1. INTRODUCTION

1.1 Diffuse parenchymal lung diseases (DPLDs)

Diffuse parenchymal lung diseases (DPLDs) or interstitial lung diseases (ILDs) represent a group of lung diseases that affect the interstitium, the vasculature and the alveolar/bronchial compartment. DPLDs can be classified into four broad categories, namely, DPLD of known causes such as drugs, environmental exposures, granulomatous DPLD (for example sarcoidosis), rare forms of DPLD (such as lymphangioleiomyomatosis (LAM)) and the idiopathic interstitial pneumonias (IIPs) (2002). Excess matrix deposition and loss of lung architecture resulting in respiratory insufficiency is the last stage of several DPLDs (Wuyts et al., 2013). Typically, DPLDs are characterized by an enhanced matrix deposition, which results in decreased lung compliance and an inefficient gas exchange. A common feature of some DPLDs is the persistent injury to the alveolar epithelium, which results in a continuous activation of innate repair mechanisms. This results in the activation of fibroblasts and an increased amount of collagen being produced in the lung together with many other proteins in the lung matrix (Tomashefski et al., 2000; Hardie et al., 2009).

1.2 Idiopathic Pulmonary Fibrosis (IPF)

Idiopathic pulmonary fibrosis (IPF) is a disease of unknown origin and typically affects middle-aged and especially elder people. It is progressive in nature and ultimately fatal. IPF is associated with severe dyspnea (Nightingale et al., 2000). One risk factor which has been described to contribute to the development of IPF is smoking (Baumgartner et al., 1997; Taskar and Coultas et al., 2006). Other diseases such as hernia and gastroesophageal reflux disease (GERD) have also been discussed, as have been exposure to pesticide, animal dust, petrochemicals, farming etc. (Iwai et al., 1994; Miyake et al., 2005; Noth et al., 2012; Raghu et al., 2006; Taskar and Coultas 2006).

IPF, one of the most common forms of idiopathic interstitial pneunomias (IIPs) and interstitial lung diseases (ILDs), has a 5 year mean survival rate as low as 20% (Wuyts et al., 2013). The prevalence of IPF has been suggested to range between 2-29 patients in 100,000 people, with an estimated prevalence 0.2% of all people aged 75 and above (Raghu et al., 2011). Several epidemiological studies demonstrated that the incidence of IPF has been on the rise in the last couple of decades (Gribbin et al., 2006; Navaratnam et al., 2011). IPF spreads across ethnicities and encompasses both rural and urban areas (Nathan et al., 2011). It is predominant in males as compared to females and the incidence increases with age (Raghu et al., 2006; Fernandez Perez et al., 2010).

Diagnosis of IPF relies on a high-resolution computed tomography (HRCT), which typically shows a pattern of usual interstitial pneumonia (UIP). Other known causes of ILD need to be ruled out before confirming the diagnosis of IPF. In patients showing absence of a definite UIP pattern on HRCT, IPF might still be diagnosed based on combinations of results from surgical lung biopsy (SLB) and HRCT (Raghu et al., 2011). However, the need for lung biopsy has been greatly reduced because of the recognition of distinct HRCT patterns by different ILDs.

The histological pattern defining IPF is also UIP, characterized by temporal and spatial heterogeneity, loss of regular lung architecture, and proof of fibroblast foci and missing other features. The disease usually originates in the sub-pleural region of the lung and develops towards the central region. Regions in the immediate vicinity of subpleural parenchmya are often regions of severe scar tissue and honeycombing marked by irregular epithelial airspaces and dense fibrosis as shown in Fig.1 (Wolters et al., 2014).

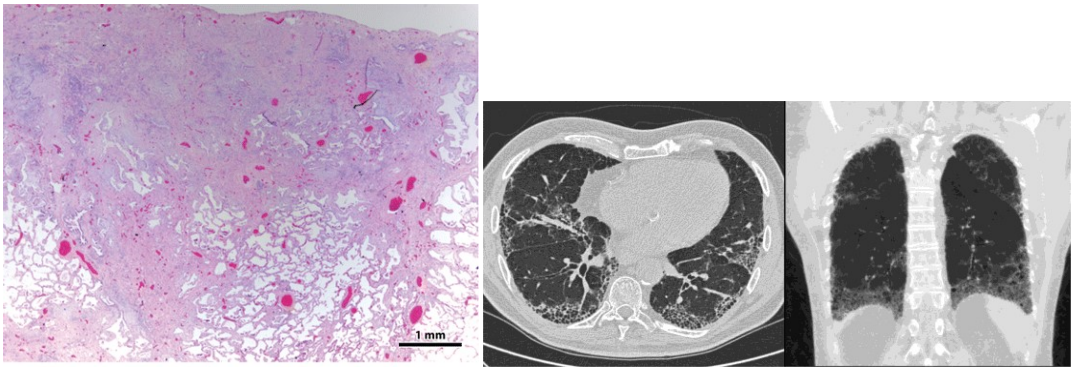

Fig. 1: Histopathological and radiographic features of usual interstitial pneumonia. A. Representative picture of an IPF lung with usual interstitial pneumonia showing sub-pleural accentuation of dense fibrosis together with irregular epithelial airspaces. Hematoxylin and eosin-stained lung section visualised at magnification of X20 (Wolters et al., 2014). **B**. HRCT image of chest from an IPF patient showing heterogenous lung alterations, reticulation, and sub-pleural honeycombing (Oldham and Noth, 2014).

Although there is no existing therapy for IPF so far, pirfenidone, a non-steroidal drug and nintedanib, a triple tyrosine kinase inhibitor targeting VEGF, FGF and PDGF are being prescribed to delay the worsening of IPF (Maher, 2010). However, lung transplantation still serves as the only available approach to increase the life span of IPF patients (Ryu et al., 2014). Initially, IPF was thought to be caused by chronic inflammation but anti-inflammatory drugs did not prove to be beneficial for IPF patients, casting doubts on the role of inflammation in driving the disease (Selman et al., 2001). Later on, the concept of epithelial injury evolved, wherein repeated injury to alveolar epithelial cells and failure to trigger a proper wound healing response by these cells is currently believed to be a major

mechanism leading to progressive lung fibrosis (Selman and Pardo, 2006). Many genetic or environmental factors contribute to influence the severity of the epithelial cell injury. Inflammation, when present, appears to be a secondary response and not the primary triggering factor in IPF (Gross and Hunninghake, 2001). Although multiple cell types are indicated to contribute to the pathogenesis of IPF, chronic injury to alveolar epithelial cell type II (AECII) is an accepted key event that triggers the disease process in IPF (Selman and Pardo 2006). Additionally, fibroblast foci, covered by hyperplastic AECIIs are a hallmark feature in an IPF lung (Katzenstein and Myers 1998). AECII are the classical secretory cells in the lung, which synthesize, store and secrete the surface tension reducing surfactant (surfactant proteins and phospholipids) into alveolar spaces and also produce compounds of the innate immune defense system (Tierney, 1989). In non-familial, sporadic forms of IPF, chronic ER stress, mitochondrial dysfunction and lysosomal stress are prominent findings in the AECII of these patients and may largely explain the extensive apoptosis of the epithelium under these conditions (Korfei et al., 2008; Lawson et al., 2008). ER stress, DNA damage and excessive AECII apoptosis are also found in familial IPF (Tanjore et al., 2012).

1.2.1 Genetic risk factors

As indicated in the previous chapter, fibrotic remodeling may be initiated by a repetitive insult or injury to the alveolar epithelium. This insult or injury may result from genetic factors (familial forms of IPF) to the environmental components, usually ending up as a combination of several factors. Mutations in surfactant protein-A (SP-A) & SP-C (Guillot et al., 2009; Mulugeta et al., 2005), the surfactant lipid transporter ATP-binding cassette sub-family A member 3 (ABCA3) (Crossno et al., 2010), telomerase (hTERT) (Alder et al., 2008) have all been shown to result in IPF or other related forms of ILD. Mutations in surfactant proteins result in alveolar damage, ER stress or unfolded protein responses (UPR) (Chibbar et al., 2004). 50% of children suffering from severe idiopathic pneumonias show a mutation in SP-C while the remaining 50% cases are sporadic (Nogee et al., 2001). The ELMOD2 gene, involved in interferon related antiviral response regulation, has been recently implicated in IPF, where a decrease in expression of ELMOD2 mRNA was observed in lungs from IPF patients as compared to the healthy controls (Pulkkinen et al., 2010). Another gene which has been recently implicated in the development of pulmonary fibrosis is *MUC5*. *MUC5* was shown to be overexpressed in the IPF lungs as compared to the healthy controls although the mechanism or the role of *MUC5* in the development and progression of IPF is not well understood yet (Seibold et al., 2011).

1.2.2 Environmental risk factors

Genetic risk factors for IPF when come together with environmental risk factors results in a dangerous mix, which is well known in the scientific research circles involved in IPF studies as "multiple hit hypothesis". It has been hypothesized that viruses are the initiators of fibrosis but studying viruses is highly complicated due to lack of sensitive reproducible cultures from the respiratory samples of the patients although the availability of molecular methods like PCRs has been instrumental in extending our understanding (Wuyts et al., 2013). Viral infection which has been most often cited in IPF cases is the EBV (Tang et al., 2003). Patients carrying EBV infections are known to have suffered from the repetitive injury to the epithelial cells, which has been postulated as a critical mechanism for the IPF pathogenesis (Katzenstein and Myers, 1998). Overwhelming evidence is available with respect to the role of EBV in IPF, for example, both protein and DNA expression of EBV has been found in samples from IPF patients with EBV proteins which are known to be expressed during the lytic phase of the viral infection cycle localizing to the AEC in IPF patients (Egan et al., 1995; Stewart et al., 1999). Another study involving two IPF patients treated with antiviral therapy has shown signs of stability in progression of IPF (Tang et al., 2003).

Another significantly elaborated factor believed to play a significant role in development and progression of IPF is transforming growth factor (TGF-β1). It has been noted that cytokine TGF- β1, a profibrotic cytokine showed an increased expression levels as a byproduct of proliferation of fibroblasts and fibrotic remodeling (Tomashefski, 2000).TGF-β1 can be found in an inactive form in the interstitium of the lung under normal conditions but upon injury to lung it gets activated (Sato et al., 1990; Sheppard, 2006). Activated TGF-β1 then binds to TGF-β1 receptors thereby resulting in a series of signaling cascades which play critical roles in the development of fibrosis. TGF-β1 via its interaction with TGF-β1 receptor kinase (ALK5) receptor can activate Smad proteins which activate downstream signaling in a cell type dependent manner (Barcellos-Hoff et al., 1994; Crawford et al., 1998). For example, TGF-β1 has been implicated in epithelial-mesenchymal transition (EMT) signalling via activation of Smad proteins (Varga and Jimenez, 1986). Blocking of TGF-β1 activation by blocking its receptor was protective against bleomycin induced lung fibrosis (Tomashefski, 2000). Apart from lung, pivotal roles for TGF-β have also been indicated also in the other organs, namely kidney and liver (Scotton and Chambers, 2007).

1.3 ANIMAL MODELS OF PULMONARY FIBROSIS

Several models of lung fibrosis have been developed so far, which include the bleomycin model, the fluorescein isothiocyanate model, asbestosis models, silica instillation model, age based models for studying fibrosis, models based on overexpression of cytokines such as TGF-α,β, interleukins, genetic models such as SFTPC, SFTPA2, TERT and mutations in the genes responsible for the development of Hermansky-Pudlak syndrome (HPS), radiation induced fibrosis model, alveolar type II cells injury via diphtheria toxin and lung injury due to acid instillation. One common feature in many of these animal models is the alveolar epithelial cell apoptosis which might result from several cellular stress events like oxidative stress, DNA damage, lysosomal stress and ER stress (B et al., 2013).

Asbestosis is a fibrotic lung disease which shows a remarkable similarity to human IPF in terms of UIP histopathology (Kishimoto et al., 2011; Roggli et al., 2010). One difference between asbestosis and IPF is that asbestosis has a slower progression as compared to IPF, and this goes along with lower number of myofibroblastic foci (Roggli et al., 2010). Animal models of asbestosis are based either on inhalation or intratracheal instillation of asbestos. Although intratracheal instillation results in fibrosis, which develops much more rapidly as compared to inhalation, this model is limited by the unequal distribution of asbestos between the lung lobes. It is also observed that intratracheal instillation of asbestos results in fibrosis being more central as compared to inhalation which results in a subpleural fibrotic remodelling. Intratracheal application of asbestos results in fibrosis already at day 7, whereas it may take up to a month to develop fibrosis with inhalation. Oxidative stress and injured AECIIs have also been observed in the asbestosis models in response to inhalation application due to the deposition of asbestos fibers (Sanchez et al., 2009).

Another murine model for lung injury which results in fibrosis is based on intratracheal administration of Fluorescein isothiocyanate (FITC), leading to lung fibrosis within a time span of 2-3 weeks (Moore and Hogaboam 2008; Moore et al., 2001; Roberts et al., 1995). Fibrosis is correlated specifically to the sites of FITC deposition, offering the advantage to study the injured regions using techniques such as immunofluorescence (Lawson et al., 2013). Another advantage of this model is that the fibrosis induced by FITC is robust and shows a long-lasting effect upto 9 months (Lawson et al., 2013). The drawback of this model is the variability in the effects of FITC which can be due to the difference in preparation of FITC, differences in the preparation of FITC (old vs freshly prepared) or size of FITC aggregates depending upon the sonification protocol (Sanchez et al., 2009).

TGF-β is a well characterized pro-fibrotic cytokine and is increased in fibrotic lungs prior to collagen synthesis (Fernandez and Eickelberg, 2012). Overexpressing TGF-β in mouse lungs resulted in increased mono-nuclear cell infiltration together with a two fold increase in total lung collagen content and apoptosis of epithelial cells (Lee et al., 2004; Sime et al., 1997). In addition, overexpression of TGF-β resulted in accumulation of myofibroblasts and epithelial-mesenchymal transition.

A mouse model based on direct injury to AECII was recently developed in which the diptheria toxin receptor was expressed under the control of SP-C promoter (Sisson et al., 2010). Repeated exposure of mice to diptheria toxin intraperitoneally resulted in AECII injury and thereby hyperplastic alveolar epithelial cell proliferation, followed by interstitial thickening resembling IPF. The specific advantage of this model is the ability to study the direct downstream effect of targeted epithelial cell injury towards the development of lung fibrosis.

Since IPF has a remarkable age-related onset, development of lung fibrosis has been studied. In aged animals, studies have shown that older mice are more prone to develop bleomycin induced pulmonary fibrosis as compared to younger ones (Sueblinvong et al., 2012). Additionally, older male mice show increased susceptibility to bleomycin as compared to older female mice (Redente et al., 2011). A similar, age dependent, predisposition to lung fibrosis has been observed in senescence-prone mice as compared to senescence-resistant mice (Xu et al., 2009). Deletion of genes responsible for receptor of the advanced glycation end products (RAGE) or relaxin results in a phenotype which is susceptible to spontaneous development of lung fibrosis (Englert et al., 2008; Samuel et al., 2003). Extended experimental time periods, high costs of animal maintenance and choosing the appropriate age remain potential drawbacks of this model.

The bleomycin model of pulmonary fibrosis has been the most extensively used model for understanding the pathophysiology of pulmonary fibrosis. Bleomycin induced lung fibrosis has been developed in a range of animals, including rats, mice, guinea pigs, hamsters, dogs, rabbits and primates (Degryse and Lawson 2011; Moore and Hogaboam 2008). Several delivery routes for bleomycin administration have been well established, such as intratracheal, intraperitoneal, subcutaneous and intravenous, out of which intratracheal delivery has been the delivery route of choice (Degryse and Lawson 2011; Muggia et al., 1983).

The bleomycin model of lung fibrosis has been attributed to excessive inflammation, apoptosis and necrosis of AECII due to DNA damage, oxidative stress and generation

of free radicals (Moeller et al., 2008; Moore and Hogaboam, 2008). Bleomycin administration in mice can induce fibrosis in a relatively short time ranging from 2 weeks to 12 weeks, depending on the delivery method chosen. Additionally, lung fibrosis development in response to bleomycin was also observed to be strain specific. For example, C57Bl/6 mice are more sensitive to the bleomycin induced lung injury and prone to fibrosis development as compared to the other strains (B, Lawson et al., 2013). Classically, the bleomycin model of lung fibrosis is based on a single exposure to bleomycin that resolves after few weeks of treatment (Lawson et al., 2005; Starcher et al., 1978; Thrall et al., 1979). Alternatively, repetitive intratracheal administration of bleomycin over several weeks (Degryse et al., 2010) was recently shown to result in lung fibrosis that persisted longer than the single administration.

1.4 Hermansky-Pudlak syndrome and respective mouse models

Hermansky-Pudlaksyndrome (HPS) was first described in 1959 by two Czech physicians, Hermansky F. and Pudlak P. HPS is typically characterized by oculocutaneous albinism (OCA) together with a bleeding diathesis due to a platelet degranulation defect and ceroid-liposfuscin accumulation (Gahl et al., 1998; Hermansky and Pudlak 1959). HPS is a rare autosomal recessive disorder linked to mutations in genes responsible for protein trafficking and organelle function. So far, nine different mutations resulting in HPS have been reported, namely HPS1-HPS9, out of which HPS1, HPS2 and HPS4 mutations may result in pulmonary fibrosis referred to as HPS associated interstitial pneumonia (HPSIP), the most common and most serious complication of HPS (Cullinane et al., 2011; Dell'Angelica et al., 1999; Gochuico et al., 2012; Li et al., 2003; Morgan et al., 2006; Pierson et al., 2006; Suzuki et al., 2002). Albinism observed in HPS patients is not due to absence of melanosomes or melanocytes but has been ascribed to the incapability of these organelles to produce required amounts of melanin in these patients. Although HPS is seen all over the world, a large proportion of HPS patients have been reported in Puerto Rico where the incidence rate of HPS is 1 person out of every 1800 people (Witkop et al., 1990).

HPS gene products areubiquitous transmembrane proteins (Wei, 2006) that affect several lysosome-related organelles in different tissues (see Fig. 2) namely melanosomes of melanocytes, lytic granules of cytotoxic T-cells, delta granules of platelets, azurophil granules of neutrophils and lamellar bodies of lung alveolar epithelial type II cells (Weaver et al., 2002; Wei, 2006).

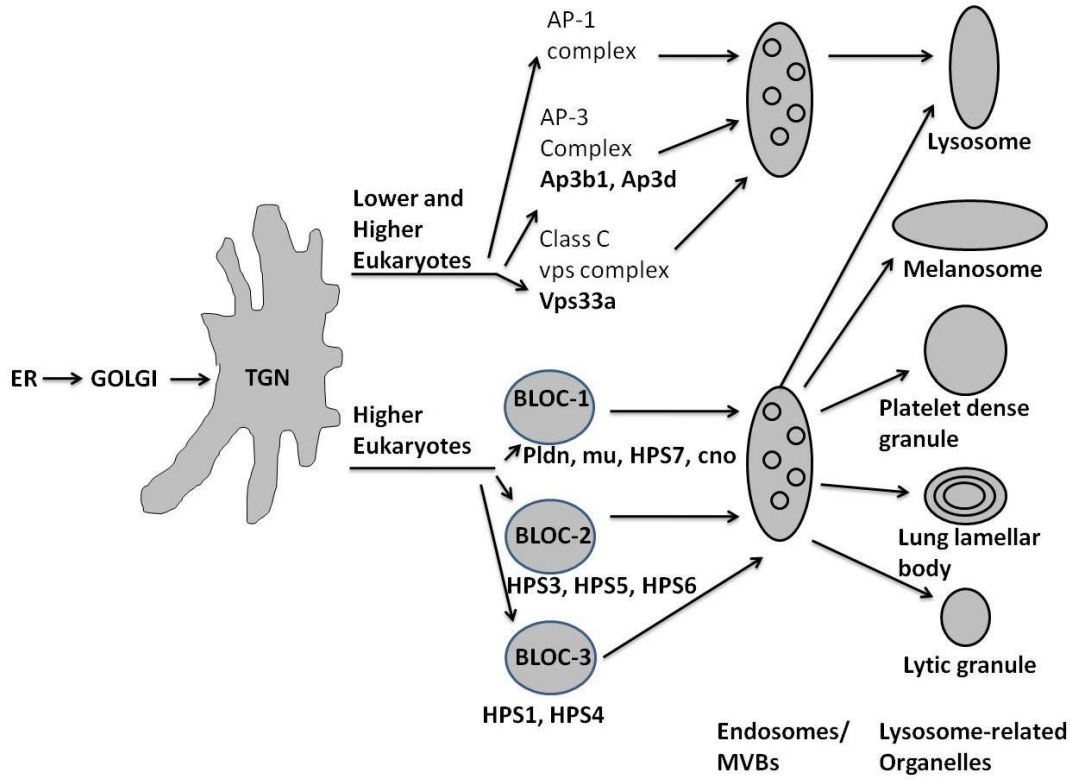

Fig. 2: HPS proteins and their significance in vesicle trafficking pathways. Different HPS proteins are involved in the generation of different lysosomal related organelles and are involved in different endocytic pathways. AP3 proteins are primarily involved in generation of lysosomes in both lower and higher eukaryotes. HPS proteins involved in the generation of BLOC complexes are found only in higher eukaryotes which are further involved in the generation of lysosome related organelles such as lytic granules, lung lamellar bodies, platelet dense granules, melanosomes, lysosomes etc. (Li et al., 2004).

1.4.1 HPS1

The *HPS1* gene on the chromosomal segment 10q23.1-q23.3 codes for a 700 a.a. protein with a molecular weight of 79.3 kDa (Bailin et al., 1997; Dell'Angelica, 2004). To date, twenty three different HPS1 mutations, which end up in a disease phenotype have been identified but the most often cited mutation found in people from Puerto Rico is the 16bp frameshift duplication in the exon 15 of *HPS1* gene (Wijnen et al. 1996).

HPS1 is the most affected HPS subtype displaying founder effects in Puerto Rico and accounts for about 50% of the HPS cases observed outside Puerto Rico (Oh et al., 1998). Majority of patients carrying HPS1 mutation in Puerto Rico show clinical phenotypes for restrictive lung disease in addition to some other noticeable clinical features including hemorrhage and granulomatous colitis (Witkop et al., 1990). Abnormal chest radiographs and abnormal high resolution computed tomography (CT) scans have been reported in

49% and 82% patients, respectively even though a normal oxygen saturation at rest was observed (Brantly et al., 2000). Pirfenidone has been shown to be effective in slowing down the progression of fibrosis in patients with residual forced vital capacity (FVC) below 50% (Gahl et al., 2002).

HPS1 is a ubiquitous cytosolic protein with a small amount of protein being membrane bound (Dell'Angelica et al., 2000). A 200 kDa BLOC-3 complex found in the cytosolic compartment was shown to have both HPS1 and HPS4 associated to each other as part of the complex (Dell'Angelica, Aguilar et al., 2000; Martina et al., 2003; Nazarian et al., 2003). Although immunoprecipitation experiments have shown a pulldown for both HPS1 and HPS4 together, there is no evidence of a direct physical interaction between HPS1 and HPS4, indicating the presence of atleast one more subunit within the BLOC-3 complex (Chiang et al., 2003; Martina et al., 2003; Nazarian et al., 2003). In HPS fibroblasts, a dispersed staining pattern for lysosome associated membrane protein-1 (LAMP1) and LAMP2 was reported instead ofthe usual perinuclear staining, while LAMP3 displayed a normal distribution pattern (Dell'Angelica, Aguilar et al., 2000). Of note, LAMP3 and LAMP1 showed localization to large vesicles in HPS1 melanocytes whereas LAMP2 showed normal distribution (Richmond et al., 2005).

1.4.2 HPS2

HPS2 encodes the β3A subunit of the heterodimeric adaptor protein complex AP-3 and is found on Chromosome 5. AP-3 is known for its function in the transport of protein cargo to transport vesicles, from where they are delivered to the lysosomes (Bonifacino and Dell'Angelica, 1999). The typical assembly of AP-3 molecule includes four main components - β3A-, μ3-, σ3- and δ- subunits. The *AP3B1* (or HPS2) gene encoding β3A-subunit consists of 1094 a.a., resulting in a protein with molecular weight of about 121.3 kDa. The role of AP3 complex is to regulate vesicular trafficking involving cargo proteins and directing them to lysosomes, platelet-dense granules, or melanosomes (Zhen et al., 1999). AP-3 adaptor complex has also been shown to be involved in the lysosomal biogenesis in yeast and melanosmal production in *Drosophila* (Lloyd et al., 1998; Odorizzi et al., 1998). AP-3 deficient cells show defects in lysosomal membrane protein trafficking where molecules which should normally be targeted to lysosomes end up accumulating inside endosomes thereby increasing the size of endosomes in the process (Sugita et al., 2002).

HPSIP due to HPS2 mutations can be separated from other forms of HPS based on the neutropenia and the resulting susceptibility to recurring respiratory infections. It resembles the Chediak-Higashi syndrome (CHS) very closely but is distinguished from

CHS by the absence of large intracellular granules. One patient diagnosed with HPS2 showed symptoms such as occulocutaneous albinism, platelet defects, a compromised immune system and at cellular level, no β3A, δ or μ3A protein was detected (Clark et al., 2003). A second patient carrying the mutations R509X and E659X showed absence of both β3A mRNA and protein resulting in a truncated form of AP3B1 complex (Huizing et al., 2002). Another patient showed severe respiratory infections, neutropenia, and hemorrhage (Huizing et al., 2002).

Two brothers with HPS2 were described by Dell'Angelica et al. where heterozygous mutations in the β3A gene were reported, with one allele encoding a deleted 21 a.a. sequence whereas other allele encoding protein with an amino acid substitution (Dell'Angelica et al. 1999). These mutations resulted in an increased degradation of β3A and destabilization of other AP-3 subunits. Both brothers suffered from neutropenia, neurological problems such as poor balance, recurrent upper respiratory infections and depressed pulmonary function (Shotelersuk et al., 2000). Another patient with two nonsense mutations resulting in loss of detectable β3A mRNA and protein and μ3 protein resulted in severe respiratory infections, neutropenia, hearing loss and hemorrhage (Huizing, 2002). Another HPS2 patient with no detectable β3A, δ or μ3A protein showed occulcutaneous albinism together with platelet defects thereby requiring immunoglobulins and prophylactic antibiotic treatments (Clark, Stinchcombe et al., 2003).

The HPS2 protein plays a critical role in trafficking of proteins towards the lysosomes (Bonifacino and Traub, 2003; Ihrke et al., 2004). Studies performed in mouse models of HPS show that only HPS mutations causing a loss of AP3 also results in an increased expression of LAMP1 (Dell'Angelica et al., 2000). Based on this observation, it was speculated that loss of AP3β1 might result in a membrane trafficking disorder. Supporting this concept, a recent report revealed that AP-3 dependent cargo transport is important for lamellar body maturation and that LAMP2 dependent peroxiredoxin-6 is impaired in HPS2 mice (Kook et al., 2016).

1.4.3 HPS4

The *HPS4* gene is located on Chromosome 22q11.2-q12.2 and encodes a 708 a.a. protein (molecular weight 76.9 kDa), expressed ubiquitously (Anderson et al., 2003; Martina et al., 2003). So far only about a dozen HPS4 patients carrying about ten different mutations have been reported. Two significant HPS4 mutations were reported in two patients, both in the carboxyl terminal, one being a deletion mutation on codon 685, the other one being an insertion mutation at codon 698. Both patients developed severe

pulmonary fibrosis ultimately resulting in death (Anderson et al., 2003; Bachli et al., 2004).

In addition to pulmonary fibrosis, one study reported that HPS4 patients exhibited clinical features like absence of platelet dense bodies and granulomatous colitis, similar to HPS1 patients (Anderson et al., 2003). Another patient with a P685del mutation, who was diagnosed with a severe case of pulmonary fibrosis, showed normal levels of melanocytes, but a decrease in melanin and ceroid content in perivascular macrophages in skin biopsy in this patient. There was also an increase in the number of AECIIs, which showed a foamy cytoplasm, and an increase in ceroid pigment in macrophages (Bachli et al., 2004).

The first mouse models of HPS were characterized about twenty years after the Czech physicians described the existence of HPS disease in 1959. These mouse models were results of non-allelic mutations which resulted in decreased pigmentation and severe bleeeding disorders (Novak et al., 1981; Novak et al., 1984). The HPS mouse models have greatly extended our understanding of the HPS disease at the molecular level with respect to biogenesis of various intracellular organelles such as lysosomes, melanosomes, lamellar bodies, and platelet dense granules. About 14 genes in mice result in HPS-like symptoms. Some of the mouse HPS genes, which have so far been analyzed at molecular level, are gunmetal (*gm*), pallid (*pa*), mocha (*mh*), pale ear (*ep*) and pearl (*pe*). Pallid mice show a severe hypopigmentation as compared to pearl and gunmetal mice which show intermediate hypopigmentation (Swank et al., 2000). Hypopigmentation in pale ear mice is limited to tail and ears. Oculocutaneous pigmentation effects are observed in pallid, pearl, and pale ear mice but no ocular hypopigmentation can be observed in gunmetal mice.

1.4.4 Mouse models of HPS

1.4.4.1 Pale ear mice

HPS1 in mice is the *pale ear* (*ep*) gene, located on Chromosome 19 and was the first HPS gene to be identified in mouse genome (Feng et al., 1997; Gardner et al., 1997). *Pale ear* gene encodes for a protein weighing 79 kDa, ubiquitous distribution in all tissues. Pale ear protein functions are still not known, but it is known to have some sequence homology to the gene responsible for Chediak-Higashi Syndrome (CHS) syndrome, which shares certain pathological features with HPS (Oh et al., 1996). *Pale ear* gene has been shown to have a very high sequence homology to human HPS1 gene,

mapped to the human Chromosome 10q23, showing that the pale ear mouse model of HPS is an appropriate model for human HPS1 disease.

1.4.4.2 Pearl mice

Pearl gene (*pe*) located on mouse Chromosome 13 codes for β3A subunit which belongs to adaptor protein AP-3 complex (Feng et al., 1999). Pearl mice as well as clinical HPS2 mutations show the same effect on AP-3, wherein a complete degradation of β3A subunit of AP3 is observed (Zhen et al., 1999).The HPS2 mouse model exhibits clinical features such as pigment dilution, impaired platelet lysosomal enzyme secretion and prolonged bleeding (Swank et al., 1998). In addition, kidney proximal tubule cells from HPS2 mice showed enlarged multi-lamellar structures which resemble lysosomes (Zhen et al., 1999). Even though mutations in β3A gene in humans and mice are different, the net effect of these mutations on the AP-3 complex is very similar. Trafficking of the lysosomal membrane proteins such as LAMP-1, LAMP-2, CD63 etc. has been shown to be defective in AP-3 deficient cells (Dell'Angelica et al., 1999; Le Borgne et al., 1998).

1.4.4.3 HPS1/2 double mutant mice

HPS1/2 double mutant mice, also known as *pale ear/pearl* (*ep/pe*) mice were obtained by crossing the naturally occurring pale ear (HPS1) mice with pearl (HPS2) mice (Feng et al., 2002). Double mutant mice show morphological defects in melanosomes belonging to retinal pigment epithelium (RPE), prolonged bleeding and an increase in levels of lysosomal enzymes in kidneys but not in other organs such as liver, spleen or brain (Feng et al., 2002). These mice characteristically show AECII features such as increased size, foamy appearance, aberrant lamellar bodies and a decreased survival rate (Guttentag et al., 2005; Lyerla et al., 2003). In addition to this, these mice also show a defect in surfactant processing and secretion resulting in accumulation of hydrophobic surfactant proteins, SP-B and SP-C in the lung tissues of these mice (Guttentag et al., 2005). It has also been shown that the double mutant mice model of HPS develops spontaneous fibrotic remodeling of lung as observed in HPS associated interstitial pneumonia (HPSIP) (Mahavadi et al., 2010). In HPS1/2 mice, an increased alveolar dysfunction, lysosomal stress together with an increase in the protein levels of Cathepsin-D has been ascribed, which might be the reason for increased apoptosis (Mahavadi et al., 2010). In addition to the lysosomal stress, the 9 month old HPS1/2 double mutant mice also displayed ER stress characterized by ATF4 induction and CHOP activation (Mahavadi et al., 2010).

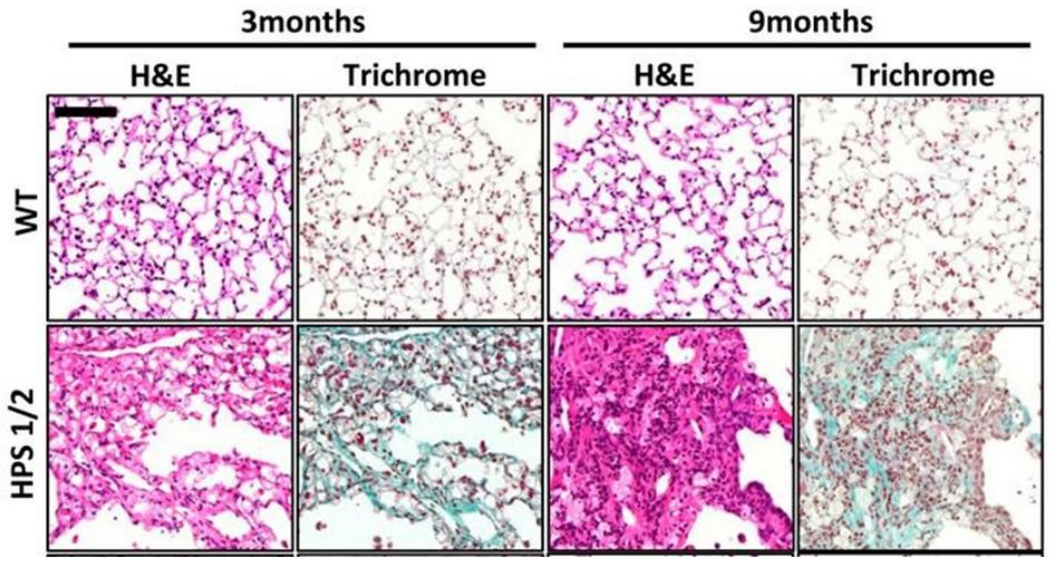

Fig. 3: H&E stained lung sections from HPS1/2 double mutant mice. Hemotoxylin and eosin stained right lung sections from HPS1/2 double mutant mice as compared to age matched WT mice at 3 months and 9 months of age. Magnification = X200, scale bar = 100 μm (Mahavadi et al., 2010).

1.4.4.4 Other HPS mice

Other HPS mice models such as Mocha, Pallid and Gunmetal mice have been described. Mocha mice carry a mutation in another subunit of AP3 complex, the δ subunit, and shows changes similar to HPS (Kantheti et al., 1998; Swank et al., 1998). In addition to HPS symptoms, these mice show balance defects, become deaf with age, and have a hyperactive phenotype (Miller et al., 1999). Mutations in the *Pallid* gene located on Chromosome 2 can result in abnormalities related to balance and posture in addition to pigmentation and platelet-dense granules related problems which are more severe in Pallid mice than other mouse mutants (Swank et al., 1998). Lung abnormalities in Pallid mice develop around one year after birth which eventually results in death of these mice (de Santi et al., 1995; McGarry et al., 1999). *Pallid* gene codes for the protein pallidin which is involved in regulation of intracellular vesicule trafficking (Huang et al., 1999). Gunmetal mice is a more severe mutant as compared to other HPS mutant mice because in addition to commonly found hypopigmentation and platelet-dense granule defects, these mice also exhibit serious problems with respect to platelet synthesis and alpha granule content (Swank et al., 1998). The defects in gunmetal mice are caused by mutations in the gene coding for the RabGGTase which results in a reduction in the amount of RabGGTase enzyme in these mice (Detter et al., 2000). RabGGTase enzyme is involved in prenylation, specifically geranylgeranylation of Rab proteins, which is critical for Rab proteins to function properly. Rab proteins play a key role in regulation of

intracellular vesicle trafficking and are involved in vesicle translocation and fusion (Pfeffer, 1999).

Proteins belonging to the HPS gene family like AP3B1 are also involved in enriching and delivery of cargo proteins in vesicles via endosomal lysosomal pathway; VPS33A is involved in vesicular trafficking to vacuoles in yeast which correspond to the lysosome - mammalian homologue (Suzuki et al., 2003); RABGGTA is involved in regulation of vesicular trafficking and organelle motility (Detter et al., 2000). Thus, lysosome associated alterations including impaired lysosomal enzyme secretion, are shown in some forms of HPS (Peden et al., 2002; Wei, 2006) and lysosomal stress was shown in HPSIP (Mahavadi et al., 2010). Especially in melanocytes derived from HPS1 patients, lysosomal membrane proteins, LAMP1 and LAMP3 were shown to be sequestered in macroautophagosome-like structures that are essential intermediate organelles of the cell's important lysosome associated degradation mechanism, commonly known as 'autophagy'.

1.5 AUTOPHAGY

Autophagy is an important, lysosome-dependent, protein quality control mechanism of the cell. It primarily aims for cellular survival and involves a series of tightly regulated steps that target long-lived proteins, dysfunctional organelles, carbohydrates, lipids, etc. to lysosomes for final degradation (Kelekar, 2005). The importance of autophagy pathway stems from the fact that the degradation products of autophagy are recycled back, hence generating energy for cell survival for example under starvation conditions (Yang and Klionsky, 2007). Degradation of damaged organelles and toxic build-up of proteins is taken care of by autophagy, thus keeping the cellular stress levels low (Lamark et al., 2009; Mortensen et al., 2010). However, under certain settings like aging or during neurodegeneration, autophagy has also been implicated to cause apoptosis (Azad et al., 2008; Yousefi et al., 2006).

Classically, autophagy has been characterized as macroautophagy, microautophagy and chaperone mediated autophagy (CMA). Out of the three, macroautophagy is the most well studied and understood pathway both *in vivo* and *in vitro*. Macroautophagy also offers the possibility to be visualized using a simple light microscope with the aid of fluorescently tagged proteins or with an electron microscope (Klionsky et al., 2008). Cytosolic proteins or the organelles, which are supposed to be degraded, via macroautophagy (Fig. 4A), are often referred to as cargo and are encapsulated by a double layer limiting membrane called autophagosome. These autophagosomes with the entrapped cargo fuse with lysosomes forming autophagolysosomes. Once fused with

highly acidic lysosomes, the cargo gets degraded by the lysosomal enzymes inside the autophagolysosomes (Klionsky and Emr, 2000). Macroautophagy deregulation has been well implicated in the progression and development of some of the most common pathologies such as cancer and neurodegeneration among many others (Brech et al., 2009; Menzies et al., 2015).

A

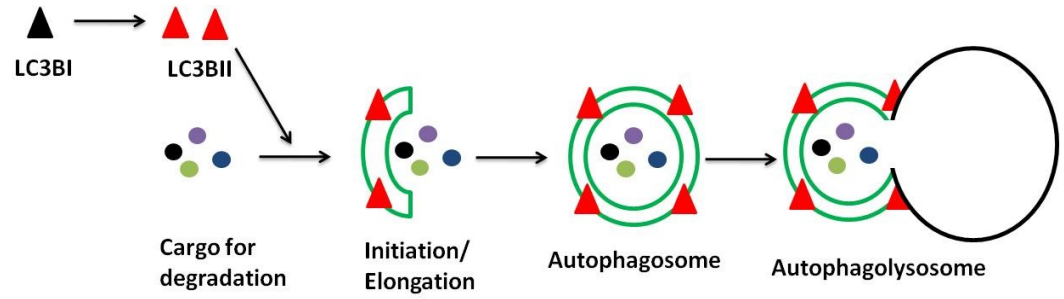

B

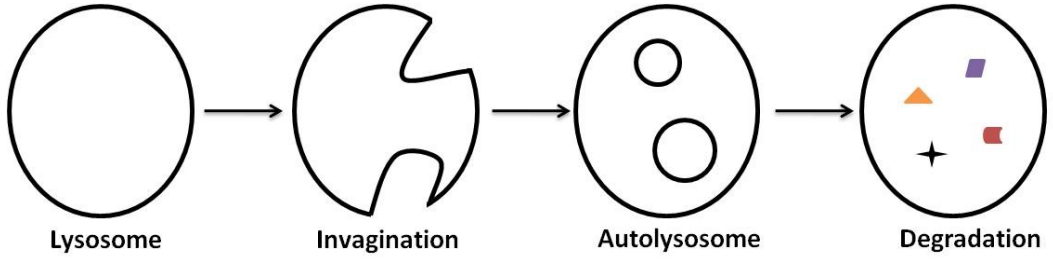

C

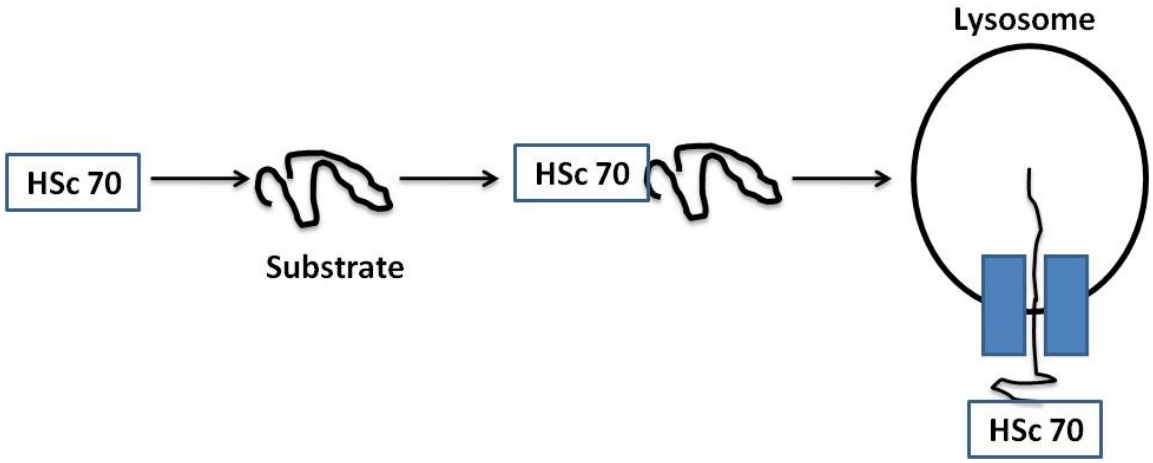

Fig. 4: Illustrations depicting different autophagy pathways. A. Macroautophagy, B. Microautophay, C. Chaperone mediated autophagy (Cuervo, 2011)

Microautophagy involves uptake of the protein cargo to be degraded by the lysomes via lysosomal invagination thereby resulting in the degradation of the protein cargo (Fig. 4B).

Under CMA pathway (Fig. 4C) proteins are labelled for degradation via the pentapeptide motif, KFERQ that gets directly translocated to the lumen of lysosomes via a complex formation which includes Hsc70 and lysosomal transmembrane protein LAMP2A (Cuervo and Dice, 2000).

1.5.1 Measuring autophagy

Several methods have been suggested to study the autophagy flux both *in vivo* and *in vitro* (Klionsky et al., 2008) out of which some of them are outlined below.

1.5.1.1 Western blots for Atg8/LC3B

Atg8 (mammalian homologue known as LC3B) is one of the most important members of the autophagy pathway. LC3B is produced as a pro-LC3B which gets cleaved at the C-terminus, followed by the conjugation to phosphatidylethanoloamine (PE-conjugated). This PE-conjugated form of LC3B known as LC3BII is then utilized by the autophagy pathway to form autophagosomes where proteins/organelles labelled for degradation are enveloped inside the double membrane vesicle labelled by LC3BII. This autophagosome then fuses with lysosomes to finally degrade the labelled proteins. Hence increase of lipidated LC3BII protein is widely used as a marker for an increased induction of autophagy or increased formation of autophagosomes.

1.5.1.2 Dynamic autophagy flux assays

Alterations in the LC3B protein levels may indicate that autophagy is induced in response to a particular treatment but to precisely assess autophagic flux, LC3BII turnover needs to be characterised in the presence or absence of autophagy inhibitors. Some of the commonly used autophagy inhibitors are chloroquine, bafilomycin, pepstatin + E64D, and ammonium chloride. Although various inhibitors of autophagy work in different ways acting at different stages of autophagy, the overall effect being loss of autophagic degradation thereby resulting in accumulation of key autophagy marker proteins together with protein/organelle cargo which was supposed to be degraded via autophagy. The difference in LC3BII levels in response to the treatment of choice plus inhibitor as compared to the LC3BII levels in response to the inhibitor alone indicates increase in autophagic flux, while unaltered or decrease in LC3BII levels in response to treatment in the presence of inhibitor as compared to inhibitor alone represents autophagy inhibition. In such cases, the increased amount of LC3BII levels in treated cells as compared to controls may primarily be due to inhibition of autophagy thereby accumulation of LC3BII, and not due to increased autophagy (Klionsky et al., 2008). Autophagic flux under different conditions is depicted in Fig. 5. Normal autophagic flux when no interventions

are made to the autophagic pathway is shown in Fig. 5A. Fig. 5B represents interventions such as treatment with autophagy inhibitor 3-MA or knockdown of autophagy protein Atg7 which result in a decrease in the lipidation potential of LC3B thereby reducing the overall flux. Fig. 5C shows how the rapamycin treatment induces increase in autophagy flux via increase in the lipidation of LC3B. Fig. 5D shows the commonly used principle for measuring autophagy flux in the presence of autophagy inhibitors where inhibitors prevent the degradation of autophagosomes resulting in accumulation of LC3BII.

Another commonly used method for analysing autophagy flux involves overexpressing GFP-LC3B in the cells and thereby assessing production of free GFP fragments in response to the treatment of choice. If there is an increase in autophagy flux post treatment, LC3B part of GFP-LC3B complex gets degraded via increased autophagic flux whereas GFP fragment being relatively more stable than LC3B in the acidic compartment of lysosomes can be detected via western blotting using GFP antibody. It is important to understand that GFP part of the GFP-LC3B as a protein is slightly more resistant to degradation as compared to LC3B but not the fluorescence of GFP as fluorescence is lost under highly acidic conditions inside the lysosomes upon formation of autophagolysosomes (Kimura et al., 2007).

Several immunofluorescence-based methods for studying changes in autophagic flux have been defined, some of the common ones being the RFP-GFP-LC3B chimera or studying the colocalization of LC3B (LC3BII being marker for autophagosomes) and LAMP1 (marker for lysosomes) indicating formation of autophagolysosomes. The RFP-GFP-LC3B chimera technique is based on the principle that the fluorescence emitted from RFP is more robust and stable under acidic conditions of lysosomes, whereas GFP fluorescence is not as stable. When the RFP-GFP-LC3B reaches autophagolysosomes, the predominant yellow fluorescence of the chimera would turn to stronger red fluorescence, indicating an increase in autophagic flux and hence degradation of GFP-LC3B leaving out only the RFP part of the chimera. Another immunofluorescence-based method involves tagging LC3B (either as green/red) and tagging LAMP1 (either as red/green depending on LC3B tag) for co-localization studies and imaging the fluorescence individually. Increase in yellow structures and quantifying the intensity of the yellow colour indicates increased autophagic flux.

A

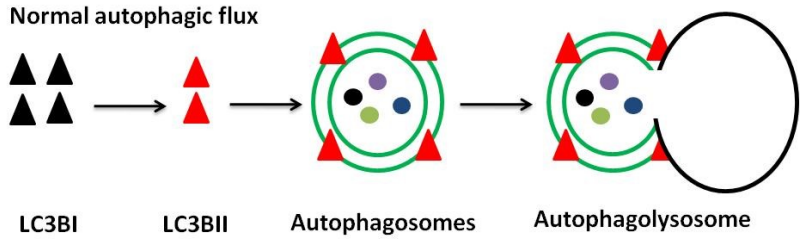

B

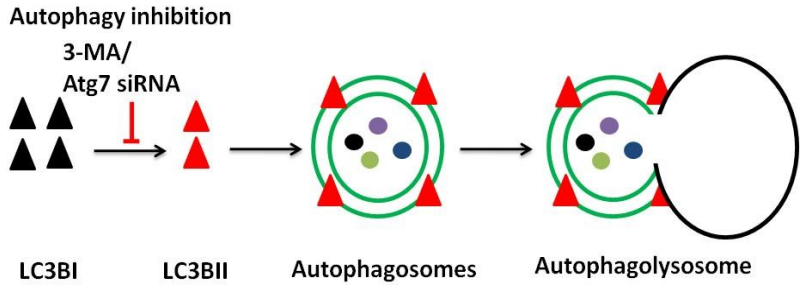

C

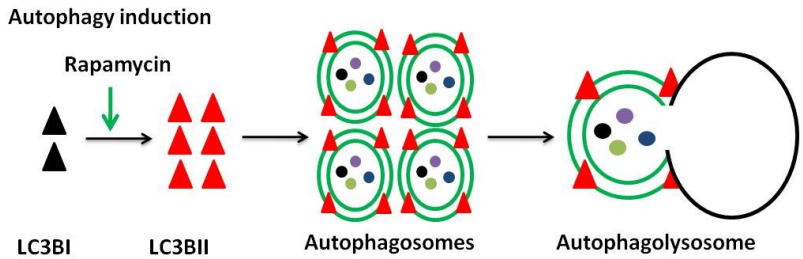

D

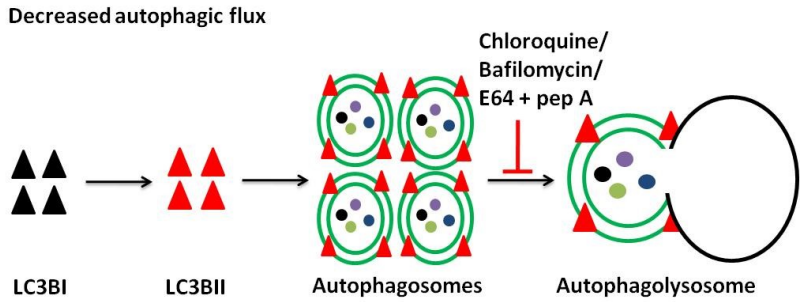

Fig. 5: Effect of different autophagy specific treatments on autophagic flux. Figure illustrates autophagy flux under different conditions, (a) normal autophagy pathway; (b) autophagy pathway when inhibited by the early-stage autophagy inhibitor, 3-methyl adenine (3-MA); (c) effect of autophagy inducer, rapamycin on the autophagic flux; (d) effect of late-stage autophagy inhibitors such as bafilomycin, chloroquine and E64/pepstatin on the autophagy pathway.

1.5.2 AUTOPHAGY IN HUMAN DISEASES

Autophagy has been studied quite extensively in development and progression of many diseases including cancer (Qu et al., 2003; Yue et al., 2003), neurological disorders (Anglade et al., 1997; Nixon, 2013), microbial infections (Liang et al., 1998; Nakagawa et al., 2004; Yuan et al., 2012) and aging related diseases (Takacs-Vellai et al., 2005; Toth et al., 2008). Recently, autophagy has gained interest in the field of pulmonary diseases since the first lung specific *Atg7* knocked out from the Clara cells in mice resulted in a number of severe airway epithelial abnormalities resulting in visible cellular swelling, loss of rough endoplasmic reticulum and a disfigured mitochondria (Inoue et al., 2011). Autophagy has been studied quite elaborately in several pulmonary disorders, such as in chronic obstructive pulmonary disease (COPD), cystic fibrosis, pulmonary arterial hypertension (PAH) and lung cancer.

Limited airflow, remodeling of small airways and predisposition to bacterial infections represent characteristic features of COPD, a disease typically caused by exposure to cigarette smoke for prolonged periods (Vestbo et al., 2013). Cigarette smoke has been shown to be consisting of approximately 4500, components which include certain heavy metals, phenolics, aromatic hydrocarbons etc. (Chen et al., 2008). Autophagy proteins such as LC3B-II, Atg4, Atg5-Atg12 complex, Atg7 etc. have been shown to be upregulated in the lung tissues of COPD patients in addition to an increased number of autophagosomes as observed under electron microscopy (Chen et al., 2008). When key autophagy proteins such as Beclin-1 and LC3B were knocked down, this resulted in a decrease in apoptosis when cells were subjected to cigarette smoke extract, establishing a link between autophagy and apoptosis under conditions of cigarette smoke extract exposure (Chen et al., 2010; Kim et al., 2008).

An autosomal recessive disorder, cystic fibrosis (CF), affiliated to a mutation in cystic fibrosis transmembrane conductance regulator (CFTR) gene, is a fatal disease and involves recurring pulmonary infections which have been attributed to highly viscous mucous blocking airway potency. The most common mutation in CFTR gene is at position 508 where phenylalanine gets deleted ($CFTR^{F508del}$) (Rommens et al., 1989). Several studies have established a defect in autophagy resulting in the accumulation of polyubiquitinated proteins together with autophagosomes (Bence et al., 2001). Another mutation in CFTR gene has also been shown to result in an increased oxidative stress together with key inflammatory response molecule transglutaminase (TG2) (Luciani et al., 2010). This increase in TG2 levels induces Beclin-1 inactivation and hence

accumulation of the autophagy substrate protein, SQSTM1/p62 protein (Luciani et al. 2010).

Pulmonary hypertension (PAH) is defined by a pulmonary arterial pressure higher than 25 mm Hg while resting or higher than 30 mm Hg while exercising, together with a mean pulmonary-capillary wedge pressure being below 15 mm Hg (Farber and Loscalzo, 2004). PAH typically starts in the pulmonary vasculature with initial events of insults and apoptosis, which are followed by excess proliferation of endothelial and smooth muscle cells together with a potential to avoid apoptosis and hence be able to proliferate uncontrolled (Dromparis et al., 2013). This kind of tissue remodelling results in a progressive occlusion of pulmonary arteries and is fatal in most cases (Semenza, 2011). Autophagy marker proteins are increased in the lung samples collected from PAH patients, with epithelial cells characteristically showing an increase in the lipidated form of LC3B as compared to healthy lung tissue (Lee et al., 2011). On one hand LC3B knockout mice showed severe form of PAH as compared to wild type controls in response to chronic hypoxia conditions, suggesting a protective role of LC3B. On the other hand, knockdown of Beclin1 was protective to fetal lambs suffering from persistent PAH by increasing the angiogenesis in pulmonary artery suggesting a negative role of autophagy pathway mediated by Beclin-1 (Lee et al., 2011; Teng et al., 2012). The role of autophagy in PAH is currently unclear and deserves future investigation.

Autophagy has been well studied and established for playing a significant role in the development and progression of carcinogenesis per se, but the role of autophagy in the field of lung cancer is still in an early stage. Studies performed on human lung adenocarcinoma have found an inverse correlation of the expression of Beclin-1 with tumor size (Won et al., 2012). Beclin-1 levels were found to be decreased in non-small cell lung carcinoma (Liu et al., 2011). Autophagy has also been shown to control levels of a GTPase-RhoA thereby playing a key role in maintaining genomic stability (Belaid et al., 2013).

Lysosomal storage disorders (LSDs) have also been shown to display defects in the autophagy pathway resulting in the accumulation of autophagosomes because of autophagic flux inhibition (Ballabio 2009; Ballabio and Gieselmann, 2009). Absence of lysosomal markers from the LC3B positive structures, indicating a defect in autophagolysosomes production, has been observed in several mouse models of LSDs such as juvenile neuronal ceroid lipofuscinosis (Cao et al., 2006), Batten disease (Koike et al., 2005), mucopolysaccharidosis type IIIa (Settembre et al., 2008) and others. Defects in LAMP2A, either on the basis of genetic mutations or a defective processing,

resulting in a dysfunctional chaperone mediated autophagy (CMA) pathway, have been implicated in LSDs like Danon disease (Fidzianska et al., 2007) and mucolipidosis IV (Venugopal et al., 2009), respectively.

Not many studies so far have been attributed to the role of autophagy in the development and progression of DPLDs. More recent studies on the regulation of autophagy in lung fibrosis report that autophagy is either not activated or is insufficient in patients with IPF and that TGFβ-1 inhibits autophagy in lung fibroblasts *in vitro* (Araya et al., 2013; Patel et al., 2012). Another study revealed an alteration in the Bcl-2-binding protein Beclin1, providing a hint towards a dysfunction in the autophagy/apoptosis system in IPF fibroblasts (Ricci et al., 2013). Knockdown of key autophagy proteins, namely LC3B or Beclin-1, have been shown to increase the levels of fibronectin and α-smooth muscle actin in the fibroblasts upon treatment with TGF-β (Patel et al., 2012). A more recent study revealed that bleomycin induces autophagy flux and that mice deficient in the autophagy gene Atg4B exhibited severe fibrosis (Cabrera et al., 2015). Nevertheless, the precise role of autophagy within the alveolar epithelial cells largely remains unexplored in IPF as well as in animal models of lung fibrosis.

2. OBJECTIVES

In this study, we hypothesized that autophagy pathway may play an important role in the development of lung fibrosis. For this purpose, we analyzed autophagy in two models: the HPS1/2 mouse model and the bleomycin model. To test our hypothesis, the following objectives were identified:

1. Analyze the autophagy pathway in animal models of lung fibrosis as well as in *in vitro* models.

2. Perform experimental gain/loss of function experiments to assess the impact of altered autophagy on the cellular phenotype.

3. Identify interaction partners for HPS1 protein.

4. Identify interaction partners for MAP1LC3B protein.

3. MATERIALS AND METHODS

3.1 Materials

3.1.1 Reagents

Reagent	Company
2-(4,2-hydroxyethyl)-piperazinyl-1-Ethansulfonate (HEPES)	Sigma Aldrich, Germany
2-amino-2-hydroxymethyl-1,3-propanediol (TRIS)	Roth, Germany
2-mercaptoethanol	Sigma Aldrich, Germany
Acrylamide solution, Rotiphorese® Gel30	Roth, Germany
Albumine, Bovine Serum (BSA)	Roth, Germany
Agarose (DNA electrophoresis)	Carl Roth
Ammonium persulfate (APS)	Roth, Germany
Bacto-Trypton	BD-Biosciences
Bacto-Yeast extract	BD-Biosciences
Bacto-agar	BD-Biosciences
Bleomycin	Hexal
Brilliant blue-G	Sigma
Bromophenol blue	Merck
Citric Acid	Thermoscientific, USA
Dharmafect	Thermoscientific
Dimethyl Sulfoxide (DMSO)	Sigma Aldrich, Germany
DMEM-F12 medium	Gibco, Germany
Dulbecco's phosphate buffered saline (PBS)	PAA, Austria
Dynabeads	Invitrogen
Endotoxin free maxi prep kit	Qiagen
Ethanol 99,5%	Roth, Germany
Ethylenediamine-tetraacetic acid (EDTA)	Sigma Aldrich, Germany
Fetal calf serum (FCS)	Roth, Germany
Gel red	Biotium
Glycergel® mounting medium	Dako, Germany

Glycerol	Roth, Germany
HotstarTaq® DNA polymerase kit	Qiagen
HPS1-myc-DDK clone (hu)	Origene
Hydrobeta-estradiole	Sigma Aldrich, Germany
Hydrochloric acid (HCl) 32%	Sigma Aldrich, Germany
Hydrocortisone	Sigma Aldrich, Germany
Isopropanol	Roth
Insulin-transferring-selenium (ITS)	PAN biotech
L-glutamate	Gibco
Lipofectamine®	Invitrogen
Methanol 99,9%	Roth, Germany
Milk powder	Sigma
Miniprep kit	Qiagen
Normal donkey serum	Johnson Immuno
N,N,N',N'-tetramethyl-1,2-diaminomethane (TEMED)	Sigma Aldrich, Germany
$Na_2HPO_4.2H_2O$	Merck, Germany
Nucleotide mix (dNTPs)	Qiagen, Germany
Omniscript® RT kit (200)	Qiagen
Opti-MEM medium	Gibco
Oligo (dT) primer	Roche, Germany
One shot top10 competent E.coli cells	Invitrogen
Page Ruler™ prestained protein ladder	Thermo scientific, USA
Paraffin, Paraplast Plus®	Sigma Aldrich, Germany
Paraformaldehyde (PFA)	Sigma Aldrich, Germany
PCR purification kit	Qiagen
Penicillin/Streptomycin	PAA, Austria
Pierce® BCA protein Assay Kit	Thermo scientific, USA
Pierce® ECL plus western blotting substrate	Thermo scientific, USA
Potassium Chloride (KCl)	Merck, Germany
Primers	Metabion
QIAquick Gel extraction kit	Qiagen
Rnase inhibitor	Roche, Germany
Restriction enzymes and buffers	New englandbiolabs

Roti®-Histofix 4%	Roth, Germany
HPS siRNA	Santa-cruz biotechnology
Saccharose	Roth, Germany
Scrambled siRNA	Santacruz biotechnology
Sodium citrate tribasic dehydrate	Sigma Aldrich, Germany
Sodicum dodecyl sulfate (SDS)	Sigma Aldrich, Germany
Sodium hydroxide (NaOH)	Sigma Aldrich, Germany
T4 DNA ligase	New englandbiolabs
Triton-X-100	Sigma Aldrich, Germany
Trypsin/EDTA	PAA, Austria
Turbofect®	Thermo scientific
Tween-20	Sigma Aldrich, Germany
ZytoChem HRP-DAB kit	Zytomed, Germany

3.1.2 Equipments

Instrument	**Manufacturer**
Autoclave	
Analytical balance	IKA®
Burner	Campingaz
Cell culture hood	Heraeus-Thermo scientific
Cell culture plates (10 cm)	Sarstedt, Germany
Cell culture plates (6 well)	Sarstedt, Germany
Centrifuge (table-top)	Hettich 200
8-well chamber slides	VWR
Cooling centrifuge	Hettichmikro 200R
Centrifuge (rotina 380R)	Hettich
Dynal magnetic stand	Dynal Biotech
Agarose gel apparatus	Keutz labor technic
Falcon tubes	BD Falcon, USA
Filter tips	Axygen scientific
Glass slides for IHC	Langenbrinck, Germany
Hemocytometer	W. SchrechHofheim
Thermocyler (semi-quantitative)	Bio-rad
Cell culture incubator	Thermo scientific
Orbital incubator SC 50	Stuart

Magnetic stirrer	Heidolph, Germany
Mini-PROTEAN® tetra cell	Biorad
Microwave oven	Severin
Microscope	Nikon eclipse Ts-100
Mirax scanner	Carl Zeiss, Germany
MJ. mini thermal cycler	Bio-rad
Nanodrop spectrophotometer	Thermo scientific
Nitrile gloves	Ansell, Germany
Power supply box	Consort
Parafilm	Pechiney plastic packaging
pH meter	Hanna instruments
PVDF trasnfer membrane	Thermoscientific
IHC slide scanner	Hamamatsu
Scalpels	Feather, Germany
Shaker	Grant-bio
Semi dry transfer cell	Bio-rad
Space and short plates	Bio-rad
Thermo mixer	Ika®
Vortexer	VWR
Water bath	Julabo

3.2 Methods

3.2.1 RNA isolation

RNA isolation from adhered cells was performed using the commercial kit RNEASY® plus mini kit (Qiagen) following the protocol provided by the manufacturer. Cells were washed with PBS and suspended in lysis buffer containing 1% β-mercaptoethanol. The lysate was subsequently passed through gDNA eliminator spin column and flow through was mixed with 70% ethanol. The solution was then passed through spin columns where RNA gets bound to the membrane. The membrane is subsequently washed with wash buffers and then transferred to a clean eppendorf tube where high quality RNA is obtained dissolved in RNase free water. The quality and concentration of this RNA is measured using Nanodrop® spectrophotometer. RNA samples are stored at -80℃.

3.2.2 Reverse transcription

Total complimentary DNA (cDNA) was prepared from isolated RNA using Omniscript® reverse transcription kit from Qiagen. 10 µl mastermix was prepared using components provided from the kit which was further mixed with 2 µg RNA suspended in 10 µl RNase free water and pipetted into PCR tubes. PCR tubes were incubated at 22°C for 10 min followed by incubation at 37°C for 65 min in PCR block. Final concentration of cDNA obtained is around 100 ng/µl. The cDNA obtained is then stored at -20°C.

RT components	Volume (µl)	Final concn.
10X RT buffer	2	1X
5mM dNTP mix	2	0,5 mM
50µM Oligo dT primers	0,5	1,25 µM
Rnase inhibitor (20 U/µl)	0,5	0,5 U
Omniscript^{TM} RT (4 U/µl)	1	2 U
Rnase free H_2O	4	
Total	10	

3.2.3 Semiquantitative PCR

Semiquantitative PCR is used to study the changes in transcription of genes in response to different treatments or under disease conditions. Genes of interest are amplified using gene specific forward and reverse primers which anneal to the DNA at specific temperature followed by extension and elongation using the properties of Taq DNA polymerase and added nucleotides in the reaction mixture for a certain number of cycles. Semiquantitative PCRs were performed using HotStarTaq DNA polymerase kit from Qiagen following the manufacturer's guidelines.

PCR components	Volume (µl)	Final concn.
10X buffer	2.5	1X
dNTPs (10 mM)	0.5	0,2 mM
Forward primer	1	0,6 µM
Reverse primer	1	0,6 µM
Taq polymerase (5 U/µl)	0.25	1,25 U
cDNA template	x	1 ng
Rnase free H_2O	19.75 - x	
Total	25	

After the PCR, sample buffer is added to every PCR eppendorf and sample is loaded on the agarose gel which contains a DNA intercalating dye such as Ethidium Bromide or Gel Red. DNA bands are separated on the agarose gel using electrophoresis. Negatively charged DNA moves towards positive terminal and gets separated based on size of DNA fragments. These DNA fragments are then visualized using UV lights fitted into the commercial Geldoc system from Biorad.

Program conditions	**Temperature (℃)**	**Time**
Initial denaturation	94	20 min
Denaturation	94	30 s
Annealing	Annealing temp.	30 s
Extension	72	1 min/KB
30 cycles		
Final extension	72	10 min

Gene (hu/m)	**Accession number**	**Forward primer**	**Reverse primer**
HPS1 (hu)	NM_000195.3	5'GGACTTCTTGC TGGTGAAGAG3'	5'CATCTGGAGTT TGTACCCCATG3'
p62 (hu)	NM_003900.4	5'TGGACCCATCT GTCTTCAAA3'	5'TCTGGGAGAGG GACTCAATC3'
β-actin (hu)	NM_001101.3	5'ACCCTGAAGTA CCCCATCG3'	5'CAGCCTGGATAG CAACGTAC3'
GAPDH (hu)	NM_002046.5	5'ACCCAGAAGACT GTGGATGG3'	5'GTGTCGCTGTTGA AGTCAGAG3'
LC3B (m)	AF255953.1	5'TGCCCGTCCT GGACAAG3'	5'CACACTCACC ATGCTGTG3'
p62 (m)	NM_011018.2	5'GGCCACCTCT CTGATAGCTT3'	5'ATTGGGATCT TCTGGTGGAG3'
β-actin (m)	NM_007393.4	5'CTGGTCGTAC CACAGGCATT3'	5'ATGTCACGCA CGATTTCCCT3'

50X TAE buffer	Amounts
Tris	242 g
Acetic Acid (99.9%)	57,1 ml
0,5M EDTA	100 ml
H_2O	Upto 1000 ml

50X Loading buffer	Amounts
Glycerol	5 ml
50X TAE buffer	200 µl
Bromophenol blue	4 mg
H_2O	make final volume 10 ml

3.2.4 Cloning

The process of cloning genes into vector backbones consists of several stages. First stage of cloning a gene is the amplification of the gene of interest. Using the specially designed amplification primers coupled to the sequence specific for the restriction enzyme of choice.

Plasmid (hu/m)	Forward primer	Reverse primer
Myc-LC3B (m)	5'TATTATGGATCCATGCCG TCCGAGAAGACCTT3'	5'TATTATAAGCTTCACAGCC ATTGCTGTCCCG3'
GFP-p62 (m)	5'CAGAGAATTCCA TGGCGTCGTTCA3'	5'TGTCGGATCCTCA CAATGGTGGAG3'
GFP-HPS1 (hu)	5'TATATAAAGCTTCCAT GAAGTGCGTCTTGGTGGC3'	5'TATATAGAATTCCCGA GCAGGGGGATACGGGA3'

Upon amplification of the gene of interest, the amplified product is subjected to the PCR purification using QIAquick PCR purification kit from QIAGEN. After purification, the PCR product and the vector backbone are restricted with the restriction enzymes which have been chosen for cloning of the gene into the backbone. Restriction digestion was carried out for 6-12 h at 37°C.

On the following day restriction digested fragments of interest are separated from the irrelevant fragments by running the samples on the agarose gel. After the fragments have separated enough, the agarose gel is cut out and the relevant DNA fragments are purified from the gel using QIAquick gel extraction kit from QIAGEN. Next step in the process of cloning is to ligate the restriction enzyme digested DNA segments of gene of interest and vector backbone. Ligation reaction was carried out at 4℃ overnight.

Vector digestion master mix	**Volume (µl)**
Vector (3-5µg)	5
Compatible buffer (10X)	3
Restriction enzyme 1 (10U/µl)	0,5
Restriction enzyme 2 (10U/µl)	0,5
H_2O	21
Total	30

PCR product digestion master mix	**Volume (µl)**
PCR product	50
Compatible buffer (10X)	7
Restriction enzyme 1 (10U/µl)	0,5
Restriction enzyme 2 (10U/µl)	0,5
H_2O	12
Total	70

Ligation master mix	**Volume (µl)**
Vector DNA	1
Insert DNA	5
10X ligase buffer	1
T4 DNA ligase	1
H_2O	2
Total	10

On the following day, ligation reaction is used to perform transformation of the ligation reaction into the TOP10® bacterial cells from invitrogen. Transformation protocol is as follows:

1. Briefly centrifuge vial contaning TOP10 cells once thawed and gently tap the vial to resuspend bacterial cells homogenously.
2. Pipette ligation reaction into the vial of competent cells.
3. Incubate on ice for 30 min.
4. Incubate at 42℃ in water bath for 30 s and immediately transfer the vial back to ice.
5. Add 250 µl SOC medium to each vial and incubate shaking at 37℃ for 1 h.
6. Spread 50 µl and 150 µl of the ligation solution onto agar plates containing selection marker specific for the vector backbone and incubate overnight at 37℃.
7. On the following day select isolated colonies from the agar plate and inoculate 5 ml of LB media containing selection antibiotic marker with the selected colonies.
8. Incubate overnight shaking at 37℃.
9. On the following day, from the cultures prepare glycerol stocks containing 600 µl of autoclaved glycerol and 500 µl overnight grown bacterial culture. Transfer the glycerol stocks to -80℃.
10. Using the remaining overnight cultures perform Miniprep using QIAprep Spin Miniprep kit from QIAGEN following manufacturer's protocol.
11. The plasmid DNA isolated from miniprep is restriction digested with the restriction enzymes originally used for preparing clones to confirm "Insert Release" thereby validating the positive clones from the negative clones.

Digestion master mix	**Volume (µl)**
DNA sample	5
Compatible buffer (10X)	2
Restriction enzyme 1 (10U/µl)	1
Restriction enzyme 2 (10U/µl)	1
H_2O	11
Total	20

Restriction digestion is performed for atleast 2 h upto overnight at 37℃ followed by running the restriction digested samples on agarose gel and confirming the positive clones. Once confirmed, the samples are submitted for sequencing to make sure that the clones do not contain any mutations which might have occurred during the process

of cloning. Once the sequencing data confirms the sequence of the gene of interest, already prepared glycerol stocks were used to generate endotoxin free stocks of plasmids using EndoFree® Plasmid Maxi Kit from QIAGEN.

3.2.5 Plasmid transfections

Plasmid transfections to the cells, A549 and MLE12 were made using Lipofectamine® or Turbofect® depending on different plasmids used for transfection. 1 µg DNA was used for transfecting 1 well of a 6 well plate. Transfection medium was changed after 4 h with a fresh medium without any transfection agent when Lipofectamine® was used for transfection but there was no such change of medium when Turbofect® was used.

3.2.6 Protocol for transient transfection with plasmids:

1. Appropriate number of cells was plated per well on Day 1.
2. On Day 2, 1 µg plasmid DNA was mixed with 4 µl lipofectamine or 6 µl turbofect depending upon the plasmid. Final volume of the solution was made 200 µl and incubated for 20 min at room temperature.
3. The final volume was made 2 ml and added per well which was supposed to be transfected.
4. In case of lipofectamine, transfection medium was aspirated after 4 h and replaced with fresh medium without any transfection reagents.

Plasmid (hu/m)	Transfection reagent
Myc-LC3B (m)	Turbofect
GFP-LC3B (m)	Turbofect
GFP-p62 (m)	Turbofect
HPS1-myc-DDK (hu)	Lipofectamine
GFP-HPS1 (hu)	Lipofectamine
GFP-TFEB (m)	Lipofectamine

Table above shows list of plasmids used for transfection and the transfection reagent which was correspondingly used for those plasmids.

3.2.7 Protein isolation

3.2.7.1 Protein isolation from cultured cells

Cultured cells were harvested and suspended in lysis buffer containing protease inhibitor. Once suspended in lysis buffer, cells were snap frozen in liquid nitrogen and

then thawed three times followed by incubation on ice for 30 min. After this, cells were centrifuged at 13,000 RPM using cooling centrifuge at 4℃. Supernatants were transferred to clean eppendorf tubes and stored at -80℃.

Protein extraction buffer	Concentration
Tris	50 mM
NaCl	150 mM
EDTA	5 mM
Triton-X-100	1%
Na-deoxycholate	0,5%
Protease inhibitor cocktail Complete™	4%

3.2.7.2 Protein isolation from animal/human tissues

At the time of harvesting tissues from mice these tissues were snap frozen in liquid nitrogen and stored at -80℃. Before preparing protein homogenate from these tissues, a small piece of lung tissue (approximately 50-80 mg) was chopped and suspended in lysis buffer mentioned earlier together with 1,4 mm and 2,8 mm zirconium oxide beads and then homogenized at a very high-speed using Precellys® (programmed at 2 cycles of 20 s at 5500 RPM). After homogenization, protein samples were centrifuged at 13,000 RPM at 4℃. Supernatants were transferred to fresh eppendorf tube and stored at -80℃.

3.2.8 Bicinchoninic acid (BCA) assay

BCA was used to determine protein concentration in these protein samples. BCA was performed using Pierce® Protein Assay Kit following manufacturer's guidelines. BCA assay is a 2-step reaction where in step one copper gets chelated to the proteins in alkaline environment resulting in light blue complexes. In next step the bicinchoninic acid (BCA) makes a reaction with reduced cuprous ions producing a purple color product. The intensity of purple color signifies the protein concentration in the sample with a more intense purple color meaning a higher protein concentration and a weaker purple color meaning a lower protein concentration. This absorbance can be measured using a spectrophotometer with an absorbance around 562 nm. Since BCA is performed in a 96 well plate, an ELISA reader (SpectraFluor Plus, Tecan) was used to measure the absorbance of the samples. Based on the optical density readings from spectrophotometer concentrations of the samples, protein concentrations are determined. BSA was used as standard spanning a range of concentrations ranging from 7.8 µg/ml to 2 mg/ml.

3.2.9 SDS Polyacrylamide Gel Electrophoresis (PAGE)

SDS-PAGE is performed to separate group of proteins based on their molecular weight under the influence of an electric field. Before loading the protein sample on the acrylamide gel, the protein sample is mixed with loading buffer which contains β-mercaptoethanol and incubated at 95℃ for 10 min on the heating block.

Loading Buffer (4X)	Amount
SDS	1,6 g
Tris/HCl, ph 6,8	4,8 ml tris-HCl (1M)
Glycerol	8 ml
Bromophenol blue	8 mg
β-mercaptoethanol	1 ml (freshly added)
Water	Upto 20 ml

Depending on the molecular weight of the protein of interest different acrylamide percent gels are used.

Components	Resolving gel				Stacking gel
	8%	10%	12%	15%	4%
Rotiphorese	2,66 ml	3,33 ml	4 ml	5 ml	1,33 ml
Dividing gel buffer	3,33 ml	3,33 ml	3,33 ml	3,33 ml	0
Stacking gel buffer	0	0	0	0	2ml
Dest. water	3,87 ml	3,20 ml	2,53 ml	1,53 ml	6,75 ml
10% APS	50 µl	50 µl	50 µl	50 µl	100 µl
10% SDS	100 µl	100 µl	100 µl	100 µl	100 µl
TEMED	10 µl	10 µl	10 µl	10 µl	10 µl

** Volumes provided for resolving gel in the table are for 1 gel

***Volumes provided for stacking gel in the table are for 3-4 gels

Resolving gel buffer	Amounts
Tris (1.5M)	18,17 g
pH	8,8
H_2O	Upto 100 ml

Stacking gel buffer	Amounts
Tris (0.5M)	6,05 g
pH	6,8
H_2O	Upto 100 ml

SDS running buffer (10X)	Amount
Tris	30.2 g
Glycine	144 g
SDS	10 g
Water	Upto 1000 ml

3.2.10 Immunoblotting

Immunoblotting involves transfer to proteins from acrylamide gel to the polyvinylidene (PVDF) membrane known as western blotting followed by incubation of the membrane with the antibodies against protein of interest. This incubation with antibodies allows us to detect the protein of interest on the membrane. Proteins separated on the acrylamide gel under the electric field are transferred to a 0.45 µm PVDF membrane using a semi-dry transfer chamber also under the electric field. PVDF membrane is incubated in methanol for 1 min to activate the membrane before using it for the transfer.

After transfer of proteins to the PVDF membrane, the membrane is blocked with 5% milk buffer made in 1X-TBST for 1 h to reduce the non-specific binding of the antibody to the proteins. After blocking, membranes are transferred to the antibody solutions prepared in 5% milk buffer and incubated overnight shaking at 4℃. Next day membranes are washed with 1X-TBST followed by incubation with secondary antibody labelled with horseradish peroxidase prepared in 5% milk buffer targeting primary antibody for 1 h at room temperature shaking. After incubation with secondary antibody, the membranes are thoroughly washed with 1X-TBST and taken for developing. Protein bands are visualised by incubating membranes with Pierce ECL substrate for western blotting using chemiluminiscence properties. Images of the membrane were made using imaging system from INTAS®. Quantification of the western blots was performed using ImageJ software.

Transfer buffer	Amounts
Tris	6.04 g
Glycine	28.8 g
Methanol	400 ml
H_2O	Upto 2000 ml

10X TBST buffer	Amounts
NaCl	176 g
Tween20	20 g
Tris	48 g
H_2O	Upto 2000 ml
pH	7,5

Milk Buffer	Amounts
Milk powder	5%
1X TBST	-

3.2.11 Immunohistochemistry

Detection and localization of genes in the lung tissues harvested from mice and humans was performed using immunohistochemistry (IHC) by using specific antibodies against specific antigens. Lung tissues harvested from mice or from humans were fixed using phosphate-buffered formaldehyde solution (Roti®-Histofix 4%, ph 7.0) overnight at 4℃. Following overnight incubation in the formaldehyde solution tissues were transferred into embedding cassette and then stored at 4℃ in phosphate-buffered saline. This was followed by dehydration in a tissue processor (ASP 300S, Leica) overnight and then embedded into the paraffin using Leica embedding unit (EG 1140H, Leica). Tissues were cooled down on a cooling plate which was then followed by sectioning of the lung tissue to a thickness of 3 µm using a microtome. These cut sections of the lung tissue were then mounted on to the glass slides. These slides were then incubated in a heating oven set at 37℃ for 6-12 h and then stored at room temperature until used for immunostainings.

10X PBS buffer	Concentration
NaCl	1,37 M
KCl	26,8 mM
$Na_2HPO_{4.2}H_2O$	64,6 mM
KH_2PO_4	14,7 mM
Water	-

Before subjecting the slides mounted with lung tissues to the immunohistochemistry protocol, slides were incubated in an oven set at 60℃ for 2 h followed by deparaffinization in xylene for 10 min. Followed by deparaffinization, slides were hydrated by passing them through decreasing ethanol concentration solutions of 99.6%, 96%, 80%, 70% and finally 50%, incubated in each solution for 3 min. After passing the slides through alchohol series, slides were washed in PBS and then boiled in citrate buffer for antigen retrieval three times for 10 min.

After boiling the slides in citrate buffer, slides were washed in PBS and then subjected to the protocol provided by the manufacturers of ZytoChem HRP kits (DAP/Fast red). Tissue sections were incubated in the blocking solution for 5 min followed by incubation with primary antibody targeting specific antigen of interest overnight at 4℃. Next day, slides were washed with 1X PBS and incubated with biotinylated secondary antibody for 10 min. Slides were washed with 1X PBS and incubated with the Streptavidin HRP-conjugate solution for 10 min. Slides were washed and incubated with substrate solution, either DAB or Fastred. All slides were incubated with the substrates for equal amount of time. The enzyme-substrate reaction was stopped by putting the slides in water. Slides were counterstained for the nucleus using hematoxylin solution by incubating for 30 s after which slides were washed under running water until water runs clear. The stained sections were mounted with the Glycergel® mounting medium and left to dry. These slides were scanned using scanning device (Hamamatsu) and analyzed.

Lung tissues from HPS-1 patients were procured either from post-mortem lungs or explanted lungs. Written informed consent was obtained and subjects were enrolled in protocol (04-HG-0211) which was approved by the National Human Genome Research Institute's Institutional Review Board. Lung tissue slides were received from Dr. Bernadette R. Gochuico (MD, Bethesda). Lung tissue samples used as control, procured from the organ donors have been described earlier (Korfei et al., 2013).

3.2.12 Immunofluorescence and quantification

Cells cultured in 8 well chamber slides post treatments were washed with PBS followed by fixing cells with 4% PFA prepared in PBS. Cells were incubated with 4% PFA for 10 min and then washed 3X with PBS. Fixed cells were then permeabilized with 0.5% Triton X-100 for 5 min at room temperature. Following permeabilization, cells were washed with PBS. Cells were blocked with 10% donkey serum prepared in PBS for 30 min at room temperature and then washed 3X with PBS. Cells were blocked again with 3% BSA made in PBS for 45 min at room temperature. After blocking, cells were incubated at 4°C overnight with antibody solutions prepared in 3% BSA. Cells were washed next day 5X with PBS and incubated with secondary antibody prepared in 3% BSA at a concentration of 1:5000 for 1 h at room temperature. Cells were washed 5X with PBS before mounting it with DAPI. Leica M205FA fluorescent stereoscope (Leica Microsystems, Wetzlar, Germany) equipped with Leica DFC360 was used to make fluorescent images using 63X lens. Image analysis was performed using Leica Application Suite Advanced Fluoresence (LAS AF) software, version 4.3, Germany. Immunofluorescent images were quantified using ImageJ plugin 'JACOP', which was used for calculating Pearson's coefficient. 15-30 randomly selected regions per well were imaged and quantified using ImageJ. Parameters for imaging and quantification were kept constant across treatments for all images. 'Costes automatic threshold' method was used for calculating Pearson's coefficient of colocalization for images with two different fluorophores.

3.2.13 Co-Immunoprecipitation and Mass spectroscopy

Method of co-immunoprecipitation (Co-IP) allows us to pull down the protein of interest (bait protein) using specific antibodies against the protein and in the process, we can pull down the other proteins (prey proteins) which are interaction partners of the target protein. In simple terms, antibody which is specific against our protein of interest is coupled to the beads (magnetic, agarose, sepharoseetc). Antibody coupled beads are incubated with the protein mixture where our protein of interest exists together with many other proteins. Incubating these beads with the protein solution for long enough duration allows the proteins to bind to the antibody which can later be separated from other protein by various methods depending on the type of beads you use for immunoprecipitation. Pulled down proteins are then analysed using MS/MS or western blots. Beads are coupled to the antibodies on day 1. Pipette 1 mg beads per 10 cm plate into a 1.5 ml eppendorf tube and wash the beads twice with PBS before resuspending the beads in 29 µl of Buffer B/mg of beads. To this suspension add 2 µg antibody for 500 µg total protein. To this antibody-beads suspension add 2/3rd volume of (PBS + antibody) solution. Incubate the beads overnight rolling at +4°C. On day 2, wash the antibody bound magnetic beads 2X with PBS and resuspend the beads in 100 µl PBS. From the protein

lysate, pipette 10% volume into a new eppendorf and label it as input. Incubate the antibody coupled beads with the protein lysate and incubate overnight rolling at +4℃. On day 3, wash the beads 1X with PBS and resuspend the beads in 100 µl PBS. Transfer this suspension to a new Eppendorf and wash again. Resuspend the beads in 50 µl PBS and add 4X sample buffer containing β-mercaptoethanol. Boil the samples at 95℃ for 10 min before continuing with SDS-PAGE followed by western blots or MS/MS analysis.

For the mass spectroscopic analysis of the pulled down proteins, pull down samples were subjected to SDS-PAGE. After the electrophoresis, polyacrylamide gels were stained with Coomasie Brilliant blue (CBB). Gels were incubated with CBB one hour at room temperature. Visible bands were cut out from the gel and each of the gel fragments were cut into smaller pieces of about 1mm per side. Gel pieces were washed twice with 50 mM Ammonium Bicarbonate (ABC)/50% EtOH solution for 20 min at room temperature. Gel pieces were then dehydrated by incubating in 100 µl absolute ethanol for 20 min (2 X 10 min) and then dried using speed vacuum for 5 min. Dried gel pieces were then incubated in 100 µl DTT (prepared in 50 mM Ammonium Bicarbonate) for 45 min at 56°C to reduce the proteins. Gel pieces were then incubated in 100 µl of 55 mM iodacetamide for 30 min at room temperature away from direct light to alkylate the proteins (block free sulphydryl group). Gel pieces were then washed with 50 mM ABC and dehydrated with absolute ethanol followed by drying the gel pieces. Proteins were then digested by incubating with 12 ng/µl trypsin for 15 min at 4°C. Gel pieces were then covered with 50 mM ABC and digested overnight at 37°C. On the following day, supernatant from the overnight incubation were collected in a clean 1.5 ml microfuge tube. Gel pieces were incubated with 100 µl 30% acetonitrile/3% trifluoroacetic acid (TFA) for 20 min at room temperature. Supernatant was collected and added to the previously collected supernatant. Gel pieces were incubated in 100µl 70% acetonitrile for 20 min at room temperature. Supernatant from the samples post incubation were collected and added to the previously collected supernatants. Collected supernatants were dried down using speed vacuum to a volume of approximately 80 µl. Samples were then loaded on stage tips and centrifuged at 2600 rpm for 4 min. Stage tips were then washed with 20 µl wash buffer and centrifuged at 2600 rpm for 2 min. Stage tips were then dried and stored at 4°C until analysis. Mass spectroscopic analysis of the samples and quantification of the signal intensities was performed by Prof. Marcus Krueger (Max plank institute, Bad Nauheim). Excel sheets contanining calculations and quantifications of the immunoprecipitated proteins were provided to us in the final form by Prof. Krueger.

3.2.14 Bleomycin treatments (*in vivo*)

10-14 weeks old were administered 0,6 µl/g ketamine 10% (100 mg/ml) and 0,3 µl/g Domitor 10% (0,5 mg/ml) dissolved in 0,7% saline to anaestheisize the mice. Post anaesthesia, 0,7% saline or bleomycin (1,0-3,0 U/kg) was administered to the mice intratracheal. Post bleomycin administration, mice were daily checked for weight, activity, respiration, and temperature parameters. After the treatment period of bleomycin, mice were sacrificed, and lungs were harvested and used according to protocols for further studies. In case of decline in vital parameters, mice were euthanized.

3.2.15 Small interfering RNA (siRNA) transfections

siRNA transfections inhibit the expression of the gene against which the siRNAs are targeted thereby inhibiting production of the protein produced by the targeted gene. The siRNA against *HPS1* (hu) was commercially obtained from Santa Cruz biotechnology® and used to silence *HPS1* gene in A549 cells. 700,000 cells were seeded per well of the 6 well culture plates previous evening and next morning the cells were transfected with 50 nM HPS1 siRNA or scrambled siRNA (Dharmacon) in serum free medium. Dermafect was used as transfection reagent for transfecting both HPS1 siRNA and scrambled siRNA. After 24 h or 48 h, cells were harvested and used for analysis of proteins and mRNA accordingly.

3.2.16 Bleomycin treatments *in vitro*

Bleomycin powder from HEXAL® was suspended in 1.5 ml NaCl giving a final concentration of 10 mU/µl and used for treating the cells under *in vitro* conditions. 1,000,000 cells were incubated per well of a 6 well plate and treated with indicated amount of bleomycin for 4 h in complete medium. After 4 h, cells were washed with PBS and harvested to extract mRNA or protein and used for further experiments.

3.2.17 Autophagy flux assays

To measure autophagy flux assays, MLE12 cells were first incubated with autophagy inhibitors, either Chloroquine (CQ) or Bafilomycin (Baf) for 1 h and then treated with indicated doses of bleomycin for 4 h. After treatment, cells were harvested, and total protein was isolated from the cells and used to perform BCA. After BCA, equal amount of protein was loaded onto the polyacrylamide gels and used to detect levels of LC3BII in the cells using western blotting.

3.2.18 Transmission electron microscopy and immunogold labelling

Electron microscopy was performed in collaboration with the groups of Prof. Dr. Matthias Ochs and Prof. Dr. Lars Knudsen, Hannover Medical School, Germany. Mice lungs were

isolated and perfusion fixed using multipurpose solution for fixation (4% paraformaldehyde, 0.1% Glutaraldehyde in 0.2 M HEPES buffer) as has been described earlier (Vasilescu et al., 2012) in Giessen. In Hannover, 3 lungs each from wild type mice and HPS1/2 mice were embedded in lowicryl resin after freeze distribution. Immunogold labelling for LC3B was performed as described earlier (Poornima Mahavadi, 2015). Gold labeling was quantitatively analyzed to determine cellular compartments with a preferential localization of LC3B. Relative labeling index (RLI) was determined by chi-squared analysis (χ^2-analysis) to statistically analyze distribution of gold labelling (Hsia et al., 2010; Mayhew and Lucocq, 2008). Three lungs per group i.e., wild type and HPS1/2 were used for the calculation and 2 sections per lung were analyzed. Volume fractions and surface densities within AECII cells were calculated using point and intersection counting for following compartments: lumen of lamellar body (LB), the limiting membrane (LM) (area of 100 nm around the limiting membrane), mitochondria (mito), nucleus and cytosol. Gold particles ($N_{gold\ observed}$) in these five compartments were counted. Gold particles were observed in cytosol were also counted. Cell size of the AECII in HPS1/2 was significantly larger than the size of wild type AECIIs. Expected number of gold particles per subcellular compartment was calculated by multiplying sum of all counted gold particles in AECIIs with volume fraction of subcellular compartment. $N_{gold\ expected}$ gives us the number of particles which we would be ending up counting if the labeling were random. $N_{gold\ observed}$ and $N_{gold\ expected}$ values were used to calculate RLI using the following formula: $RLI = N_{gold\ observed}/N_{gold\ expected}$

3.2.19 Animal ethics permissions

Bleomycin study protocol (GI 20/20-Nr. 109/2011) was approved by University Animal care committee and the Federal Authorities for Animal Research of the Regierungspraesidium, Giessen (Hessen, Germany).

Mice with naturally occuring HPS mutations (HPS1, HPS2) and HPS1/2 mice were sacrificed for the study as approved and published earlier by our research group (Mahavadi et al., 2010). Same lung samples were used for the current study.

3.2.20 Patient consent

A written and informed consent from the subjects enrolled in the protocol (04-HG-0211) was obtained. This protocol was approved by the Institutional review board of the National Human Genome Research Institute.

3.2.21 Statistical analysis

Quantification of western blots, immunofluorescence images and analyses involving comparison between multiple groups was performed using one-way ANOVA. Graphpad Prism 5.0 was used to perform statistical analysis. p value summary: * $p<0.05$, ** $p<0.01$ and *** $p<0.001$, n.s.: no significance. Immunogold labelling distribution in the ultrastructural compartments of AECII was analyzed using chi-squared analysis and degree of freedom of 4 (in case of 5 defined ultrastructual compartments). All quantifications pertaining to electron microscopy were performed by Prof. Dr. Matthias Ochs and Prof. Dr. Lars Knudsen, Hannover Medical School, Germany.

4. RESULTS

4.1 Defective autophagy in HPS1/2 mice and HPS1 patients.

To understand the effect of the HPS mutations on the autophagy pathway we first performed immunoblots on total lung homogenates of lung tissues of HPS1/2 double mutant mice as well as HPS1 and HPS2 single mutant mice belonging to two different age groups, 3 and 9 months. Immunoblots for key autophagy marker proteins namely LC3B, SQSTM1/p62, ATG7, ATG5, TFEB and LAMP2 for HPS1/2 mice were performed and compared to the age matched single mutant mice and wild type controls as shown in Fig. 6A-E. Western blot results showed an increase in autophagy marker proteins in HPS1/2 mice lungs as compared to the single mutants and controls in both 3 months and 9 months old mice. Interestingly though, in addition to the increase in the protein levels of LC3BII, which is a key marker for autophagosome production, we also observed a corresponding increase in the protein levels of the autophagy substrate protein, SQSTM1/p62, especially in the 9 months old mice. Under homeostasis conditions, the levels of p62 protein are well regulated by autophagy pathway and an increase in autophagy would result in a decrease in p62 levels. An increase in LC3BII protein levels together with an increase in p62 protein levels is therefore indicative of a defective autophagy pathway. Immunohistochemistry performed on the lungs isolated from HPS1/2 mice for the autophagy protein p62 as shown in Fig. 6G and 6H corroborated with the western blot data and showed an increase in the total levels of p62 as compared to single mutants and wild type mice. Fig. 6H is the zoomed view of HPS1/2 mice lung tissue immunostained for p62. In this image the AECII show a strong staining for p62 as compared to WT controls. To analyze HPS1/2 mice lungs at ultrastructural level, transmission electron microscopy (TEM) for these lungs was performed in collaboration with Profs. Ochs and Knudsen, Hannover. Immunogoldlabelling for LC3B showed a decrease in the amount of gold labelled LC3B from the limiting membrane of the lamellar bodies in HPS1/2 mice as compared to WT mice (Fig. 6F). An overall increase in the LC3B immunogoldlabelling was observed upon quantification in the AECII from HPS1/2 mice but this increase in LC3B was localized to the inside of the lumen of the lamellar bodies and not on the limiting membrane of the lamellar bodies, as indicated in table 1. WT mice on the other hand showed LC3B targeting to the limiting membrane of the lamellar bodies in addition to the lumen of the lamellar bodies.

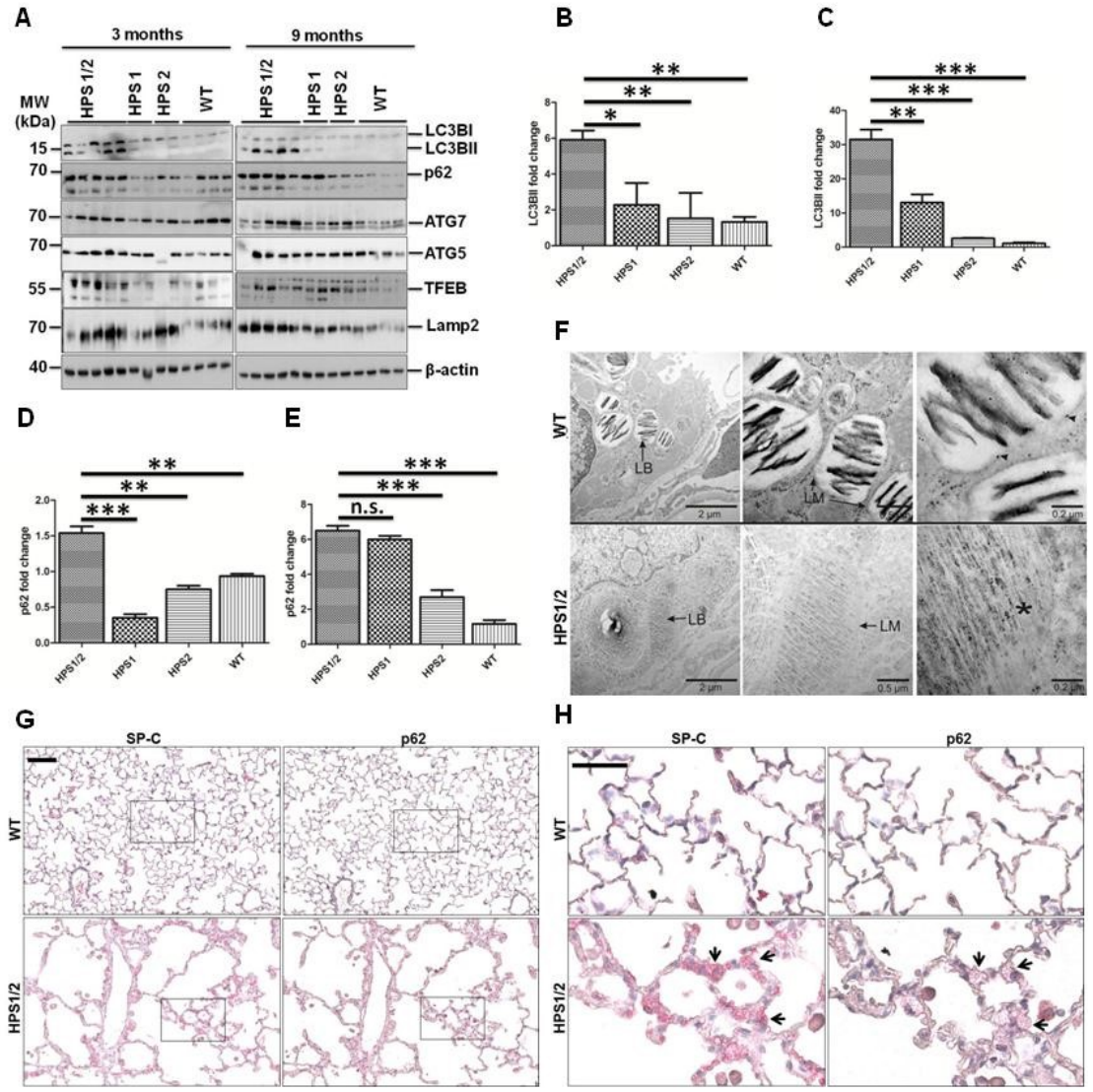

Fig. 6: Defective autophagy in HPS1/2 double mutant mice. A. Western blots from total lung homogenates of 3 months and 9 months old mice for autophagy marker proteins. **B & C**. Densitometric quantification for LC3BII/LC3BI ratio, 3 and 9 months, respectively. **D** & **E**. Densitometric quantification for p62 protein, 3 and 9 months, respectively. **F**. LC3B immunogoldlabelling on HPS1/2 and WT lung sections showing lamellar bodies within AECIIs. Arrowheads show LC3B gold labelling found on the limiting membrane of lamellar bodies in WT mice whereas asterix denotes LC3B gold labelling inside the lumen of the lamellar bodies in HPS1/2 mice. These images are representative images from three independent experiments. **G**. Immunohistochemical stainings for autophagy marker protein p62 (red) and AECII marker protein pro-SP-C (red) from HPS1/2 mice lungs. Magnification = X200 Scale bar = 100 µm **H**. Zoomed in view of AECIIs from the HPS1/2 mice lung section stained for LC3B and AECII marker protein SP-C. Magnification = X400 Scale bar = 50 µm for middle panel, 100 µm for the left and right panel. *-p<0.05, **-p<0.01, ***-p<0.001, n.s.: no significance. HPS1/2 mice: n=5, HPS1 mice: n=2, HPS2 mice: n=2, WT mice: n=4 mice. (Ahuja et al., 2016)

Compartment	RLI (control)	RLI (HPS1/2)	χ^2 (control)	χ^2 (HPS1/2)
LB	4.55	1.58	681.33	**393.64**
LM	3.69	0.38	131.63	**28.05**
mito	0.22	0	39.47	**47.03**
Nucleus	0.05	0.06	63.37	**86.91**
Cytosol	0.41	0.06	72.71	**458.18**
Total			**988.51**	**1013.81**

Table 1: LC3B immunogoldlabelling distribution pattern in HPS1/2 mice as compared to control mice. 50 AECIIs from 2 sections in HPS1/2 mice and 30 AECIIs from 2 sections in WT mice were randomized followed by counting the gold particles within different cellular compartments. Relative labelling index (RLI) and Chi-squared value (χ^2) were calculated for these gold particles. LB - interior of lamellar body, LM - limiting membrane, mito - mitochondria.

In addition to the mice data, we also performed immunostaining for LC3B and p62 on lung sections from HPS1 patient where we observed a weak staining for LC3B in the AECII and a strong staining for p62 in the AECII of the HPS1 patient lung section (Fig.7 & Fig.8). Taken together, these results so far show increased LC3BII together with an increase in the protein levels of autophagy substrate protein p62, indicating defective autophagy pathway under conditions of HPSIP.

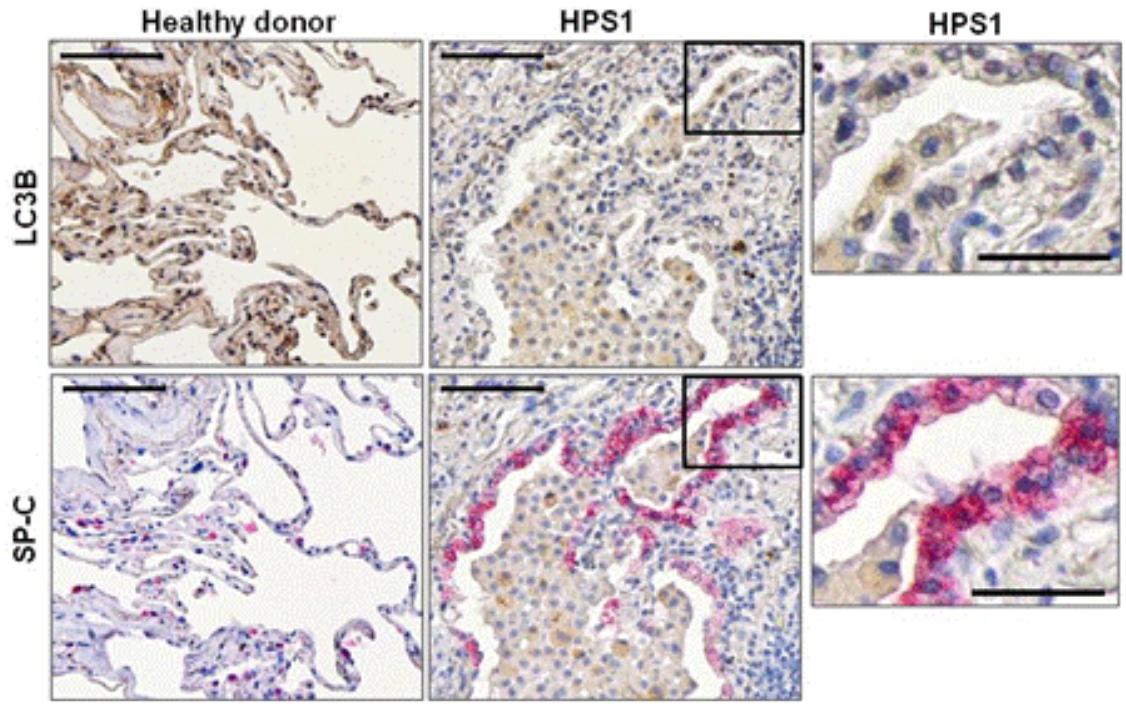

Fig. 7: Weak staining for LC3B in AECII of the lung from HPS1 patient. A. Immunostaining for LC3B (brown) and SP-C (red) was performed on the serial sections of the lung from one HPS1 patient. Maginification= X200, Scale bar = 100 µm. **B.** Higher magnification images from the same section. Magnification = X400, Scale bar = 50 µm. Representative images from three independent experiments. HPS1 lungs: n=1, Healthy donor: n=2. (Ahuja et al., 2016)

4.2 HPS1 knockdown in A549 cells results in a defective autophagy together with increase in apoptosis marker proteins.

Our results from patient and mouse samples suggested defective autophagy in HPSIP. To further confirm our results, we performed *in vitro* studies where knock down of HPS1 gene in A549 cells was performed followed by an assessment of the autophagy parameters. To establish the knockdown at mRNA level, we made a knockdown of HPS1 and harvested samples at 24 h and 48 h post knockdown. Scrambled, mock and untreated samples were all harvested at 48 h times point. After harvesting the cells, total mRNA was isolated from the cells and converted into cDNA. From this cDNA, semiquantitative PCR was performed for HPS1 using HPS1 (hu) specific primers. Knockdown of HPS1 was successful at mRNA level at both 24 h and 48 h, as can been seen from the representative image of an agarose gel in Fig. 9A and densitometry for the same in Fig. 9B.

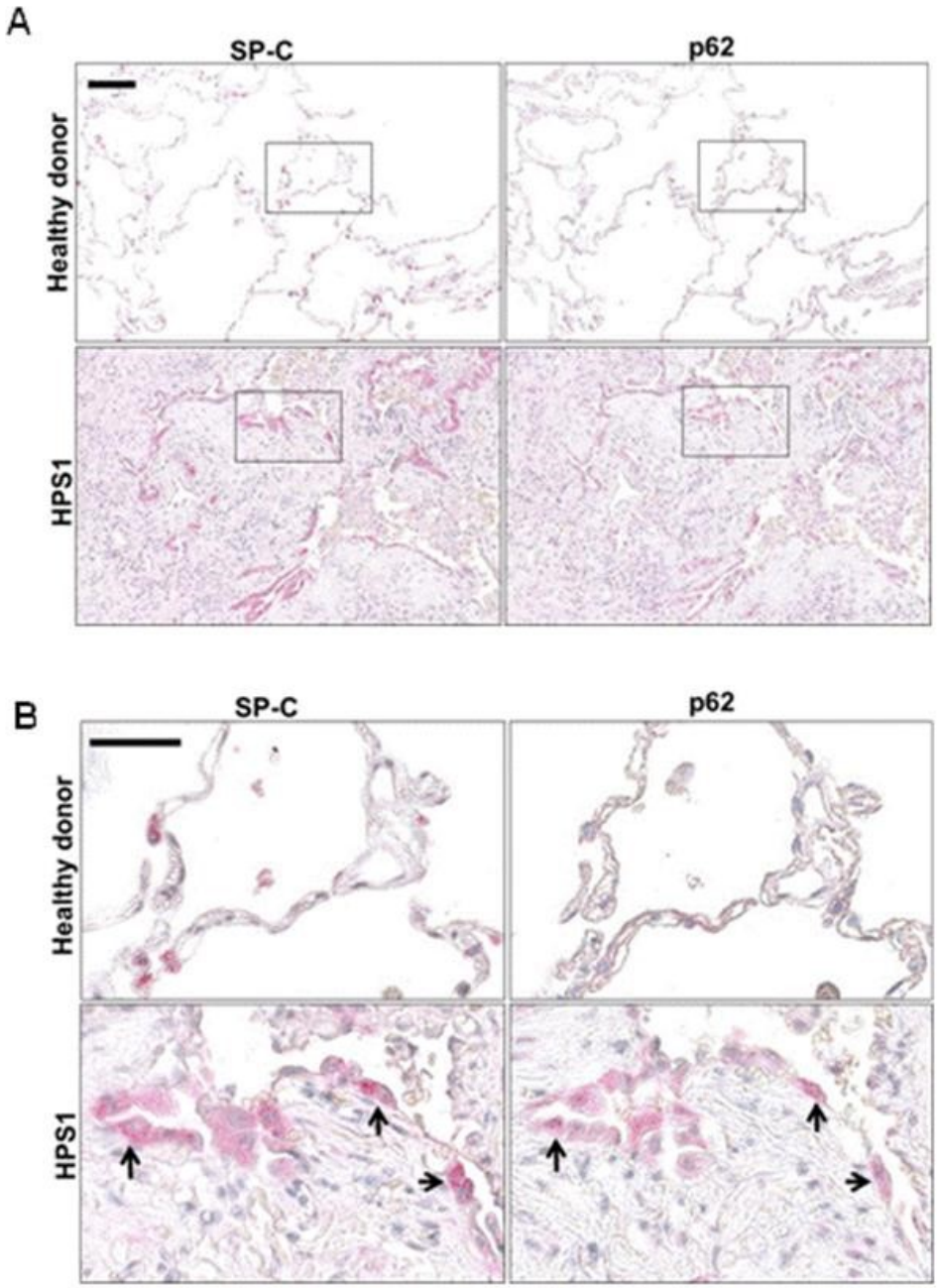

Fig. 8: **Increased staining for p62 in AECII of the lung from HPS1 patient. A**. Immunostaining for p62 (red) and SP-C (red) was performed on serial sections of the lung from one HPS1 patient. Magnification= X200, Scale bar = 100 µm. **B.** Higher magnification images from the same section. Arrows indicate AECIIs staining for p62. Magnification = X400, Scale bar = 50 µm. Representative images from three independent experiments. HPS1 lung: n=1, Healthy donor lung: n=2. (Ahuja et al., 2016)

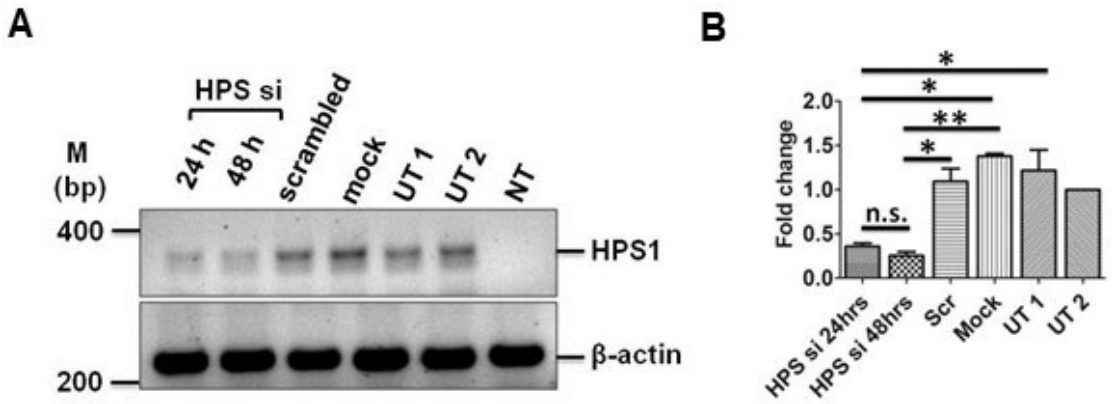

Fig. 9: **HPS1 knockdown in A549 cells. A**. Representative image of an agarose gel post semi-quantitative PCR analysing the expression levels of HPS1 (hu) mRNA post HPS1 knockdown for 24 h and 48 h of knockdown. Actin was used as loading control for the semiquantitative PCR. UT1 - untreated sample 1, UT2 - untreated sample 2, NT - no template sample. **B**. Densitometry for mRNA levels of HPS1 post siRNA treatment for HPS1 knockdown. *-p<0.05, **-p<0.01, ***-p<0.001. Results from three independent experiments. (Ahuja et al., 2016)

HPS1 siRNA transfected cells, scrambled transfected, mock transfected and untransfected cells were harvested 24 h post siRNA transfection and total protein were harvested from these cells. Total protein extracts were then used to run SDS-PAGE gels and immunoblotted for autophagy marker proteins LC3B and p62, as shown in Fig. 10A. In line with the *in vivo* data, our *in vitro* data showed an increase in LC3BII/LC3BI ratio together with an accumulation of p62 protein levels post HPS1 siRNA transfection, but not with scrambled or mock transfected and untransfected cells. This increase in p62 protein levels, together with an increase in the LC3BII/LC3BI ratio, is indicative of a block or a defect in autophagy pathway. Densitometric quantification of LC3BII/LC3BI ratio and p62 levels in Fig. 10B and 10C respectively followed by statistical evaluation showed significant results, according to which LC3BII and p62 protein levels were greatly upregulated in HPS1 siRNA transfected but not in scrambled or untransfected cells (Fig. 10A-C).

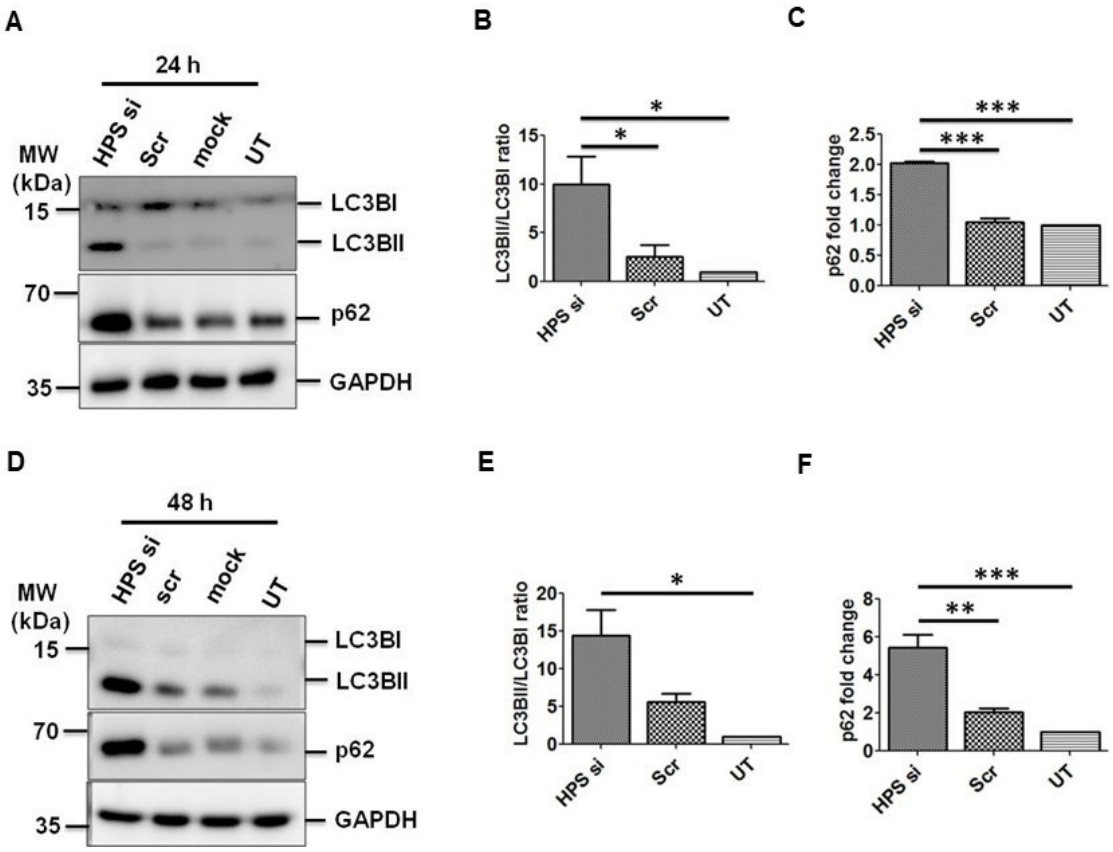

Fig. 10: **HPS1 knockdown in A549 cells results in defective autophagy causing accumulation of p62. A**. Representative western blot images for the autophagy marker proteins LC3B and p62 post HPS1 (hu) specific siRNA transfection for 24 h as compared to scrambled siRNA transfection(scr) and untransfected samples (UT). GAPDH was used as loading control for this experiment. **B** and **C**. Densitometries for LC3B and p62 post 24 h treatment with HPS1 (hu) siRNA as compared to scrambled and untransfected samples. **D**. Representative western blot images for the autophagy marker proteins LC3B and p62 post HPS1 specific siRNA transfection for 48 h as compared to scrambled and untransfected samples. GAPDH was used as a loading control. **E** and **F**. Densitometries for LC3B and p62 post 48 h treatment with HPS1 siRNA as compared to scrambled and untransfected samples. *-p<0.05, **-p<0.01, ***-p<0.001, n.s.: no significance. Results from three independent experiments. (Ahuja et al., 2016)

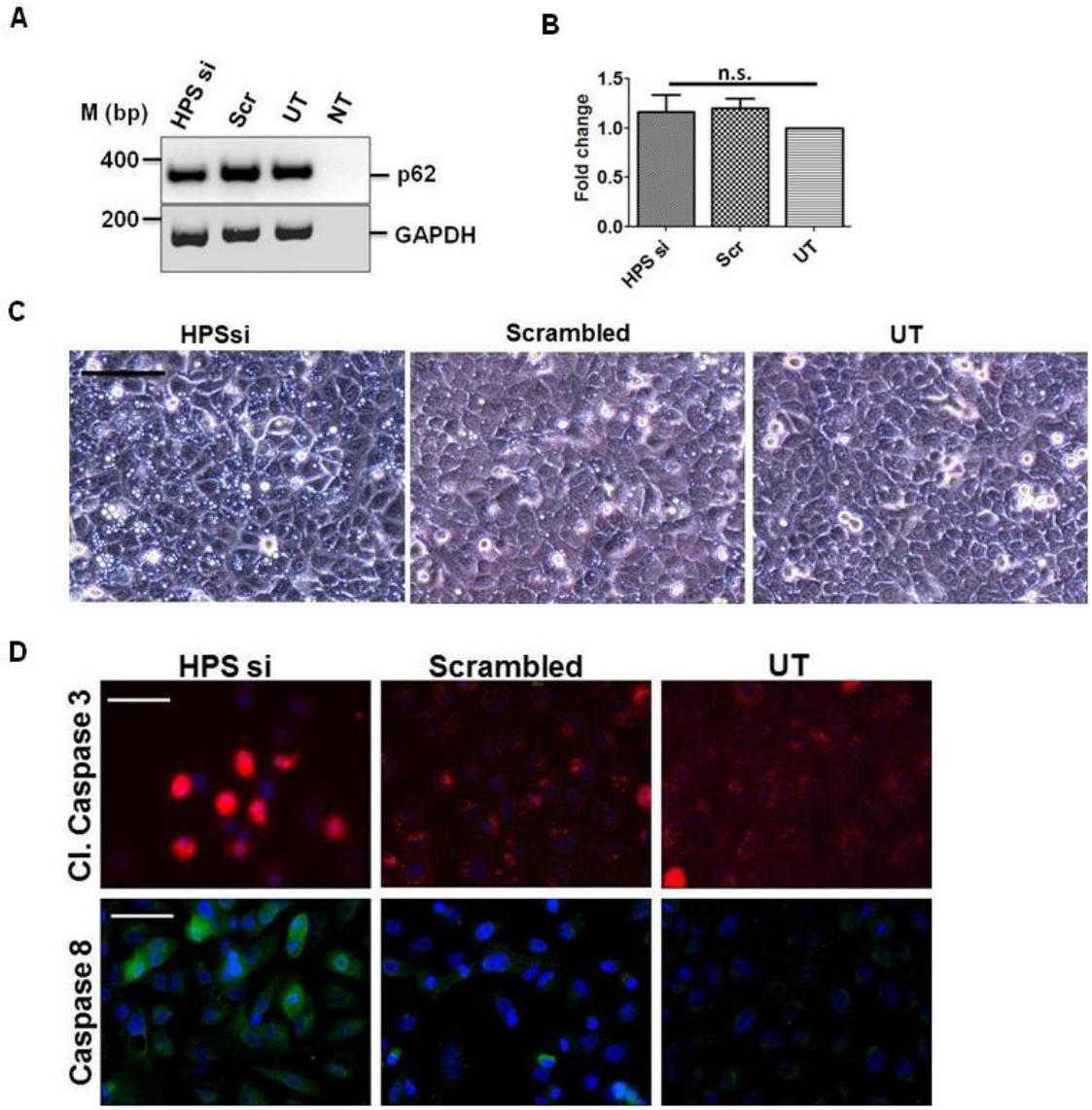

Fig. 11: **HPS1 knockdown induces vacuolar accumulation and activation of caspases in A549 cells. A**. Representative agarose gel image for semiquantitative PCR to show changes in mRNA levels of p62 post 24 h of HPS1 siRNA transfection as compared to scrambled and untransfected samples. GAPDH was used as a loading control. **B**. Densitometry for p62 mRNA levels post HPS1 siRNA transfection for 24 h as compared to scrambled siRNA and untransfected samples. **C**. Phase contrast microscope image for the A549 cells post 24 h of HPS1 (hu) knockdown as compared to scrambed or untransfected cells (UT). Scale bar = 100 µm. **D**. Representative immunofluorescence images for apoptosis markers cleaved caspase-3 (red) and caspase-8 (green) 24 h post HPS siRNA transfection as compared to scrambled and untransfected samples. Nuclei were stained using DAPI (blue). Scale bar = 10 µm. *-$p<0.05$, **-$p<0.01$, ***-$p<0.001$, n.s.: no significance. Results from three independent experiments. (Ahuja et al., 2016)

To understand if increase in p62 protein levels were caused by the autophagy defect or due to increased mRNA, we performed semi-quantitative PCR post HPS siRNA

transfection for 24 h using primers specific for p62 (hu). It can be seen in the representative agarose gel image shown in Fig. 11A and densitometry for the same shown in Fig. 11B that the mRNA levels for *p62* do not change in response to HPS1 siRNA transfection as compared to scrambled or untransfected cells. Taken together, this clearly shows that the knockdown of HPS1 in A549 cells results in a problem with autophagy pathway. In addition to western blot for autophagy marker proteins 24 h post HPS1 siRNA transfection, we also performed western blot for the autophagy marker proteins from the cells transfected with HPS1 siRNA for 48 h. As shown in the representative western blot image Fig. 10D and densitometry for the same shown in Fig. 10E and 10F, the protein levels for autophagy marker proteins LC3B and p62 remained high as compared to controls even after 48 h post transfection. From here on, for any further experiments regarding knockdown of HPS1, we chose to restrict our experiments to 24 h timepoint, since keeping the cells for 48 h post HPS1 siRNA transfection subjected the cells to a lot of stress and resulted in an increased cell death easily observed under the light microscope. A549 cells post HPS1 siRNA knockdown also showed an increase in vacuolar structures inside the cells when observed under phase contrast light microscope as shown in Fig. 11C. It is well established that autophagy inhibition can result in appearance of this kind of vacuolar structures in the cells. Well known autophagy inhibitor chloroquine (CQ) is a commonly known chemical which produces similar vacuolisation. Fig. 11D is a representative immunofluorescence image showing increase in the protein levels of pro-apoptotic proteins cleaved caspase-3 (red) and caspase-8 (green) post HPS1 siRNA transfection for 24 h as compared to scrambled transfected and untransfected cells.

4.3 Overexpressing LC3B reverts HPS1 knockdown induced accumulation of p62 in A549 cells.

The next step was to study autophagic flux post HPS1 siRNA transfection. According to the autophagy research guidelines, the most common way for studying autophagic flux is by using autophagy inhibitors, followed by the analysis of lipidation of LC3BII to confirm an increase or decrease in autophagy flux. The limitation that we faced in using autophagy inhibitors to study autophagy flux was that the cells, which were already under the stress of HPS1 siRNA transfection, were very sensitive to cell death induction. Therefore, using any kind of autophagy inhibitor would result in a very high cell death making it hard to study the flux. To overcome this problem, we used the GFP cleavage assay to study autophagy flux. Cells were transiently transfected with GFP-LC3B followed by HPS1 siRNA transfection for 24 h. As controls, cells were transfected with scrambled siRNA, mock siRNA and another set of cells was left untransfected. Empty

GFP vector was used as a control to show the free GFP band on western blot. As shown in Fig. 12A, a free GFP fragment was observed in response to HPS1 siRNA transfection in the cells which were pre-transfected with GFP-LC3B. A free GFP band was not observed in cells transfected with scrambled or mock siRNA or in untransfected cells. This result was a surprise to us, as we did not expect a free GFP band coming up post HPS1 siRNA transfection since results until now indicated a defective autophagy pathway in response to HPS1 knockdown. We also observed a loss of HPS1 knockdown induced vacuolar structures in the presence of GFP-LC3B (Fig. 12B).

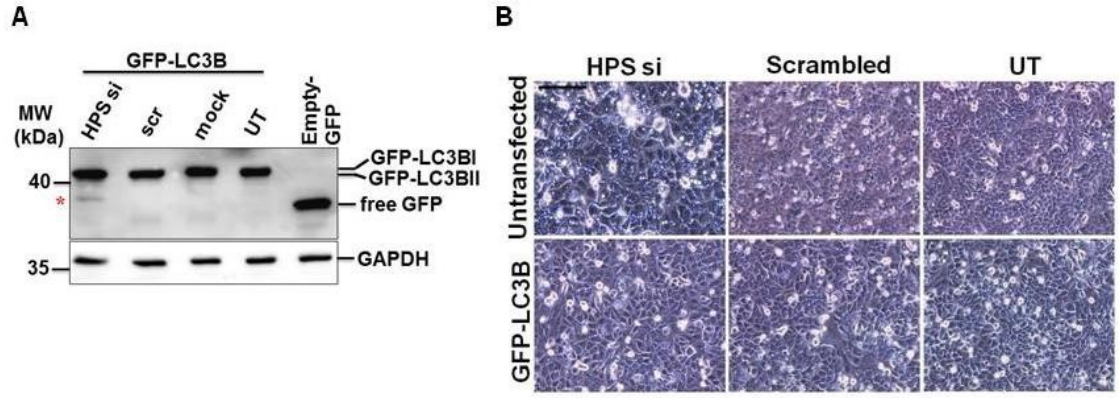

Fig. 12: Overexpressing LC3B reverts HPS1 knockdown induced vacuolarization in A549 cells. A. A549 cells were transfected with GFP-LC3B and then followed by HPS1 siRNA transfection for 24 h. Scrambled, mock and untransfected were used as controls against HPS1 siRNA transfection. Empty GFP transfection is a control against GFP-LC3B transfection. Immunoblot was performed using antibody against GFP. GAPDH was used as loading control. Asterisk (*) indicates free GFP fragment. **B**. Phase contrast images of the cells post HPS1 knockdown showing vacuolisation in the cells which were not transfected with GFP-LC3B but the cells which were transfected with GFP-LC3B, no vacuolar structures are visible. Scale bar = 100 µm. Results from three independent experiments. (Ahuja et al., 2016)

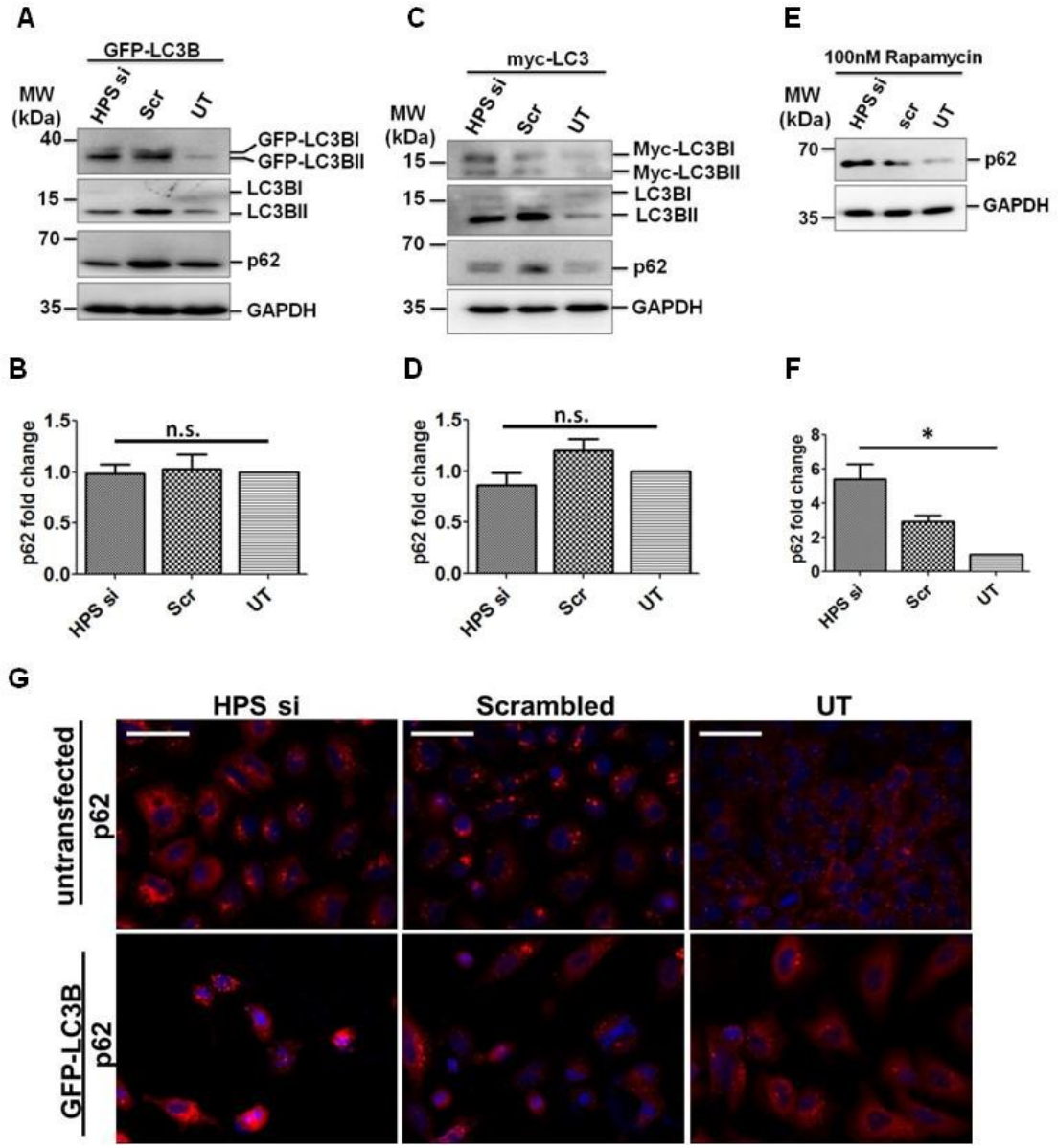

Fig. 13: Overexpressing LC3B revert HPS1 knockdown induced accumulation of p62 in A549 cells but treatment with rapamycin does not. A. Representative western blot image immunoblotted for the indicated autophagy proteins from the total cell lysates of the cells which were transfected with GFP-LC3B before knocking down HPS1. GAPDH was used as loading control. **B**. Densitometry for p62 levels post HPS1 knockdown in the cells transiently transfected with GFP-LC3B before knockdown. **C**. Representative western blot image immunoblotted for the indicated autophagy proteins from the total cell lysates of the cells which were transfected with myc-LC3B before knocking down HPS1. GAPDH was used as loading control. **D**. Densitometry for the p62 levels post HPS1 knockdown in the cells transiently transfected with myc-LC3B before knocking down HPS1. **E**. A549 cells were treated with 100 nM rapamycin before transfecting the cells with HPS1 siRNA. After 24 h of transfection, cell lysates from these treatments were immunoblotted for indicated autophagy proteins. GAPDH was used as loading control. **F**. Densitometry for p62 levels post HPS1 siRNA treatment in presence of 100 nM rapamycin. **G**.

Representative immunofluorescent images showing p62 (red) protein levels post HPS1 siRNA transfection as compared to scrambled transfected or untransfected cells with or without transient overexpression of GFP-LC3B. Scale bar = 10 μm. *-p<0.05, **-p<0.01, ***-p<0.001, n.s.: no significance. Results from three independent experiments. (Ahuja et al., 2016)

Further, we performed western blots for the autophagy marker proteins LC3B and p62 post HPS1 siRNA transfection in presence of GFP-LC3B. Representative western blots shown in Fig. 13A and densitometry for p62 levels shown in Fig. 13B showed us that the amount of p62 protein in HPS1 siRNA transfected cells did not show any accumulation as compared to scrambled transfected or untransfected in presence of transiently transfected GFP-LC3B. This data indicated to us that overexpressing GFP-LC3B in A549 cells before knocking down HPS1 protected the cells against the possible cytotoxic effects of p62 accumulation. To further examine if this effect was specific for LC3B overexpression, or if the effect was casually linked to the GFP tag, we repeated the experiment using myc-LC3B instead of GFP-LC3B. Fig. 13C and the densitometry for the experiment shown in Fig. 13D indicated that p62 protein levels did not change significantly after HPS1 siRNA transfection in the presence of transiently transfected myc-LC3B. Next, we asked if treatment with autophagy inducers, for example, rapamycin would have similar results like GFP/myc-LC3B with respect to p62 levels. To answer this question, we treated the cells with 100 nM rapamycin before transfecting the cells with HPS1 siRNA. 24 h post siRNA transfection, cells were harvested and subjected to immunoblotting for p62. As shown in Fig. 13E & 13F, rapamycin treatment did not protect cells against HPS1 knockdown induced p62 accumulation. We next performed immunofluorescence for p62 in the cells subjected to HPS1 knockdown with or without GFP-LC3B. As shown in Fig. 13G, reduced fluorescence signal for p62 was observed in response to HPS1 knockdown in the presence of GFP-LC3B as compared to HPS1 knockdown alone, supporting our previous observations. These results clearly show us that the overexpression of exogenous LC3B protects A549 cells against accumulation of p62 in response to HPS1 knockdown.

4.4 HPS1 knockdown results in loss of autophagolysosomes formation but overexpression of LC3B restores the formation of autophagolysosomes in these cells.

Our data so far indicates that HPS1 knockdown induces p62 accumulation in otherwise untreated cells, but not in cells overexpressing LC3B. We hence asked how the overexpression of LC3B helps against p62 accumulation in the absence of HPS1 protein. To answer this question, we further analyzed the formation of autophagolysosomes post HPS1 knockdown in the presence or absence of transiently overexpressed LC3B. As

shown in Fig 14A, co-immunofluorescence analysis for LC3B (red, Fig. 14A, upper panel) and LAMP1 (green, Fig. 14A, second panel) showed no colocalization for LC3B and LAMP1 as is evident from the lack of yellow spots in the overlay panel (Fig. 14A, third panel) indicating there is a lack of autophagolysosomes formation. On the other hand, scrambled and untransfected cells did show LC3B and LAMP1 colocalization. Overexposed images (Fig. 14A, fourth panel) revealed similar readouts. Colocalization for LC3B and LAMP1 was quantified using ImageJ plugin "JACOP" where Pearson's coefficient was calculated using Coste's automatic threshold method. Details about this plugin have been provided in the material and methods section. Densitometry for LC3B and LAMP1 colocalization based on Pearson's coefficient is shown in Fig. 14B, where a clear and significant decrease in colocalization is visible in HPS1 siRNA transfected cells as compared to scrambled and untransfected cells. In addition to that, we also quantified the colocalization signals of LC3B and DAPI (nucleus) using the same method to calculate Pearson's coefficient. Densitometry data shown in Fig. 14C clearly shows a significantly increased nuclear localization of LC3B in response to HPS1 siRNA versus scrambled siRNA or non-transfected cells. Taken together these results indicated to us that a knockdown of HPS1 in A549 cells results in nuclear trapping of endogenous LC3B which explains the lack of autophagolysosomes post HPS1 siRNA transfection and the accumulation of p62 protein.

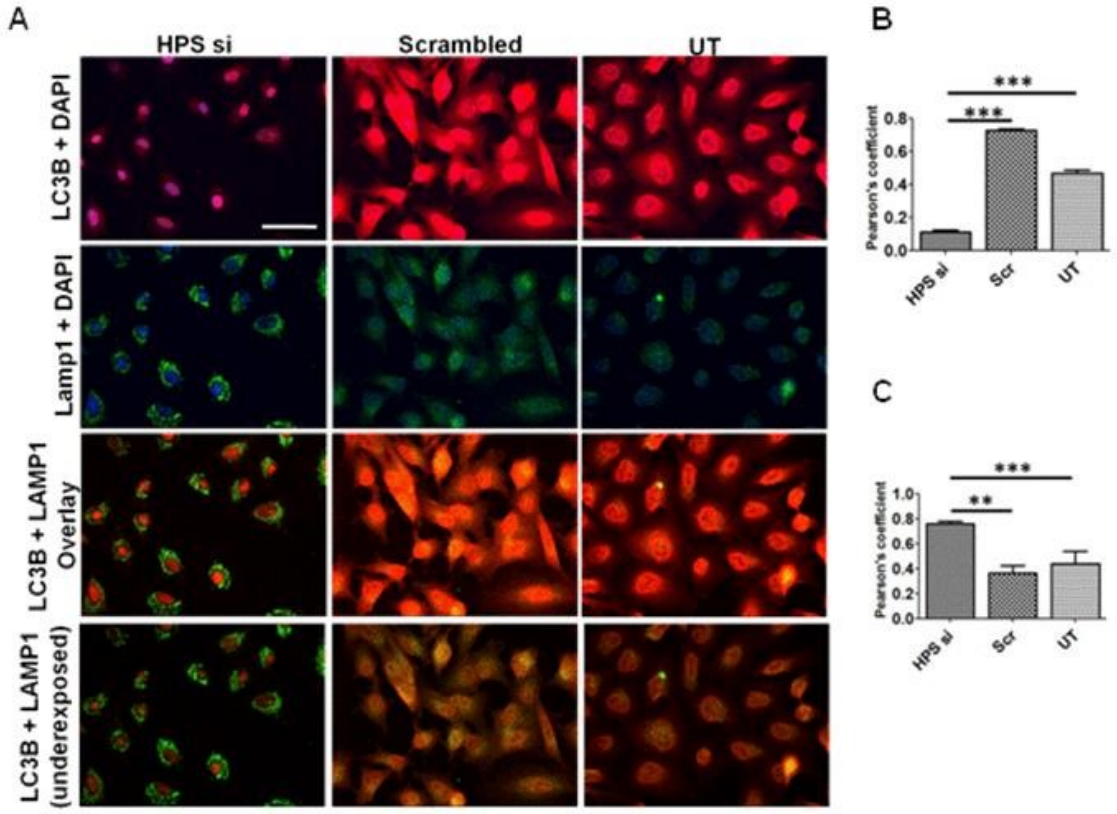

Fig. 14: HPS1 knockdown results in loss of autophagolysosomes formation. A. A549 cells were transfected with HPS1 siRNA, scrambled siRNA or left untreated (UT). 24 h post transfection cells were fixed and subjected to immunofluorescence protocol for the endogenous LC3B (red) and LAMP1 (green) Scale bar = 10 μm. **B**. Densitometry for endogenous LC3B and LAMP1 colocalization post HPS1 knockdown for 24 h. **C**. Densitometry for endogenous LC3B and DAPI (nucleus) colocalization post HPS1 knockdown for 24 h. *-p<0.05, **-p<0.01, ***-p<0.001, n.s.: no significance. Results from three independent experiments. (Ahuja et al., 2016)

To answer whether any additional LC3B expression promotes autophagy under conditions of HPS1 knockdown, we performed an additional immunofluorescence experiment, where A549 cells were transfected with GFP-LC3B, followed by HPS1 siRNA or scrambled siRNA transfection for 24 h. Afterwards, cells were fixed and subjected to the immunofluorescence protocol for GFP-LC3B (green) and LAMP1 (red). As was expected, GFP-LC3B did show cytosolic presence and colocalized with LAMP1, being visible in the representative immunofluorescence image in Fig. 15A as yellow spots in the overlay panel. Densitometry using the same method of calculating Pearson's coefficient as explained earlier clearly showed no difference between colocalization signal, Fig. 15B for GFP-LC3B and LAMP1 for HPS1 knockdown samples as compared to scrambled and untransfected cells. Fig. 15C shows the densitometric calculation for the colocalization of GFP-LC3B and DAPI (nucleus) not indicating any kind of GFP-LC3B colocalizing with DAPI. Taken together, these results clearly indicate that upon HPS1 knockdown, additional transfection of cells with exogenous LC3B protects against p62 accumulation.

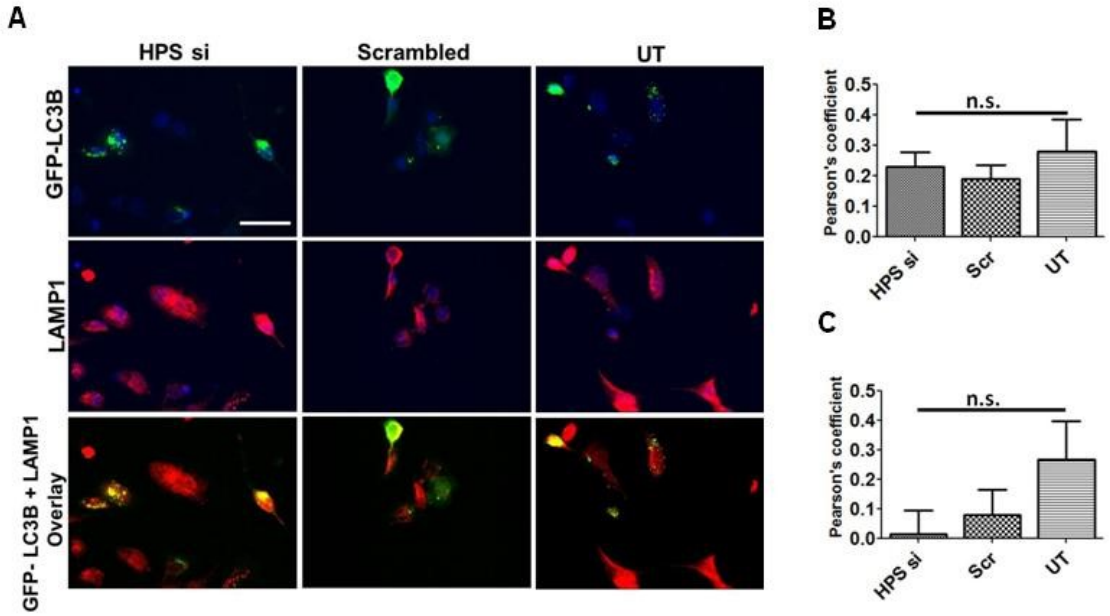

Fig. 15: Overexpression of LC3B restores the formation of autophagolysosomes in A549 cells post HPS1 knockdown. A. A549 cells were transiently transfected with exogenous GFP-LC3B followed by HPS1 siRNA transfection. Scrambled siRNA transfected and untransfected cells were used as controls. 24 h post siRNA transfection, cells were fixed and subjected to immunofluorescence for exogenous GFP-LC3B (green) and endogenous LAMP1 (red). Scale bar = 10 µm. **B**. Densitometry for exogenous GFP-LC3B and endogenous LAMP1 colocalization HPS1 knockdown for 24 h. **C**. Densitometry for exogenous GFP-LC3B and DAPI (nucleus) 24 h post siRNA transfection. *-p<0.05, **-p<0.01, ***-p<0.001, n.s.: no significance. (Ahuja et al., 2016)

4.5 Proposed mechanism for defective autophagy under HPS1 knockdown conditions

Under healthy conditions, lysosomes fuse with autophagosomes to degrade their toxic cargo with the help of cellular p62 thereby regulating the levels of cellular waste (Fig. 16, left panel). Under conditions of HPS1 knockdown, this fusion between lysosomes and autophagosomes seems to be inhibited. This inhibition then results in toxic accumulation of cellular waste together with increased levels of p62 (Fig. 16, middle panel). Upon exogenous LC3B overexpression, this fusion between autophagosomes and lysosomes is restored, thereby regulating the levels of p62 in the cells and preventing the buildup of toxic cargo inside the cells (Fig 16, right panel).

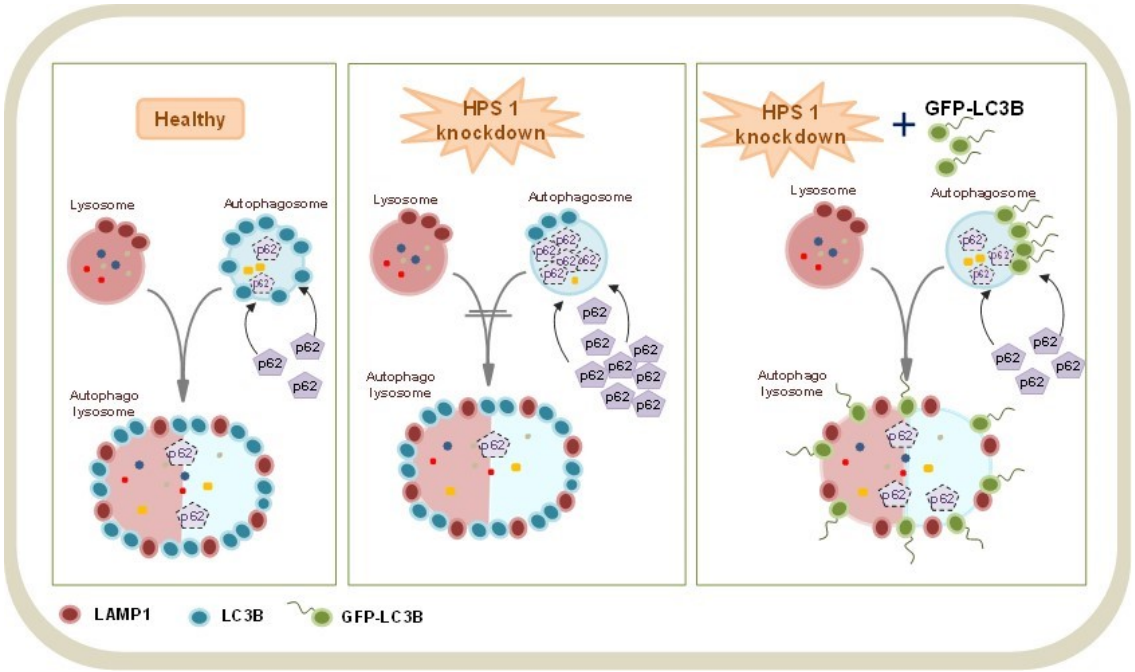

Fig. 16: Proposed mechanism for HPS1 knockdown induced autophagy inhibition and exogenous LC3B mediated autophagy rescue in A549 cells. (Ahuja et al., 2016)

4.6 Bleomycin treated mice show increase in autophagy marker protein levels belonging to both macroautophagy and chaperone mediated autophagy pathways.

Our next aim is to analyze the regulation of autophagy in bleomycin model of lung fibrosis. Age matched C57BL/6 mice were treated with bleomycin and sacrificed at days 7, 14, 21 or 28 days. Saline treated mice were used as controls and lungs from these mice were harvested at day 28. Shock frozen lungs were harvested and used to prepare total protein lung homogenate for performing western blots or fixed and used to prepare serial sections for immunostainings. As shown in Fig. 17A, western blots for key autophagy marker proteins such as LC3B, p62, TFEB, Atg5-Atg12 complex and Atg7 were performed. Densitometric quantifications for LC3B, p62 and beclin-1 are shown in Fig 17B, 17C and 17D, respectively. A significant increase in the autophagy marker proteins was observed in the lung homogenates at different time points of bleomycin treatment as compared to the vehicle treated controls. The profound increase in LC3BII levels in bleomycin vs. vehicle treated lungs, reflecting increased lipidation of LC3B, indicated possible increase in the number of autophagosomes. In addition, another key autophagy protein, transcription factor EB (TFEB), which is responsible for lysosomal biogenesis and referred to as master regulator of autophagy, showed a significant increase in bleomycin as compared to vehicle treated mice. Other autophagy proteins involved at different stages of autophagy, such as Atg7 and Atg5-Atg12 complex, were also found to be increased on protein level as compared to controls. However, SQSTM1/p62 was also found to be increased in bleomycin treated mice as compared to vehicle treated mice lungs. As indicated in the introduction and in the HPS results chapter, an increase in p62 protein levels together with an increase in autophagy proteins would, however, be considered as a sign for a decreased or defective autophagy.

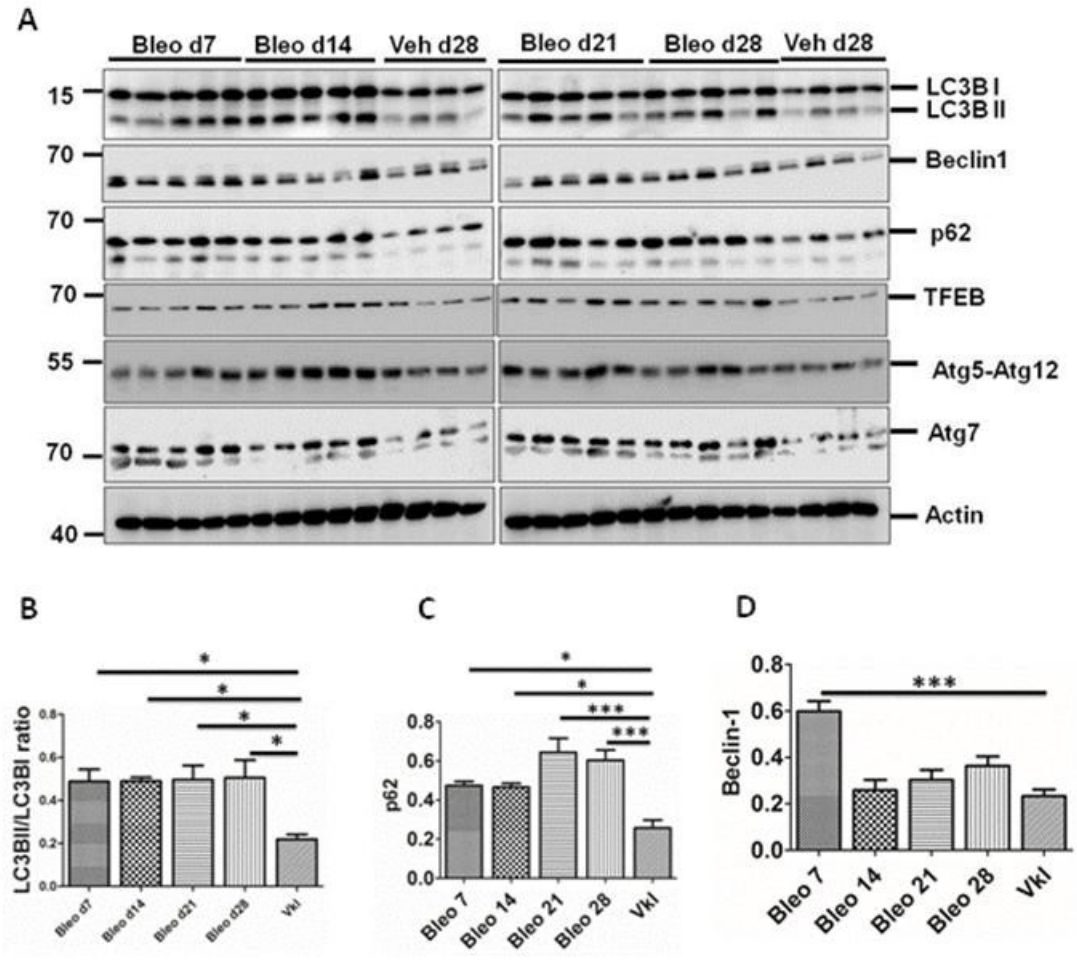

Fig. 17: Bleomycin treated mice show increase in autophagy marker protein levels belonging to macroautohphagy pathway on western blots. A. Lungs were harvested from bleomycin treated mice and total protein was harvested from these lungs and used to perform western blots for key macroautophagy marker proteins. Representative western blot image showing differences between different treatment groups against controls for the indicated macroautophagy marker proteins. Actin was used as loading control. **B**. Densitometry for LC3BII/LC3BI protein levels in bleomycin treated mice lungs. **C**. Densitometry for p62 protein levels in bleomycin treated mice lungs. **D**. Densitometry for Beclin-1 in bleomycin treated mice lungs. *-p<0.05, **-p<0.01, ***-p<0.001, n.s.: no significance. Bleomycin D7, D14, D21, D28 lungs: n=15, Vehicle D28 lungs: n=12.

In addition to western blots, immunostainings were performed on the lung sections for macroautophagy marker proteins LC3B and p62. An overall increased staining for LC3B and p62 was observed in AECIIs (stained by antibody against SP-C), indicating accumulation of both LC3B and p62 in bleomycin, but not in vehicle treated mice in serial sections (Fig. 18). Taken together these results corroborate with each other and support the conclusion that bleomycin treatment results in an increase in LC3B and p62 in the lungs of these mice and their accumulation in the AECII.

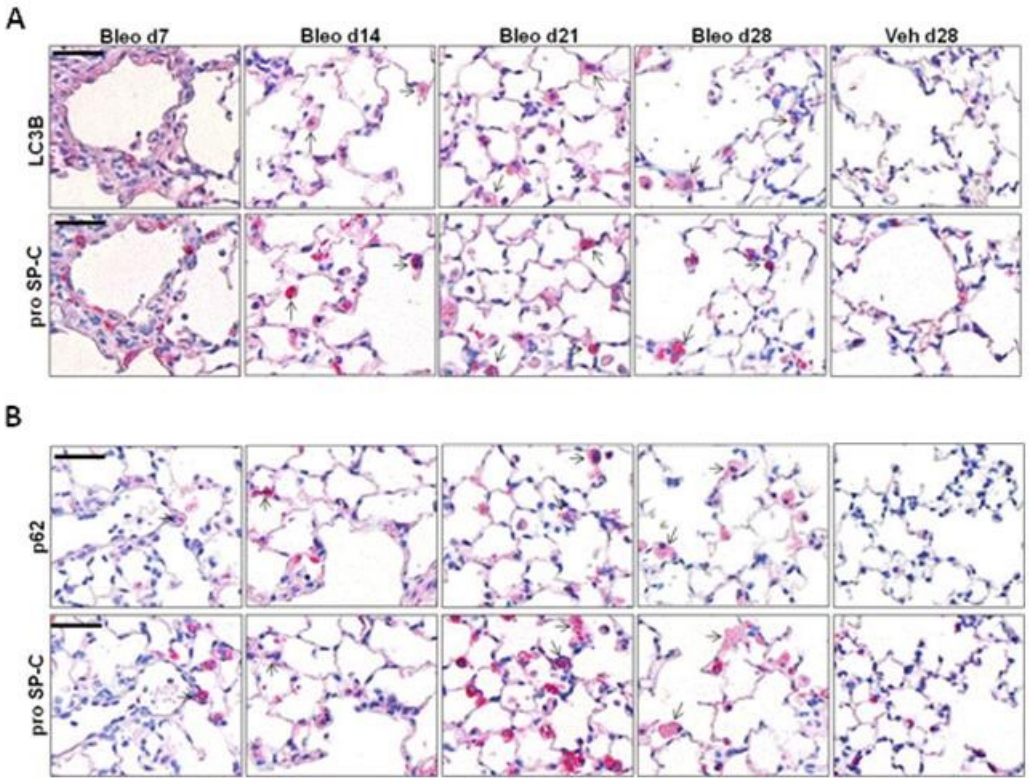

Fig. 18: Bleomycin treated mice show increase in autophagy marker protein levels belonging to macroautophagy pathway on immunohistochemistry. A & **B**. Bleomycin treated mice were sacrificed at indicated time points and lungs were harvested from these mice. Serial sections were prepared from these lungs and stained for indicated autophagy marker proteins LC3B, p62 and AECII marker protein SP-C. Magnification = X200, scale bar = 100 μm. Bleomycin D7, D14, D21, D28 lungs: n=15, Vehicle D28 lungs: n=12.

4.7 Bleomycin treated MLE12 cells do not show autophagy induction.

To further test our results from the mouse model, we next performed *in vitro* studies on MLE12 cells treated with bleomycin. We treated cells with bleomycin dose ranging was from 10 mU to 200 mU. MLE12 cells were treated with bleomycin for 4 h before the cells were harvested and total protein or total mRNA was isolated from them depending upon the experiment planned. Cells were chosen to be treated for 4 h due to the treatment limitations of the autophagy inhibitors (bafilomycin, choloroquine) which will later be used for the autophagy flux assays. Bleomycin treatment of MLE12 cells at the indicated dosages failed to produce any siginificant difference in LC3BII and p62 levels at both protein and mRNA levels as shown in Fig. 19A-F.

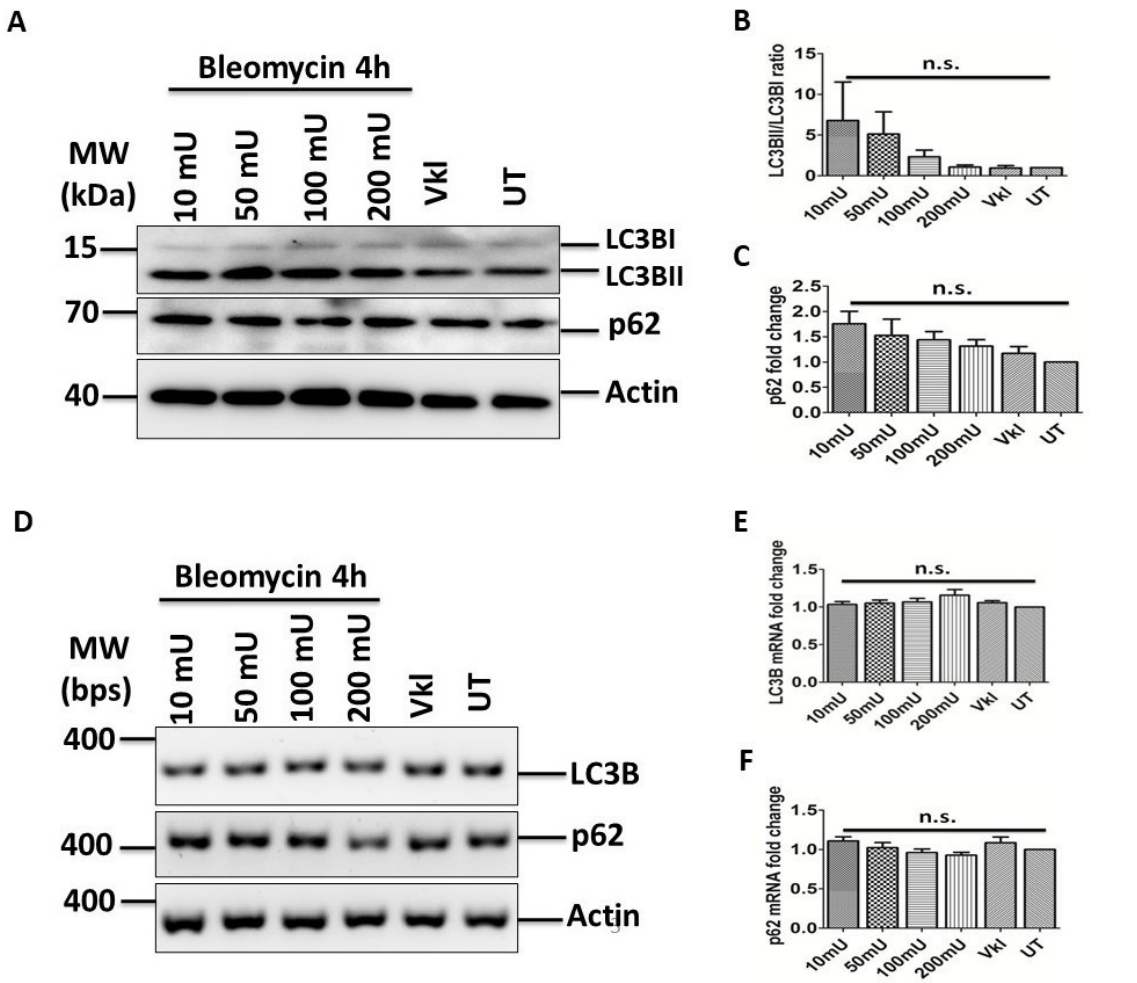

Fig. 19: Bleomycin treated MLE12 cells do not show induction of autophagy at higher doses of bleomycin. A. Representative western blot image for the key autophagy proteins in response to cells treated with the indicated dosage of bleomycin for 4 h. Actin was used as loading control. **B** & **C**. Densitometry for the protein levels of autophagy marker proteins LC3B and p62 in response to the indicated dosage of bleomycin treatment for 4 h. **D**. Representative agarose gel image for the semiquantitative PCR performed for mRNA level changes of autophagy marker proteins in response to bleomycin treatment for 4 h with the indicated bleomycin dosage. Actin was used as loading control. **E** & **F**. Densitometric quantification for the changes in the mRNA levels of the autophagy marker proteins LC3B and p62 in response to bleomycin treatment for 4 h. *-p<0.05, **-p<0.01, ***-p<0.001, n.s.: no significance.

4.8 Bleomycin treatment induces activation of caspase-3 as early as 4 h post treatment and induces swelling in MLE12 cells upon longer exposure.

Treating cells with bleomycin is known to cause increased toxicity which may result due to oxidative stress, ER stress and DNA damage. Here, we studied the effect of bleomycin on the pro-apoptotic protein cleaved caspase-3 in response to the treatment with bleomycin. We treated MLE12 cells with different doses of bleomycin for 4 h, harvested

the cells and prepared total protein lysate. This total protein lysate was used to analyze changes in the protein levels of cleaved caspase-3 in response to the bleomycin treatment. Representative western blot image shown in Fig. 20A shows a dose dependent increase in the cleavage products of caspase-3 with 200 mU of bleomycin causing the highest increase in the amount of cleaved caspase-3 as compared to other doses and controls. Densitometric quantification for the cleaved caspase-3 levels, Fig. 20B confirmed this result. Another interesting observation made under light microscope post bleomycin treatment is a characteristic increase in the size of MLE12 cells (Fig. 20C). This swelling of MLE12 cells was observed when cells were incubated with bleomycin for 24 h with a gradual increase in the amount of cell death as is visible from the representative phase contrast image but not when the cells were incubated for a shorter period. The exact reason for this swelling observed in MLE12 cells post bleomycin treatment for longer time periods is a subject of further analysis.

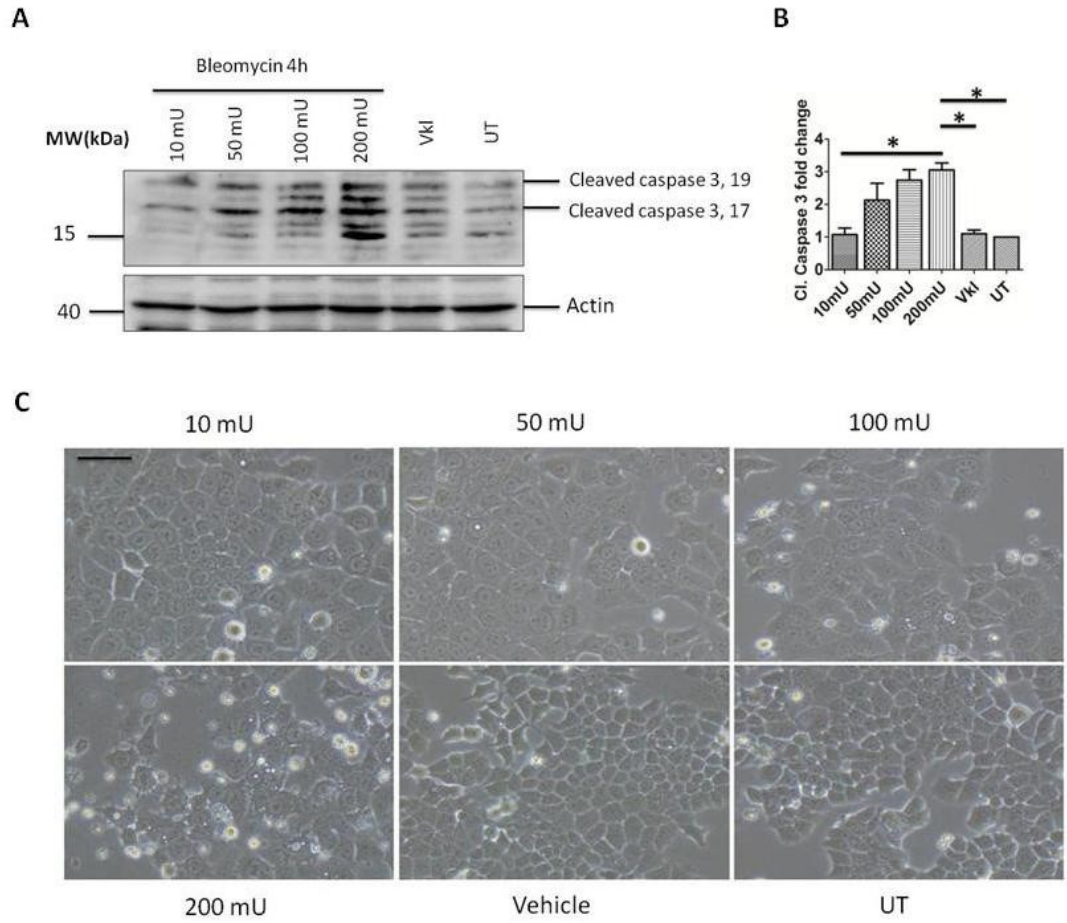

Fig. 20: Bleomycin treatment induces activation of caspase-3 as early as 4 h post treatment and induces swelling in MLE12 cells upon longer exposure. A. Representative western blot image for changes in cleaved caspase-3 (19 kDa & 17 kDa forms) levels in response to treatment with indicated dosages of bleomycin for 4 h in MLE12 cells. Actin was used as loading control. **B.**

Densitometry for the cleaved caspase-3 protein levels post bleomycin treatment with indicated dosages for 4 h. *-p<0.05, **-p<0.01, ***-p<0.001, n.s.: no significance. **C.** Representative phase contrast image of the bleomycin challenged MLE12 cells treated with indicated dosages for 4 h. Scale bar = 100 µm.

4.9 Bleomycin treatment does not increase autophagy flux.

To study autophagy flux, we pretreated the cells with well-known autophagy inhibitors chloroquine and bafilomycin for 1 h before treating the cells with bleomycin at the indicated dosages of 10 mU, 50 mU and 100 mU (Fig. 21, 22 and 23, respectively). Readouts of this experiment clearly showed that LC3BII levels did not increase when cells were treated either with 10 mU or 50 mU of bleomycin in presence of autophagy inhibitor as compared to the cells which were treated with autophagy inhibitor alone (Fig. 21, 22 and 23, respectively). Densitometric quantification also did not reveal any significant increase in autophagy flux due to bleomycin treatment at all three concentrations in the presence of inhibitors, chloroquine and bafilomycin (B & C panels of Fig. 21, 22 and 23, respectively). Taken together, based on the unaltered levels of LC3BII levels in the presence of lysosomal/autophagy inhibitors, it may be stated that bleomycin is not an autophagy inducer but on contrary it is an autophagy inhibitor and the increase in levels of LC3BII that was observed in bleomycin treated mice was not due to induction of autophagy pathway but due to inhibition of autophagic flux.

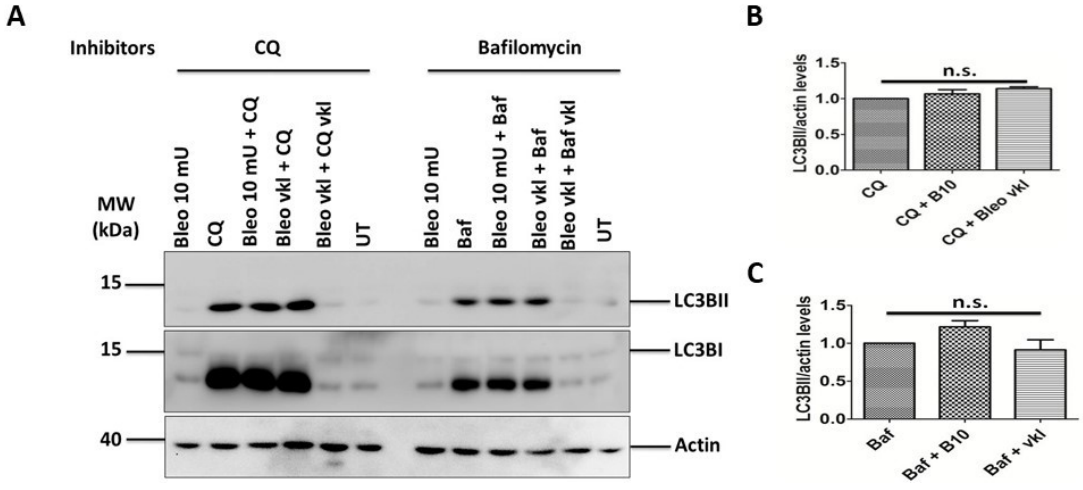

Fig. 21: Bleomycin treatment does not increase autophagy flux at 10 mU dosage. A. Representative western blot image for flux analysis in MLE12 cells treated with 10 mU bleomycin for 4 h in presence of autophagy inhibitors chloroquine (CQ) and bafilomycin (Baf) showing LC3BII levels in reponse to treatment. Actin was used as loading control. **B** & **C**. Densitometric quantification for LC3BII levels in response to 10 mU bleomycin treatment for 4 h in presence of autophagy inhibitors. *-p<0.05, **-p<0.01, ***-p<0.001, n.s.: no significance.

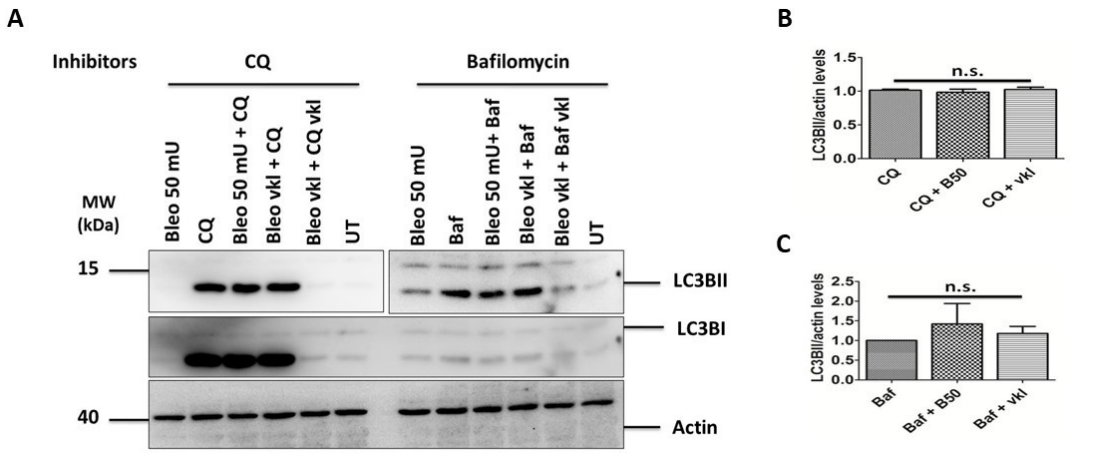

Fig. 22: Bleomycin treatment does not increase autophagy flux at 50 mU dosage. A. Representative western blot image for flux analysis in MLE12 cells treated with 50 mU bleomycin for 4 h in presence of autophagy inhibitors chloroquine (CQ) and bafilomycin (Baf) showing LC3BII levels in reponse to treatment. Actin was used as loading control. **B** & **C**. Densitometric quantification for LC3BII levels in response to 50 mU bleomycin treatment for 4 h in presence of autophagy inhibitors. *-p<0.05, **-p<0.01, ***-p<0.001, n.s.: no significance.

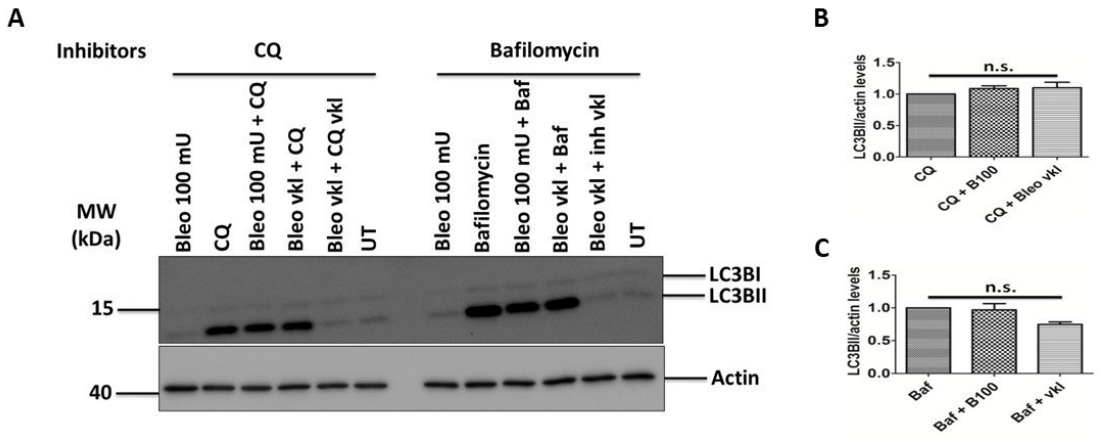

Fig. 23: Bleomycin treatment does not increase autophagy flux at 100 mU dosage. A. Representative western blot image for flux analysis in MLE12 cells treated with 100 mU bleomycin for 4 h in presence of autophagy inhibitors chloroquine (CQ) and bafilomycin (Baf) showing LC3BII levels in reponse to treatment. Actin was used as loading control. **B** & **C**. Densitometric quantification for LC3BII levels in response to 100 mU bleomycin treatment for 4 h in presence of autophagy inhibitors. *-p<0.05, **-p<0.01, ***-p<0.001, n.s.: no significance.

4.10 Bleomycin treatment does not increase formation of autophagolysosomes.

Since it is established from our previous results that bleomycin does not induce autophagy flux in MLE12 cells, we then asked if it influences the formation of autophagolysosomes. To answer this, we treated MLE12 cells with bleomycin at different concentrations of 10 mU and 50 mU for 4 h. Following bleomycin treatment, cells were

fixed and subjected to immunofluorescence protocol for colocalization study of LC3B (red) and LAMP1 (green) followed by quantification of the fluorescence signal of these two proteins using ImageJ plugin "JACOP" to calculate Pearson's coefficient of colocalization. As shown in Fig. 24, treatment of MLE12 cells with both 10 mU & 100 mU of bleomycin did not result in an increase in the number of autophagolysosomes as compared to the vehicle treated or untreated controls. An increase in the number of autophagolysosomes in response to bleomycin treatment would have suggested the protective role of autophagy but a complete lack of any kind of increase in autophagolysosomes from the autophagic flux assay studies indicate that autophagy is inhibited by bleomycin.

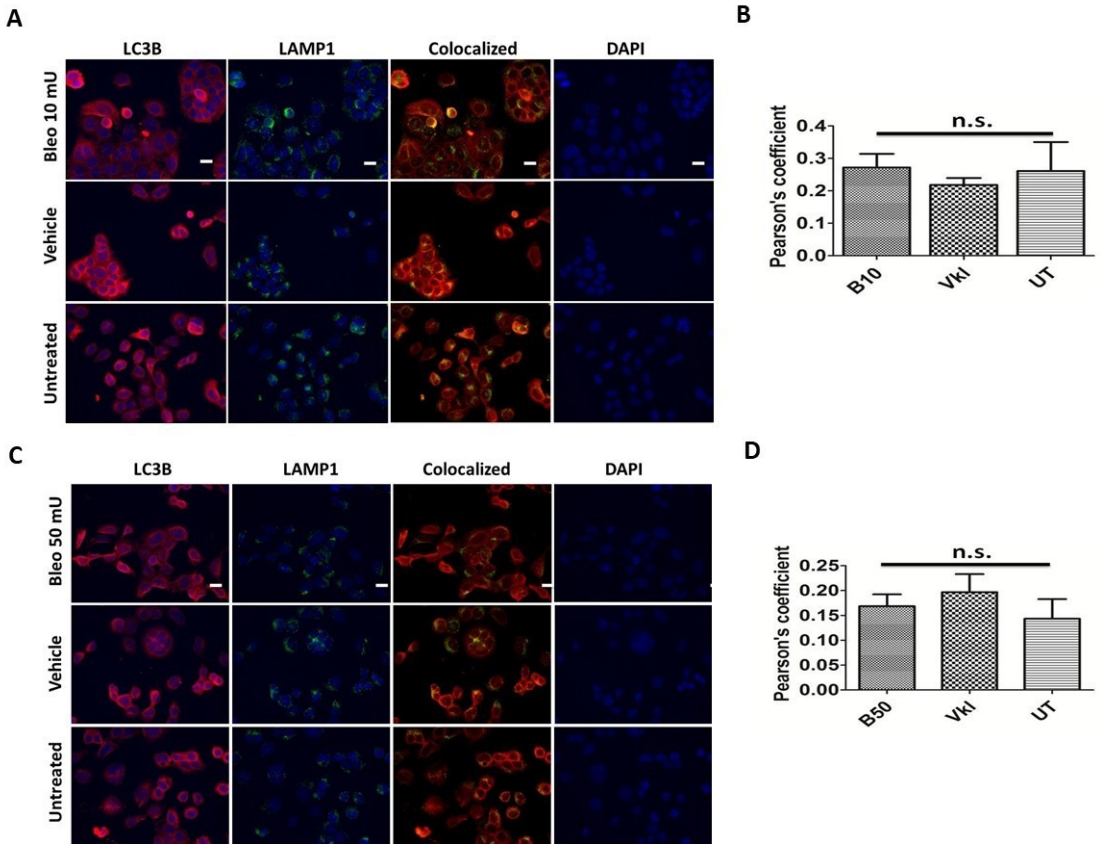

Fig. 24: Bleomycin treatment does not increase formation of autophagolysosomes. A. Representative immunofluorescent images for LC3B (red) and LAMP1 (green) showing formation of autophagosomes in response to 10 mU bleomycin treatment as compared to vehicle treated or untreated cells. DAPI (blue) shows nuclear staining. **B**. Densitometric quantification for the colocalization of the immunofluorescent signals from LC3B and LAMP1 based on calculation of Pearson's coefficient showing changes in formation of autophagosomes in response to 10 mU bleomycin treatment as compared to vehicle treated and untreated cells. **C**. Representative immunofluorescent images for LC3B (red) and LAMP1 (green) showing formation of autophagosomes in response to 50 mU bleomycin treatment as compared to vehicle treated or

untreated cells. DAPI (blue) shows nuclear staining. **D**. Densitometric quantification for the colocalization of the immunofluorescent signals from LC3B and LAMP1 based on calculation of Pearson's coefficient showing changes in formation of autophagosomes in response to 50 mU bleomycin treatment as compared to vehicle treated and untreated cells. *-p<0.05, **-p<0.01, ***-p<0.001, n.s.: no significance.

4.11 Overexpressing TFEB before treating cells with bleomycin (10 & 50 mU) does not increase autophagic flux.

Transcription factor EB (TFEB), as indicated before, is a 'master regulator' of autophagy genes. Hence as an attempt to induce autophagy following bleomycin treatment, we overexpressed GFP tagged TFEB in MLE12 cells before treating them with bleomycin. Cells transfected with GFP-TFEB (Fig. 25) showed a protein band at approximately 100 kDa when probed with antibodies against both GFP and TFEB at the same location but not when the cells were transfected with GFP alone or in untransfected cells. This confirmed the overexpression of GFP-TFEB. To test the effect of GFP-TFEB overexpression on autophagy flux, we pre-treated the cells transiently overexpressing GFP-TFEB with autophagy inhibitors chloroquine and bafilomycin for 1 h followed by bleomycin treatment at two different dosages (10 mU, Fig. 26A and 50 mU, Fig. 26D) for 4 h. Cells were then harvested, and total protein was isolated from these different treatment groups. This protein lysate was used to perform western blotting for autophagy marker proteins LC3B and p62. In addition to autophagy marker proteins, immunoblots were also performed for GFP and TFEB to confirm that all groups of cells used in this experiment were positive for GFP-TFEB. At both bleomycin doses (10 mU and 50 mU), autophagy was not increased as indicated by unaltered LC3BII levels upon overexpression of GFP-TFEB followed by bleomycin treatment (Fig. 26B, 26C, 26E, and 26F). This clearly indicates that the bleomycin mediated block in autophagy is not restored by exogenous TFEB *in vitro* indicating that bleomycin is a strong inhibitor of autophagy.

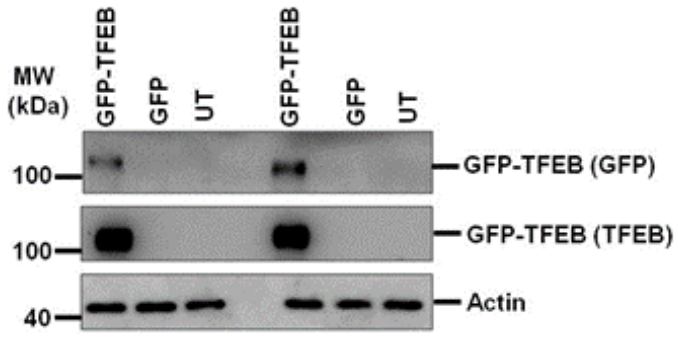

Fig. 25: MLE12 cells overexpressing GFP-TFEB. Representative western blot showing overexpression of GFP-TFEB in cells transiently transfected with plasmid coding for GFP-TFEB, GFP (empty vector) or untransfected cells. Immunoblots were performed for antibodies against GFP and TFEB to confirm the overexpression. Actin was used as loading control.

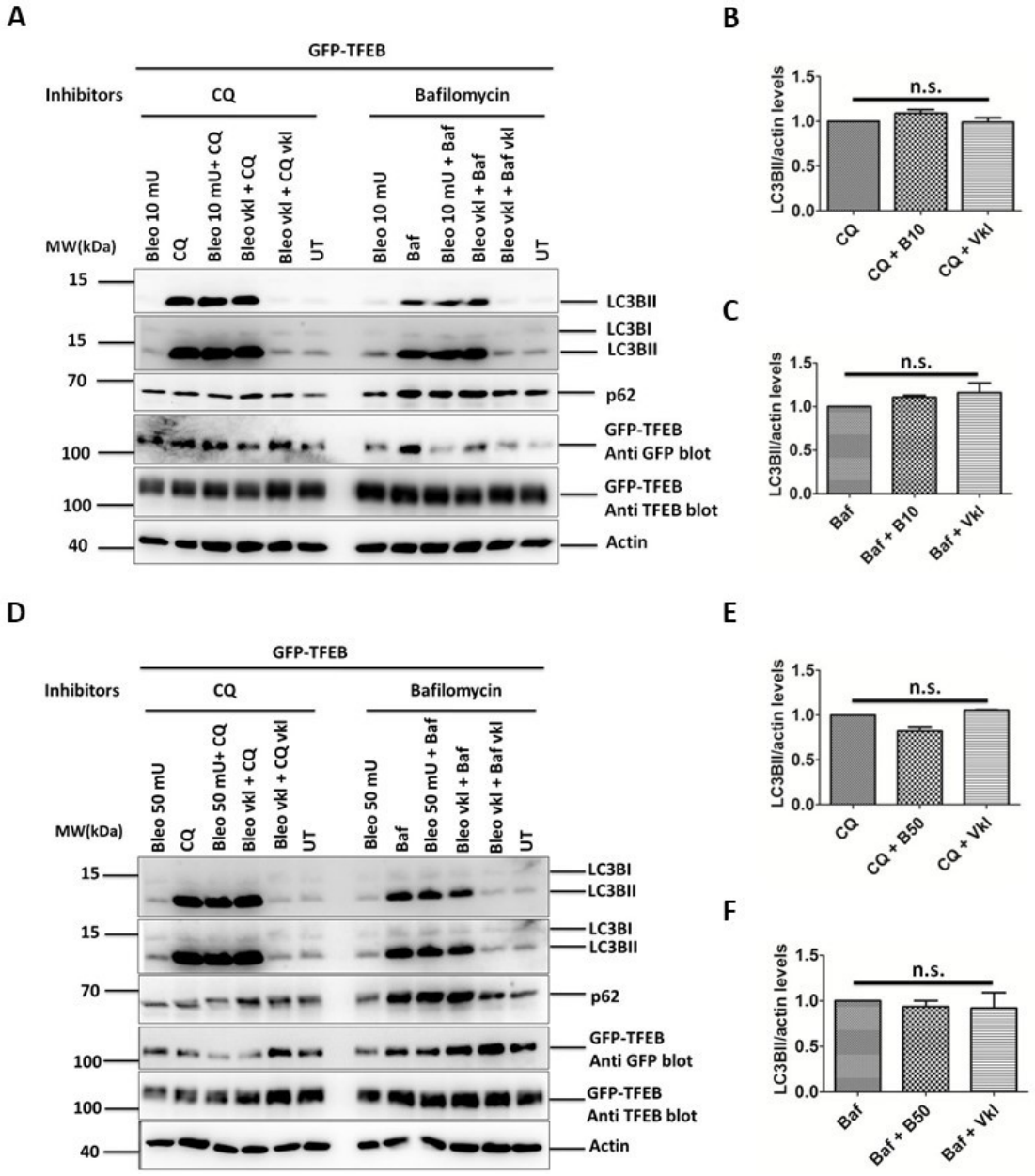

Fig. 26: Overexpressing TFEB before treating cells with bleomycin does not increase autophagic flux. A. Representative western blot image for the autophagy flux assay performed on MLE12 cells transiently transfected with GFP-TFEB is shown. Cells were treated with 10 mU bleomycin in presence of autophagy inhibitors chloroquine (CQ) and bafilomycin for 4 h. Protein lysate was used to study LC3BII and p62 protein levels in these cells. GFP and TFEB blots were performed to confirm overexpression of GFP-TFEB in all cells. Actin was used as loading control. **B** & **C**. Densitometric quantification for the autophagy flux assay showing changes in LC3BII turnover in response to 10 mU bleomycin in presence of autophagy inhibitors performed on

MLE12 cells transiently overexpressing GFP-TFEB. **D**. Representative western blot image for the autophagy flux assay performed on MLE12 cells transiently transfected with GFP-TFEB is shown. Cells were treated with 50 mU bleomycin in presence of autophagy inhibitors chloroquine and bafilomycin for 4 h. Protein lysate was used to study LC3BII and p62 protein levels in these cells. GFP and TFEB blots were performed to confirm overexpression of GFP-TFEB in all cells. Actin was used as loading control. **E** & **F**. Densitometric quantification for the autophagy flux assay showing changes in LC3BII turnover in response to 50 mU bleomycin in presence of autophagy inhibitors performed on MLE12 cells transiently overexpressing GFP-TFEB. *-p<0.05, **-p<0.01, ***-p<0.001, n.s.: no significance.

4.12 Identifying interaction partners of HPS1 protein.

To understand the functions of HPS1 protein, myc tagged human HPS1 was first amplified and the plasmid was purified using endotoxin free maxi plasmid purification kit. The purified plasmid was overexpressed in A549 cells as described in the methods section and the myc antibody was used to pull down the myc-tagged HPS1. Empty myc vector transfection was used as control for the co-immunoprecipitation assay. After pulldown, a portion of the pulldown sample was used to confirm the pulldown and the other part was used to perform LC-MS/MS to identify proteins which interact with HPS1. Sample processing and preparation for LC-MS/MS analysis is given the methods section. As shown in Fig. 27, immunoprecipitation of HPS1 was confirmed by western blotting using antibody against HPS1 and myc.

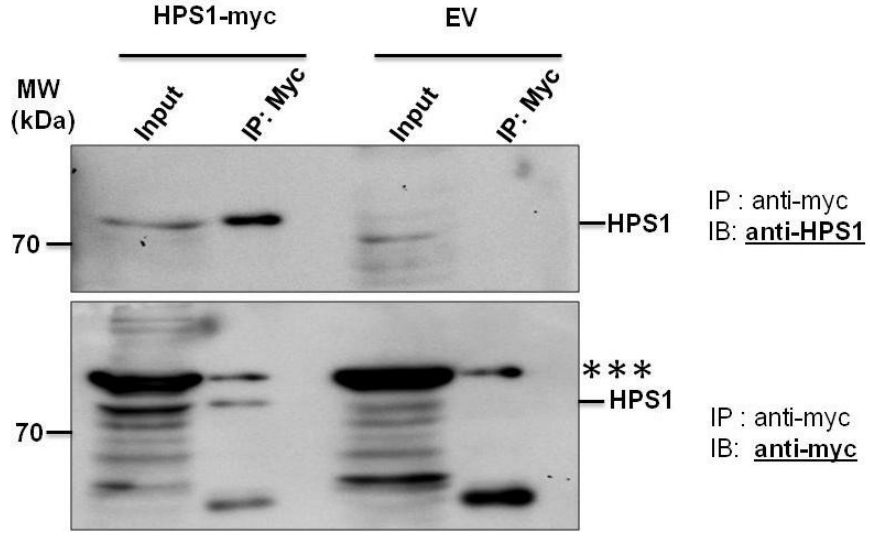

Fig. 27: Immunoprecipitation of HPS1-myc (hu) overexpressed in A549 cells. HPS1-myc was overexpressed in A549 cells and immunoprecipitated using an anti-myc antibody. Western blots show HPS1-myc immunoprecipitated from cells transfected with HPS1-myc as compared to the cells transfected with empty vector (EV). *** - non-specific cross reaction with samples by the myc antibody.

About 300 interaction partners were identified for the overexpressed HPS1 protein after mass spectroscopy of the pulldown sample. Out of those proteins, key interaction partners identified from MS/MS analysis are presented in Table 2.

Classification	Identified proteins
Autophagy related	**Atg3**
Mevalonate pathway	**Mevalonate kinase**
	Diphophomevalonate decarboxylase
	phosphomevalonate kinase
	farnesyl pyrophosphate synthase
Microtubule related	**MAP6**
	Tubulin alpha chain like 3
Vesicle trafficking	**Vps28**
	BNIP1
	Sec23ip
	Prenylatedrab acceptor protein
	Clathrin light chain B
	Syntaxinbindng protein
	Vamp
	Snap 25
	Rab3gap1
	Golgi phosphoprotein 3
	exocyst complex component 2
Extracellular matrix protein	**ECM1**
	Focal Adhesion kinase 1
	Claudin 1
Other important proteins	**Plasminogen activator inhibitor 1 (SERPINE1)- a profibrotic mediator,**
	Anaphase promoting complex subunit 7 (ANAPC7)

Table 2: List of novel interaction partners (shortlisted) after the MS/MS analysis of immunoprecipitated HPS1-myc.

Some of the proteins which play a direct role in the autophagy pathway, like Atg3 show that HPS1 proteins might be involved in the direct regulation of autophagy and are supporting our results showing autophagy deregulation post HPS1 knockdown in A549 cells. Atg3 plays an active role in the conjugation of LC3B to the lipid phosphatidylethanolamine (PE), which is a critical step in the autophagosomal biosynthesis (Ichimura et al., 2000). Atg3 has also been shown to be a direct target of caspase-8 and plays a vital role in regulating autophagy under conditions of cell death and survival (Oral et al., 2012). Interaction of proteins belonging to the microtubule family like MAP6 and tubulin alpha chain like 3 may indicate involvement of HPS1 protein in the cytoskeleton. Microtubules have been shown to be playing a key role in the autophagosome trafficking although the exact mechanism has not yet been fully understood. Immunoprecipitation of proteins involved in mevalonate pathway together with HPS1 protein opens yet another area to study the role of HPS proteins. The mevalonate pathway plays a key role in prenylation of Rab proteins and Rab proteins are essential regulators of vesicle trafficking. The HPS mouse model, *gunmetal mouse*, carrying a mutation in Rabggta results in defects in prenylation and has been shown to have defective trafficking pathways resulting in accumulation of melanosomes together with prolonged bleeding (Seixas et al., 2013). Other proteins like vacuolar sorting protein-28, syntaxin binding protein, Vamp, Rab3gap1 etc. further indicate the importance of HPS1 protein in the vesicle trafficking pathway regulation. Pulldown of proteins belonging to extracellular matrix family such as ECM1, claudin-1, focal adhesion kinase-1 etc. further reveal a possible direct role of HPS1 protein in the development of HPSIP, since these proteins have been studied in relation to IPF and tumors (Lagares et al., 2012; Lappi-Blanco et al., 2013; Wang et al., 2003).

4.13 Identification of alveolar epithelial cell specific interaction partners for LC3B.

Our lab has previously demonstrated that knockdown of LC3B under increased autophagy conditions due to amiodarone treatment in MLE 12 cells decreased the extent of amiodarone induced apoptosis of the cells (Mahavadi et al., 2015). Here, we show that exogenous LC3B is protective under HPS1 knockdown conditions (Figure 14 & (Ahuja et al., 2016)). Addtionally, LC3B has been shown to be pivotal in certain cell types and especially in osteoclasts which are secretory cells containing secretory lysosomes like the alveolar epithelial cells, the lipidation of LC3B determines the secretory function (Chung et al., 2014). Mouse LC3B was amplified from healthy mouse lung and cloned into myc-tagged-PCMV3 vector and overexpressed in MLE12 cells as detailed in the methods section. Antibody against myc-tag coupled with magnetic beads was used to immunoprecipitated myc-tagged LC3B from the overexpressing cells. Empty vector

transfections and untransfected cells were used as control for the experiment. Immunoprecipitation of myc-LC3B was confirmed by western blots using antibody against LC3B. LC3B tagged with myc protein shows a slight shift above the endogenous LC3B because of the extremely small size of myc protein (about 2 kDa) shown in Fig. 28. These samples after immunoprecipitations were processed and prepared for LC-MS/MS analysis. About 249 LC3B interacting proteins were identified.

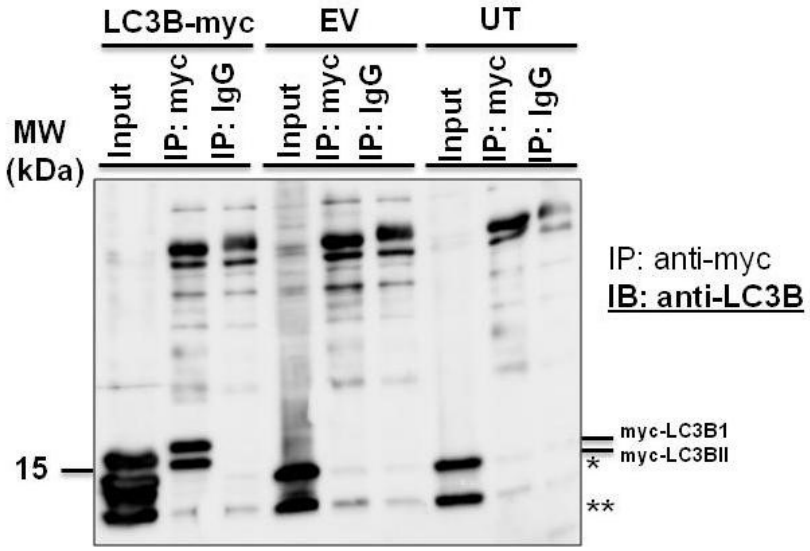

Fig. 28: Immunoprecipitation of myc-LC3B (m) overexpressed in MLE12 cells. myc-LC3B was overexpressed in MLE12 cells and immunoprecipitated using anti-myc antibody. Western blot showing myc-LC3B immunoprecipitated from cells transfected either with plasmid encoding myc-LC3B, empty vector carrying myc alone and untreated cells.

Table 3 shows a selection of proteins, known as well as novel partners for LC3B identified in this study. Many other proteins, which are not very well understood, might well be involved in the regulation of LC3B, and hence autophagy.

Classification	Related proteins
Autophagy related	**BAG3**
	VPS4b (vacuolar protein sorting associated protein 4B)
Acetylation	**Naa (N-acetyltransferase)**
E3 Ub-ligase	**RBX1**
	TRIM23
Lysosomal protein	**NCU-G1**
Other importantproteins	**Phospholipid scramblase**

	LAMTOR1 (late endosome/lysosome biogenesis)
	Drebrin 1 (neuronal growth, implicated in Alzheimers)

Table 3: List of interaction partners of interest shortlisted after the MS/MS analysis of immunoprecipitated HPS1-myc.

LC3B has been majorly understood as a protein which is mainly referred to as autophagosomal marker helping us understand regulation of autophagy pathway but to limit the function of LC3B only as autophagosomal marker might be undervaluing of an important protein. There are interaction partners of LC3B which are well known such as SQSTM1/p62 but understanding more proteins with which LC3B interacts would further allow us to understand the role and function of LC3B and the pathways beside autophagy pathway it might be involved in. VPS4b has previously been shown to be involved in vesicular trafficking and autophagsome maturation in mammalian cells, any direct evidence of direct interaction with LC3B has not yet been shown (Lin et al., 2012). LC3B deacetylation is critical for the LC3B to be able to shuttle across nuclear membrane into the cytosol and participate in the autophagosome formation (Huang et al., 2015) thereby hinting at the possibility of LC3B having Naa as a direct interaction partner. Ubiquitination has been well accepted as a method of protein targeting to the autophagosomes for the degradation with proteins like optineurin playing a bridge between ubiquitylated proteins and autophagy machinery, not much has been studied and understood in terms of the roles of E3 ubiquitin ligases. Immunoprecipitation of Ubiquitin ligases like RBX1 and TRIM23 as interaction partners of LC3B might well provide further evidence into the possible roles of these ligases towards autophagy pathway. Proteins like phospholipid scramblase and LAMTOR1 have been shown to be regulating autophagy pathway (Mastorci et al., 2016; Zada et al., 2015). Phospholipid scramblase is involved in the phospholipid translocation across lipid bilayer of cell membrane thereby being involved in lipid metabolism, thrombosis as well as apoptosis. LAMTOR1 protein is a part of Ragulator complex whose main role is amino acid sensing and activating mTORC1. It is also involved in the late endosomal/lysosomal biogenesis and cholesterol homeostasis.

5. DISCUSSION

In the current study, two models of pulmonary fibrosis, the HPS model and the bleomycin model were studied to understand the significance and role of autophagy pathway in the development and progression of the disease. We reported that the autophagy pathway in HPS1/2 mouse model *in vivo* and under *HPS1* knockdown conditions *in vitro* in A549 cells is defective, as demonstrated by the p62 accumulation and by the absence of autophagosome-lysosome fusion. Overexpression of MAP1LC3B before knocking down *HPS1* rescued the autophagy pathway by promoting autophagosome-lysosome fusion, thereby decreasing the accumulated p62 protein levels *in vitro*. Further, co-immunoprecipitation of the overexpressed HPS1 (myc tagged) protein with subsequent mass spectrometry analysis revealed about 280 novel interaction partners. Bleomycin model although showed an increase in the levels of autophagy marker proteins under *in* vivo conditions, treatment with bleomycin under *in* vitro conditions resulted in a defective autophagy. TFEB overexpression was used to rescue bleomycin induced defect in autophagy pathway as TFEB is known to be the master regulator of autophagy. Overexpression of TFEB did not rescue the bleomycin-induced defective autophagy *in vitro.* Both models of pulmonary fibrosis used in this study display defective autophagy. Further, analysis of MAP1LC3B interacting proteins revealed novel binding partners within the alveolar epithelial cells. Taken together, this study concludes that autophagy pathway does play an important role in the development of lung fibrosis in the studied mouse models.

5.1 Lysosomal stress and Hermansky-Pudlak syndrome

It is well-established that HPS affects lysosomal related organelles (LROs) and lamellar bodies (LBs) are one of the LROs that are affected by many of the HPS mutations. LBs are extremely important cellular organelles that store and secrete surfactant material to maintain surface tension in the lung. Previous work from our group revealed that cathepsin D, a lysosomal stress marker was increased in the AECII under HPSIP conditions and contributed in their apoptosis (Korfei et al., 2008). Apart from this, HPS proteins are well known to be involved in development and biogenesis of lysosome related organelles and any kind of mutation in these HPS gene products can result in a defect in lysosomal trafficking and secretion resulting in loss of cellular homeostasis. Biogenesis of organelle complex-3 (BLOC-3) is a large protein complex known to be comprised of two HPS proteins, HPS1 and HPS4 (Nazarian et al., 2003). Although exact

functions of this complex are not yet very well known, it has been shown that this complex can regulate distribution and microtubule dependent movement of lysosome related organelles in the cells (Falcon-Perez et al., 2005). Autophagy has not been directly analyzed under HPSIP conditions so far with the exception of one study in melanocytes isolated from HPS1 patients: tyrosine related proteins and lysosome associated membrane proteins, LAMP1 and LAMP3 get degraded via membranous structures which resemble macro-autophagosomes (Boissy et al., 1998).

Out of all HPS proteins known, HPS2/adaptor protein-3 complex is one of the most well researched HPS proteins. HPS2 is characterised by mutations in β3A subunit of the adaptor protein-3 complex and this complex is known to play role in sorting of membrane proteins from endosomes to lysosomes or to tissue specific lysosome related organelles and cells which lack AP-3 protein show targeting of LAMP1 and LAMP2 proteins non-specifically (Peden et al., 2004). AP-3 deficient fibroblasts showing misdirected LAMP2, a key protein involved in fusion of autophagosomes and lysosomes to form autophagolysosomes, show a deregulated autophagy pathway implicating that autophagy might well be involved in other forms of HPS as well. Previous studies of HPS1/2 double mutant mice have shown instances of early lysosomal stress which might be due to the accumulation of autophagosomal membranes in these mice (Mahavadi et al., 2010). On similar lines and supporting all this available data, the current study shows that autophagy, a very important lysosomal degradation pathway is defective under HPSIP conditions. This defect in autophagy pathway might be one of the key factors involved in typically observed apoptosis in AECII of HPS1 patients in addition to other phenotype such as increase in the size of AECIIs. Accumulation of p62 (as observed in HPS associated lung fibrosis) labeled cargo in cells lacking functional autophagy pathway can result in generation of oxidative stress, ER stress, unfolded protein response which might eventually lead the cells towards apoptotic pathways.

Our conclusion that the HPS1/2 double mutant mice have a loss of functional autophagy pathway is based on p62 accumulation in both lung homogenates as well as in lung sections. It is a well-established fact that a defect in autophagy pathway would result in accumulation of p62 protein which under conditions of homeostasis is supposed to be degraded via autophagy (Puissant et al., 2012). In addition to immunoblots, we also observed increase in p62 staining in lung sections from HPS1/2 mice as compared to controls together with an increase in LC3B protein levels. Electron microscopy data from these mice further showed us that the LC3B protein observed on the limiting membrane of lamellar bodies isolated from AECII in control mice was missing from the limiting membrane of the lamellar bodies in HPS1/2 mice. All these results taken together clearly

indicate defective autophagy pathway in HPS1/2 mice. In addition to the *in vivo* data, we also presented compelling evidence from *in vitro* studies that knockdown of HPS1 in A549 cells resulted in increased amount of LC3B lipidation i.e., LC3BII protein levels and a simultaneous accumulation of p62 protein levels. To provide autophagy flux data for this study we chose to perform GFP cleavage assay which involves production of free GFP from the overexpressed GFP-LC3B as a product of increased autophagy flux. To our surprise we observed free GFP fragment in response to HPS1 knockdown in A549 cells which transiently overexpressed GFP-LC3B. This was opposite to our claim that HPS1 knockdown results in autophagy becoming dysfunctional. But to our interest and of note, we also observed that cells overexpressing GFP-LC3B did not show accumulation of p62 post HPS1 knockdown. In addition to this, cells overexpressing GFP-LC3B show a co-localization of GFP-LC3B and LAMP1 indicating formation of autophagolysosomes even after knockdown of HPS1 which was clearly missing when HPS1 was knocked down in the absence of GFP-LC3B. The HPS1 knockdown induced p62 accumulation was restored when cells were overexpressed with GFP-LC3B. This might protect cells against the toxic effects of p62 labeled cargo accumulation. Similar results were observed by the overexpression of myc-LC3B confirming that the readouts are not tag specific. These results fully support previous literature which show that overexpression of autophagy related proteins can protect cells or even mice against potentially toxic challenges (Mai et al., 2012; Pyo et al., 2013).

Not only HPS, but several lysosomal storage disorders (LSDs) have been shown to be characterized by a dysfunctional autophagy pathway, for example, Niemann-Pick type C (NPC) disease, a disease characterised by sphingolipidosis, has been shown to have accumulation of autophagosomes in skin fibroblasts from the NPC patients and NPC mice brain (Liao et al., 2007; Pacheco et al., 2007). It has been shown in the NPC neuropathological studies that a dysfunctional autophagy pathway can result in production of reactive oxygen species (ROS) or accumulation of ubiquitinated proteins which can be quite toxic (Lieberman et al., 2012). Diseases like Gaucher or Fabry, also characteristically marked by sphingolipidoses have also been reported to have induction of autophagy marked by lipidation of LC3B but still resulting in p62 accumulation, both in patients as well as in mouse models (Chevrier et al., 2010; Liebau et al., 2013; Osellame and Duchen, 2013; Sun et al., 2010). Some other LSDs which have been characterized by defect in autophagy pathway are Pompe disease, Dannon disease, mucolipidosis and neuronal ceroidlipofuscinoses (Koike et al., 2005; Raben et al., 2009; Tanaka et al., 2000; Vergarajauregui et al., 2008). Pompe disease has been characterised by a defective autophagosome-lysosome fusion event and thereby

resulting in the accumulation of p62 and other ubiquitinated proteins in muscle fibers (Raben et al., 2008). It has also been shown in Pompe muscle cells that the induction of exocytosis resulting in removal of autophagolysosomes was cytoprotective for the cells resulting in removal of potentially toxic buildup inside the cells (Spampanato et al., 2013). Our data on similar lines shows accumulation of autophagy substrate protein p62 in response to a defect in autophagy pathway resulting from the knockdown of HPS1 protein in A549 lung cell line. Defective autophagy and giant lamellar body degeneration may be interconnected in HPSIP conditions which needs further investigations. Additionally, we also observed LC3B localization to the nucleus and thereby not being able to form autophagolysosomes although we did observe lipidation of LC3B post HPS1 knockdown. It is well-documented that LC3B in the nucleus gets deacetylated with the help of sirtuin 1 (Sirt1) which then translocates to the cytosol where lipidation of LC3B takes place. In addition, nuclear LC3B puncta under certain settings has been previously documented (Huang et al., 2015; Karim et al., 2007; Martinez-Lopez et al., 2013). Although autophagy pathway has been quite well studied and understood, the principles guiding the processing of LC3B are not yet very well understood. Further studies on the role of nuclear LC3B may hence be important also to understand the autophagy pathway in greater detail. Atg4B is a known autophagy protein believed to play a role in acetylating LC3B post-production in the nucleus. This acetylation of LC3B is a key to holding the protein inside the nucleus until the autophagy pathway gets activated and more LC3B protein is required in the cytosol but recently it has been shown that a mutation in Atg4B protein does not impact the lipidation of exogenous GFP-LC3B resulting in production of GFP-LC3BII (Fujita et al., 2008). This result to an extent helps us understand that the exogenous over-expression of GFP-LC3B and its processing takes an alternate route thereby explaining why the overexpression of GFP-LC3B was able to reverse the p62 accumulation in A549 cells resulting from the knockdown of HPS1.

5.2 Lysosomal stress and bleomycin induced lung fibrosis

Although bleomycin model for inducing lung fibrosis is the most studied model of lung fibrosis, the underlying principles and mechanisms underlining the disease post bleomycin injury continue to be evasive especially given the fact that bleomycin mice model has a potential to heal itself. Bleomycin is impermeable to plasma membrane and hence primarily enters the cells through receptor-mediated endocytosis (Pron et al., 1999). While bleomycin is well-known to cause DNA damage (Byfield et al., 1976) as well as oxidative stress (Gao et al., 2008) in many cell types, the effect of this drug on the lysosomal structures is not yet fully elucidated. It has long been demonstrated that radiolabeled bleomycin was observed in mitochondrial as well as lysosomal fractions

(Konings and Rasker 1978). In addition, an increase in cell size and lysosomal mass was reported in lung epithelial cells, both primary AECII as well as in tumor cells (A549) following bleomycin exposure (Aoshiba et al., 2003). Of late, although the autophagy pathway was not fully characterized, Patel et. al., (Patel et al., 2012) showed that rapamycin, an mTORC1 inhibitor and subsequent autophagy inducer, attenuated bleomycin induced lung fibrosis in mice, indirectly implicating defective autophagy in this model. In full support our data also shows that bleomycin treatment indeed causes defective autophagy in lungs as well as in MLE 12 cells.

Bleomycin treated mice in our study showed an increase in the amount of autophagy proteins at all treatment time points. Autophagy marker proteins like LC3B show that the bleomycin results in an increase in the turnover of LC3BI to LC3BII indicating increased lipidation of LC3B post bleomycin treatment. The increase in lipidated LC3BII levels alone is not enough to say that the autophagy is increased. To further support a claim that autophagy has been upregulated, a commonly used method is to show a decrease in the levels of autophagy substrate protein p62 whose role in autophagy pathway is to tag the proteins and organelles to be degraded and then interact with LC3B interacting region to bind with LC3B and enter autophagosomes. These autophagosomes then fuse with lysosomes to form autophagolysosomes, thereby degrading p62 labelled cargo together with p62 (Komatsu et al., 2007; Pankiv et al., 2007). In our study we did not see a decrease in levels of p62 post bleomycin treatment together with increased lipidation of LC3B but found p62 protein to be accumulating.

To further test our understanding of the effect of bleomycin on MLE12 cells we treated the cells with different concentrations of bleomycin and studied the effect of bleomycin on autophagy related proteins. Bleomycin treatment was given in two sets of concentrations, a low range of bleomycin concentration and a higher range of bleomycin concentration. Bleomycin treatment at lower concentrations showed an increase in LC3BII levels in the protein lysate obtained from these cells after treating the cells with bleomycin for 4 h but p62 levels did not change significantly as compared to vehicle and untreated controls. SQSTM1/p62 has been shown to be transcriptionally regulated under certain conditions so it is important to show the changes in p62 protein levels are not due to an increase in the expression of p62 at mRNA level. Both LC3B and p62 did not show any change in the regulation of transcription of these genes in response to bleomycin treatment. In addition to the effect of bleomycin treatment on autophagy proteins, we also tried to establish the effect of higher doses of bleomycin on the pro-apoptotic protein cleaved caspase-3 when cells were treated with bleomycin for 4 h. As indicated in many studies before, it was interesting to note that bleomycin induces cleavage of pro-

caspase-3 protein as early as 4 h post treatment in a dose dependent manner. It is well established that autophagy pathway sits at a crossway between cell survival and cell death and autophagy has been referred to as a pro survival mechanism for the cells (Maiuri et al., 2007; Marino et al., 2014). Based on our results so far, it may be stated that the cellular stress induced by the bleomycin treatment on MLE12 cells is huge and possibly autophagic machinery is not able to adapt to this kind of stress and shuts down. Once the autophagic machinery gets shut down, it becomes imperative for the apoptotic mechanisms to kick in and try to protect the overall system by sacrificing those cells where bleomycin induced toxicity is too high. In addition to the increased levels of cleaved caspase-3 observed in MLE12 cells post bleomycin treatment, we also observed a characteristic swelling in MLE12 cells when the cells were incubated with bleomycin at higher doses for 24 h. Vehicle and untreated cells did not show any such swelling. The exact reasons for this kind of swelling are not very clear but this can also be an effect of autophagy shutdown resulting in the inability of cells to clear out the toxic buildup of the proteins and organelles which might have been damaged due to the oxidative stress or other stress inducing mechanisms of bleomycin. In addition to the cellular swelling, increase in cell death of MLE12 cells in a dose dependent manner was clearly seen under light microscope.

Our autophagy flux assay using two concentrations of bleomycin in the presence or absence of autophagy inhibitors chloroquine and bafilomycin did not show any increase in the turnover of LC3BI to LC3BII. This implicates that bleomycin is not an inducer of autophagy but an inhibitor of autophagy at either of the two concentrations used to study autophagy flux. These observations are however in striking contrast to a new study by Cabrera and colleagues (Cabrera et al., 2015), where they report enhanced autophagy following bleomycin treatment. The discripency may be attributed to the fact that Cabrera et.al. studied autophagy flux after 24 h in the presence of autophagy inhibitor chloroquine, a time point which may be too long to study autophagy flux as suggested before (Barth et al., 2010; Klionsky et al., 2016).

In addition to flux assay, we also performed immunofluorescence on bleomycin treated MLE12 cells using two different concentrations as used earlier. The immunofluorescence was performed to study changes in the colocalization pattern of the autophagosome marker LC3B and lysosomal membrane protein marker LAMP2. An increase in the colocalization of these two proteins is widely accepted as an indicator of increased autophagolysosome formation which is essential for the autophagic degradation to happen. Lack of this fusion event would result in a toxic buildup of the p62 labeled cargo inside the cells resulting in activation of apoptotic or other cell death pathways. As shown

in our immunofluorescence images for LC3B and LAMP1 colocalization, no increase in autophagolysosomal formation was observed in response to bleomycin treatment as compared to vehicle and untreated cells.

Based on the results discussed above it is clear to us that autophagy pathway has been hindered in response to bleomycin treatment and we next asked if it would be possible to rescue this autophagy defect to protect the cells from bleomycin induced damage and ultimately apoptosis. One of the approaches that we used here to overcome bleomycin induced block in autophagy pathway was to transiently overexpress GFP-TFEB in MLE12 cells before exposing them to bleomycin. TFEB has been shown to a key player in the regulation of autophagy although it has only quite recently been discovered to be playing a significant role in autophagy. It has been referred to as a "master regulator" of autophagy in addition to its significant role in lysosomal biogenesis (Sardiello et al., 2009; Zhao and Czaja, 2012). Based on our previous results where we did not see increase in the formation of autophagolysosomes, we hypothesised that increase in the number of lysosomes in MLE12 cells due to overexpression of TFEB might result in an increase in the number of autophagolysosomes thereby increasing autophagy flux. We overexpressed GFP-TFEB in MLE12 cells overnight, treated the cells with bleomycin following day with 10 or 50 mU of bleoymcin for 4 h and then analysed the changes in lipidation of LC3B protein to study the turnover of LC3BI to LC3BII in presence of autophagy inhibitors. Surprisingly, neither the turnover of LC3BI to LC3BII nor autophagy flux was increased upon GFP-TFEB overexpression. It however remains to be answered if overexpression of TFEB may prove beneficial to cells treated with higher dose of bleomycin (100 mU for example). It has been shown that cellular localization of TFEB is regulated by mTORC1 by phosphorylating it at S142. Treatment of cells with TORIN1, a selective mTOR inhibitor efficiently induced nuclear localization of TFEB, implicating a lysosome to nucleus signaling (Settembre et al., 2012). Following this line, further studies are underway to activate autophagy pathway in bleomycin treated cells using TORIN1 which might trigger the lysosome to nucleus signaling of TFEB and thereby autophagy.

5.3 Autophagy in lung health and disease

Regulation of autophagy in lung diseases represents a growing field of research. So far, increased autophagy resulting in apoptotic cell death has been shown under conditions of chronic obstructive pulmonary disease (COPD) (Chen et al., 2008). In cystic fibrosis, defective autophagy seems to occur and rescuing the autophagy pathway improved the trafficking of the cystic fibrosis transmembrane conductance regulator (CFTR) (Luciani et al., 2010). More recent studies on the regulation of autophagy in lung fibrosis report

that autophagy is either not activated or is insufficient in patients with idiopathic pulmonary fibrosis (IPF) and that TGFβ-1 inhibits autophagy in lung fibroblasts *in vitro* (Patel et al., 2012). Another study revealed an alteration in the Bcl-2-binding protein Beclin1, providing a hint towards a dysfunction in the autophagy/apoptosis system in IPF fibroblasts (Ricci et al., 2013). In addition, PINK1 dependent autophagy was indicated in IPF AECIIs (Bueno et al., 2015). Nevertheless, the precise role of autophagy within the alveolar epithelial cells largely remains unexplored in IPF as well as in animal models of lung fibrosis.We recently reported increased autophagy flux and apoptosis of AECII that is mediated by autophagy in amiodarone induced lung fibrosis (Mahavadi et al., 2015). Now, in the current study, we document that autophagy is defective in HPS associated and in bleomycin induced lung fibrosis. These observations completely corroborate with the previously reported defective autophagy within the AECII of IPF patients (Bueno et al., 2015). Based on all these different observations, it may be stated that depending on the kind of insult, autophagy is regulated differently in different models of lung fibrosis. In any case, altered autophagy (either too much or too little) triggers lysosomal stress in alveolar epithelial cells and might be a critical pathway contributing towards AECII injury and apoptosis under conditions of lung fibrosis.

5.4 Interaction partners for HPS1 and LC3B

HPS1 protein has not yet been studied in detail. So far it is known that HPS1 interacts with HPS4 in the BLOC-3 complex. Rab9 is the only direct interaction partner reported for the BLOC-3 complex (Kloer et al., 2010). Identification of interaction partners of HPS1 would hence throw light on the yet unknown cellular functions of this protein. Hence, we performed mass spectrometry analysis of myc tagged HPS1 protein following its overexpression in A549 cells and its pulldown. The full list of specific HPS1 interacting proteins was about 280 proteins which included members of vesicle trafficking, microtubule related proteins, members of the autophagy family, etc. Confirmation studies for the identified partners are currently underway. Since HPS1 is known to play important role in vesicular trafficking, the currently identified interacting partners of vesicle trafficking and microtubule associated proteins are extremely exciting to study further(Huizing et al., 2000; Natsuga et al., 2005; Shotelersuk and Gahl, 1998).

In addition, it may be of great interest to study the functional and biological significance of the HPS1 protein with the identified proteins of the autophagy pathway like ATG3 and BNIP1. This will particularly enhance our current understanding about the underlying reasons behind defective autophagy that we have reported under conditions of HPS1-lung fibrosis.

Likewise, to understand the interactome of the LC3B proteinin alveolar epithelial cells, we performed mass spectrometry analysis for LC3B-myc in MLE12 cells as a first step. We were able to identify about 250 LC3B specific interacting proteins, and the list includes both known and novel interaction partners for LC3B. While proteins like SQSTM1 (p62), Bag3, and VPS1 are known interacting proteins that were identified in our analysis, lysosomal protein NCUG1, LAMTOR1, Drebrin1 etc. are novel and are not yet reported binding partners of LC3B. Confirmational experiments including immunoprecipitation of LC3B followed by western blots of the selected proteins and reverse immunoprecipitation, meaning pulldown of the interaction partner using specific antibodies followed by western blot for LC3B are some ways to confirm the identified interaction partners in the immediate future followed by long term goals to identify the biological and functional significance of the interactions in alveolar epithelial cells and how aberration of such interactions influence and trigger alveolar epithelial injury and thereby lung fibrosis.

6. CONCLUSION

We conclude that autophagy is defective in alveolar epithelial cells of two mouse models of lung fibrosis that we used in this study, the HPS model and the bleomycin model. Such aberrant autophagy triggers lysosomal stress events which might affect other cellular stress mechanisms of the cell. This contributes towards apoptosis of this cell type ultimately leading to the development of lung fibrosis. The complexities and intricacies of the autophagy pathway in these two mouse models might be very different from each other but they are united by the fact that autophagy is silenced in the alveolar epithelial cells of both the models which might contribute towards AECII injury and thereby fibrosis. In case of HPS1 knockdown, with the overexpression of LC3B in A549 cells, we were able to reverse the HPS1 knockdown induced accumulation of p62. Although this was not the case with bleomycin treated MLE12 cells where we were not able to induce recovery of autophagic pathway, the readouts so far clearly implicate towards targeting autophagy to combat alveolar epithelial cell injury in this model. Identification and confirmation of novel interacting partners for HPS1 as well as for autophagy proteins will open new avenues to target this pathway in the context of lung fibrosis.

7. Summary

Idiopathic pulmonary fibrosis (IPF), characterized by progressive decline in lung function, is associated with histological appearance of usual interstitial pneumonia (UIP). To define pathogenesis of lung fibrosis, several mouse models have been developed. Bleomycin is the most frequently used agent to drive lung fibrosis in mice. Apart from bleomycin model, AECII injury and apoptosis were reported as important triggers in other mouse models like Hermansky-Pudlak syndrome (HPS) associated lung fibrosis and amiodarone induced lung fibrosis. HPS is an autosomal recessive disorder characterized by bleeding diathesis, occuculocutaneous albinism and pulmonary fibrosis in patients. Aim of this study is to analyze regulation of autophagy in HPSIP and bleomycin model of lung fibrosis. Autophagy is a lysosome dependent quality control mechanism of cell to maintain cellular homeostasis and promote cell survival under stressful conditions.

In our study, key autophagy proteins including LC3BII and p62 were found to be increased in HPS1/2 double mutant mice lungs. Electron microscopy revealed preferable LC3B binding to the lumen of lamellar bodies in HPS1/2 while it was found in both the lumen as well as on the limiting membrane of lamellar bodies in wildtype mice. After *HPS1* knockdown in A549 cells, p62, an autophagy substrate protein accumulated indicating defective autophagy pathway. Exogenous LC3B normalized *HPS1* knockdown induced p62 protein levels. A549 cells post *HPS1* knockdown also showed a decrease in the formation of autophagolysosomes. We overexpressed and immunoprecipitated HPS1 protein from A549 cells and identified specific autophagy related proteins as HPS1 interacting proteins via mass spectrometric analysis.

Bleomycin treated mice lungs showed increase in autophagy proteins. MLE12 cells, upon bleomycin treatment revealed decrease in autophagy flux but showed increased levels of cleaved caspase-3 indicating induction of apoptosis post bleomycin treatment.

We performed co-imunoprecipitation followed by mass spectrometric analysis to identify interaction partners for autophagy marker protein, LC3B within the alveolar epithelial cells. Our analysis revealed novel interacting partners for LC3B.

This study concludes that defective autophagy pathway observed both, in response to *HPS1* knockdown and bleomycin challenge might play a critical role in the development and progression of pulmonary fibrosis. Understanding functions of autophagy by analyzing novel interaction partners of its marker proteins within the alveolar epithelial cells may help to further understand the mechanisms behind the contribution of defective autophagy towards the development of lung fibrosis.

8. Zusammenfassung

Die idiopathische Lungenfibrose (IPF) repräsentiert eine der aggressivsten Formen von Organfibrosen. Sie ist durch eine fortschreitende Verringerung der Lungenfunktion charakterisiert und wird mit dem histologischen Erscheinungsbild einer herkömmlichen interstitiellen Pneumonie assoziiert (UIP). Um die Pathogenese der Lungenfibrose zu definieren, wurden bereits einige Mausmodelle entwickelt. Hierbei stellt Bleomycin das am häufigsten verwendete agens dar, um eine Lungenfibrose bei Mäusen auszulösen. Abgesehen von diesem Bleomycin Modell wurden auch Schädigungen der AEII und Apoptose als mögliche Auslöser erkannt, etwa bei Mausmodellen für Hermansky-Pudlak Syndrom (HPS) assoziierte Lungenfibrose und Amiodarone induzierter Lungenfibrose. HPS ist eine autosomal rezessive Erkrankung, die charakterisiert ist durch Blutungsdiathese, Ceroid-Lipofuszin Akkumulation, okulokutanen Albinismus und pulmonale Fibrose. Mutationen im HPS Gen verursachen Fehler im Proteintransport. Das Ziel dieser Studie ist es, die Regulation der Autophagie in HPSIP und im Bleomycin Modell für Lungenfibrose zu analysieren.

Bei der Autophagie handelt es sich um einen von den Lysosomen abhängigen Qualitätskontrollmechanismus einer Zelle, der darauf abzielt, die zelluläre Homöostase aufrecht zu erhalten und das Überleben der Zell in Stresssituationen zu unterstützen.

In unserer Untersuchung konnten wir zeigen, dass Autophagie Proteine inklusive LC3B Lipidation und p62 in den Lungen der HPS 1/2 Doppelmutanten Mäusen erhöht waren. Elektronenmikroskopische Untersuchungen zeigten eine zu bevorzugende LC3B Bindung an das Lumen der Lamellarkörper bei den HPS1/2, während diese sowohl im Lumen als auch in der limitierenden Membran der Lamellarkörper in wild-typischen Mäusen zu finden war. Unter HPS1 knock-down Bedingungen in A549 Zellen, akkumulierte das Autophagie Substrat Protein SQSTM1/p62, was auf einen defekten Autophagie Signalweg hindeutet. Exogenes LC3B normalisierte die von HPS1knock-down induzierten p62 Proteinlevel. A549 Zellen zeigten nach HPS1 knock-down ebenfalls eine Verringerung der Formation von Autophagie Lysosomen. Wir über-exprimierten und immunpräzipitierten HPS1 Protein aus A549 Zellen und identifizierten spezifische Autophagie bezogene Proteine wie etwa HPS1 interacting Proteine durch massenspektrometrische Analyse.

Mit Bleomycin behandelte Mäuselungen zeigten einen Anstieg der Autophagie Markerproteine. MLE12 Zellen zeigten bei Bleomycin Behandlung eine Verringerng des

Autophagie Flux, aber gesteigerte Level an gespaltenen Caspase3, was eine Induktion der Apoptose nach Bleomyzin Behandlung nahelegt.

Wir führten eine Co-Immunopräzipitation durch, gefolgt von einer massenspektrometrischen Analyse, um wichtige Interaktionspartner für das Autophagie Marker Protein LC3B in den alveolaren Epithelzellen zu identifizieren. Unsere Analyse zeigte neuartige Interaktionspartner für LC3B.

Die Studie kommt zu dem Schluss, dass defekte Autophagie Signalwege wie sie sowohl als Antwort auf HPS1 knock-down als auch bei Bleomyzin Behandlung beobachtet werden, eine Rolle bei der Entwicklung und Progression der Lungenfibrose spielen könnten. Die Funktionen der Autophagie durch die Analyse neuer Interaktionspartner ihrer Markerproteine in den alveolaren Epithelzellen zu verstehen könnte helfen, die Mechanismen hinter dem Beitrag defekter Autophagie an der Entwicklung von Lungenfibrose zu verstehen.

9. REFERENCES

(2002). "American Thoracic Society/European Respiratory Society International Multidisciplinary Consensus Classification of the Idiopathic Interstitial Pneumonias. This joint statement of the American Thoracic Society (ATS), and the European Respiratory Society (ERS) was adopted by the ATS board of directors, June 2001 and by the ERS Executive Committee, June 2001." Am J Respir Crit Care Med **165**(2): 277-304.

Ahuja, S., L. Knudsen, S. Chillappagari, I. Henneke, C. Ruppert, M. Korfei, B. R. Gochuico, S. Bellusci, W. Seeger, M. Ochs, A. Guenther and P. Mahavadi (2016). "MAP1LC3B overexpression protects against Hermansky-Pudlak syndrome type-1-induced defective autophagy in vitro." Am J Physiol Lung Cell Mol Physiol **310**(6): L519-531.

Alder, J. K., J. J. Chen, L. Lancaster, S. Danoff, S. C. Su, J. D. Cogan, I. Vulto, M. Xie, X. Qi, R. M. Tuder, J. A. Phillips, 3rd, P. M. Lansdorp, J. E. Loyd and M. Y. Armanios (2008). "Short telomeres are a risk factor for idiopathic pulmonary fibrosis." Proc Natl Acad Sci U S A **105**(35): 13051-13056.

Anderson, P. D., M. Huizing, D. A. Claassen, J. White and W. A. Gahl (2003). "Hermansky-Pudlak syndrome type 4 (HPS-4): clinical and molecular characteristics." Hum Genet **113**(1): 10-17.

Anglade, P., S. Vyas, F. Javoy-Agid, M. T. Herrero, P. P. Michel, J. Marquez, A. Mouatt-Prigent, M. Ruberg, E. C. Hirsch and Y. Agid (1997). "Apoptosis and autophagy in nigral neurons of patients with Parkinson's disease." Histol Histopathol **12**(1): 25-31.

Aoshiba, K., T. Tsuji and A. Nagai (2003). "Bleomycin induces cellular senescence in alveolar epithelial cells." Eur Respir J **22**(3): 436-443.

Araya, J., J. Kojima, N. Takasaka, S. Ito, S. Fujii, H. Hara, H. Yanagisawa, K. Kobayashi, C. Tsurushige, M. Kawaishi, N. Kamiya, J. Hirano, M. Odaka, T. Morikawa, S. L. Nishimura, Y. Kawabata, H. Hano, K. Nakayama and K. Kuwano (2013). "Insufficient autophagy in idiopathic pulmonary fibrosis." Am J Physiol Lung Cell Mol Physiol **304**(1): L56-69.

Azad, M. B., Y. Chen, E. S. Henson, J. Cizeau, E. McMillan-Ward, S. J. Israels and S. B. Gibson (2008). "Hypoxia induces autophagic cell death in apoptosis-competent cells through a mechanism involving BNIP3." Autophagy **4**(2): 195-204.

B, B. M., W. E. Lawson, T. D. Oury, T. H. Sisson, K. Raghavendran and C. M. Hogaboam (2013). "Animal models of fibrotic lung disease." Am J Respir Cell Mol Biol **49**(2): 167-179.

Bachli, E. B., T. Brack, E. Eppler, T. Stallmach, R. M. Trueb, M. Huizing and W. A. Gahl (2004). "Hermansky-Pudlak syndrome type 4 in a patient from Sri Lanka with pulmonary fibrosis." Am J Med Genet A **127A**(2): 201-207.

Bailin, T., J. Oh, G. H. Feng, K. Fukai and R. A. Spritz (1997). "Organization and nucleotide sequence of the human Hermansky-Pudlak syndrome (HPS) gene." J Invest Dermatol **108**(6): 923-927.

Ballabio, A. (2009). "Disease pathogenesis explained by basic science: lysosomal storage diseases as autophagocytic disorders." Int J Clin Pharmacol Ther **47 Suppl 1**: S34-38.

Ballabio, A. and V. Gieselmann (2009). "Lysosomal disorders: from storage to cellular damage." Biochim Biophys Acta **1793**(4): 684-696.

Barcellos-Hoff, M. H., R. Derynck, M. L. Tsang and J. A. Weatherbee (1994). "Transforming growth factor-beta activation in irradiated murine mammary gland." J Clin Invest **93**(2): 892-899.

Barth, S., D. Glick and K. F. Macleod (2010). "Autophagy: assays and artifacts." J Pathol **221**(2): 117-124.

Baumgartner, K. B., J. M. Samet, C. A. Stidley, T. V. Colby and J. A. Waldron (1997). "Cigarette smoking: a risk factor for idiopathic pulmonary fibrosis." Am J Respir Crit Care Med **155**(1): 242-248.

Belaid, A., M. Cerezo, A. Chargui, E. Corcelle-Termeau, F. Pedeutour, S. Giuliano, M. Ilie, I. Rubera, M. Tauc, S. Barale, C. Bertolotto, P. Brest, V. Vouret-Craviari, D. J. Klionsky, G. F. Carle, P. Hofman and B. Mograbi (2013). "Autophagy plays a critical role in the degradation of active RHOA, the control of cell cytokinesis, and genomic stability." Cancer Res **73**(14): 4311-4322.

Bence, N. F., R. M. Sampat and R. R. Kopito (2001). "Impairment of the ubiquitin-proteasome system by protein aggregation." Science **292**(5521): 1552-1555.

Boissy, R. E., Y. Zhao and W. A. Gahl (1998). "Altered protein localization in melanocytes from Hermansky-Pudlak syndrome: support for the role of the HPS gene product in intracellular trafficking." Lab Invest **78**(9): 1037-1048.

Bonifacino, J. S. and E. C. Dell'Angelica (1999). "Molecular bases for the recognition of tyrosine-based sorting signals." J Cell Biol **145**(5): 923-926.

Bonifacino, J. S. and L. M. Traub (2003). "Signals for sorting of transmembrane proteins to endosomes and lysosomes." Annu Rev Biochem **72**: 395-447.

Brantly, M., N. A. Avila, V. Shotelersuk, C. Lucero, M. Huizing and W. A. Gahl (2000). "Pulmonary function and high-resolution CT findings in patients with an inherited form of pulmonary fibrosis, Hermansky-Pudlak syndrome, due to mutations in HPS-1." Chest **117**(1): 129-136.

Brech, A., T. Ahlquist, R. A. Lothe and H. Stenmark (2009). "Autophagy in tumour suppression and promotion." Mol Oncol **3**(4): 366-375.

Bueno, M., Y. C. Lai, Y. Romero, J. Brands, C. M. St Croix, C. Kamga, C. Corey, J. D. Herazo-Maya, J. Sembrat, J. S. Lee, S. R. Duncan, M. Rojas, S. Shiva, C. T. Chu and A. L. Mora (2015). "PINK1 deficiency impairs mitochondrial homeostasis and promotes lung fibrosis." J Clin Invest **125**(2): 521-538.

Byfield, J. E., Y. C. Lee, L. Tu and F. Kulhanian (1976). "Molecular interactions of the combined effects of bleomycin and x-rays on mammalian cell survival." Cancer Res **36**(3): 1138-1143.

Cabrera, S., M. Maciel, I. Herrera, T. Nava, F. Vergara, M. Gaxiola, C. Lopez-Otin, M. Selman and A. Pardo (2015). "Essential role for the ATG4B protease and autophagy in bleomycin-induced pulmonary fibrosis." Autophagy **11**(4): 670-684.

Cao, Y., J. A. Espinola, E. Fossale, A. C. Massey, A. M. Cuervo, M. E. MacDonald and S. L. Cotman (2006). "Autophagy is disrupted in a knock-in mouse model of juvenile neuronal ceroid lipofuscinosis." J Biol Chem **281**(29): 20483-20493.

Chen, Z. H., H. P. Kim, F. C. Sciurba, S. J. Lee, C. Feghali-Bostwick, D. B. Stolz, R. Dhir, R. J. Landreneau, M. J. Schuchert, S. A. Yousem, K. Nakahira, J. M. Pilewski, J. S. Lee, Y. Zhang, S. W. Ryter and A. M. Choi (2008). "Egr-1 regulates autophagy in cigarette smoke-induced chronic obstructive pulmonary disease." PLoS One **3**(10): e3316.

Chen, Z. H., H. C. Lam, Y. Jin, H. P. Kim, J. Cao, S. J. Lee, E. Ifedigbo, H. Parameswaran, S. W. Ryter and A. M. Choi (2010). "Autophagy protein microtubule-

associated protein 1 light chain-3B (LC3B) activates extrinsic apoptosis during cigarette smoke-induced emphysema." Proc Natl Acad Sci U S A **107**(44): 18880-18885.

Chevrier, M., N. Brakch, L. Celine, D. Genty, Y. Ramdani, S. Moll, M. Djavaheri-Mergny, C. Brasse-Lagnel, A. L. Annie Laquerriere, F. Barbey and S. Bekri (2010). "Autophagosome maturation is impaired in Fabry disease." Autophagy **6**(5): 589-599.

Chiang, P. W., N. Oiso, R. Gautam, T. Suzuki, R. T. Swank and R. A. Spritz (2003). "The Hermansky-Pudlak syndrome 1 (HPS1) and HPS4 proteins are components of two complexes, BLOC-3 and BLOC-4, involved in the biogenesis of lysosome-related organelles." J Biol Chem **278**(22): 20332-20337.

Chibbar, R., F. Shih, M. Baga, E. Torlakovic, K. Ramlall, R. Skomro, D. W. Cockcroft and E. G. Lemire (2004). "Nonspecific interstitial pneumonia and usual interstitial pneumonia with mutation in surfactant protein C in familial pulmonary fibrosis." Mod Pathol **17**(8): 973-980.

Chung, Y. H., B. Choi, D. H. Song, Y. Song, S. W. Kang, S. Y. Yoon, S. W. Kim, H. K. Lee and E. J. Chang (2014). "Interleukin-1beta promotes the LC3-mediated secretory function of osteoclast precursors by stimulating the Ca(2)(+)-dependent activation of ERK." Int J Biochem Cell Biol **54**: 198-207.

Clark, R. H., J. C. Stinchcombe, A. Day, E. Blott, S. Booth, G. Bossi, T. Hamblin, E. G. Davies and G. M. Griffiths (2003). "Adaptor protein 3-dependent microtubule-mediated movement of lytic granules to the immunological synapse." Nat Immunol **4**(11): 1111-1120.

Crawford, S. E., V. Stellmach, J. E. Murphy-Ullrich, S. M. Ribeiro, J. Lawler, R. O. Hynes, G. P. Boivin and N. Bouck (1998). "Thrombospondin-1 is a major activator of TGF-beta1 in vivo." Cell **93**(7): 1159-1170.

Crossno, P. F., V. V. Polosukhin, T. S. Blackwell, J. E. Johnson, C. Markin, P. E. Moore, J. A. Worrell, M. T. Stahlman, J. A. Phillips, 3rd, J. E. Loyd, J. D. Cogan and W. E. Lawson (2010). "Identification of early interstitial lung disease in an individual with genetic variations in ABCA3 and SFTPC." Chest **137**(4): 969-973.

Cuervo, A. M. (2011). "Chaperone-mediated autophagy: Dice's 'wild' idea about lysosomal selectivity." Nat Rev Mol Cell Biol **12**(8): 535-541.

Cuervo, A. M. and J. F. Dice (2000). "Unique properties of lamp2a compared to other lamp2 isoforms." J Cell Sci **113 Pt 24**: 4441-4450.

Cullinane, A. R., J. A. Curry, C. Carmona-Rivera, C. G. Summers, C. Ciccone, N. D. Cardillo, H. Dorward, R. A. Hess, J. G. White, D. Adams, M. Huizing and W. A. Gahl (2011). "A BLOC-1 mutation screen reveals that PLDN is mutated in Hermansky-Pudlak Syndrome type 9." Am J Hum Genet **88**(6): 778-787.

de Santi, M. M., P. A. Martorana, E. Cavarra and G. Lungarella (1995). "Pallid mice with genetic emphysema. Neutrophil elastase burden and elastin loss occur without alteration in the bronchoalveolar lavage cell population." Lab Invest **73**(1): 40-47.

Degryse, A. L. and W. E. Lawson (2011). "Progress toward improving animal models for idiopathic pulmonary fibrosis." Am J Med Sci **341**(6): 444-449.

Degryse, A. L., H. Tanjore, X. C. Xu, V. V. Polosukhin, B. R. Jones, F. B. McMahon, L. A. Gleaves, T. S. Blackwell and W. E. Lawson (2010). "Repetitive intratracheal bleomycin models several features of idiopathic pulmonary fibrosis." Am J Physiol Lung Cell Mol Physiol **299**(4): L442-452.

Dell'Angelica, E. C. (2004). "The building BLOC(k)s of lysosomes and related organelles." Curr Opin Cell Biol **16**(4): 458-464.

Dell'Angelica, E. C., R. C. Aguilar, N. Wolins, S. Hazelwood, W. A. Gahl and J. S. Bonifacino (2000). "Molecular characterization of the protein encoded by the Hermansky-Pudlak syndrome type 1 gene." J Biol Chem **275**(2): 1300-1306.

Dell'Angelica, E. C., V. Shotelersuk, R. C. Aguilar, W. A. Gahl and J. S. Bonifacino (1999). "Altered trafficking of lysosomal proteins in Hermansky-Pudlak syndrome due to mutations in the beta 3A subunit of the AP-3 adaptor." Mol Cell **3**(1): 11-21.

Detter, J. C., Q. Zhang, E. H. Mules, E. K. Novak, V. S. Mishra, W. Li, E. B. McMurtrie, V. T. Tchernev, M. R. Wallace, M. C. Seabra, R. T. Swank and S. F. Kingsmore (2000). "Rab geranylgeranyl transferase alpha mutation in the gunmetal mouse reduces Rab prenylation and platelet synthesis." Proc Natl Acad Sci U S A **97**(8): 4144-4149.

Dromparis, P., R. Paulin, T. H. Stenson, A. Haromy, G. Sutendra and E. D. Michelakis (2013). "Attenuating endoplasmic reticulum stress as a novel therapeutic strategy in pulmonary hypertension." Circulation **127**(1): 115-125.

Egan, J. J., J. P. Stewart, P. S. Hasleton, J. R. Arrand, K. B. Carroll and A. A. Woodcock (1995). "Epstein-Barr virus replication within pulmonary epithelial cells in cryptogenic fibrosing alveolitis." Thorax **50**(12): 1234-1239.

Englert, J. M., L. E. Hanford, N. Kaminski, J. M. Tobolewski, R. J. Tan, C. L. Fattman, L. Ramsgaard, T. J. Richards, I. Loutaev, P. P. Nawroth, M. Kasper, A. Bierhaus and T. D. Oury (2008). "A role for the receptor for advanced glycation end products in idiopathic pulmonary fibrosis." Am J Pathol **172**(3): 583-591.

Falcon-Perez, J. M., R. Nazarian, C. Sabatti and E. C. Dell'Angelica (2005). "Distribution and dynamics of Lamp1-containing endocytic organelles in fibroblasts deficient in BLOC-3." J Cell Sci **118**(Pt 22): 5243-5255.

Farber, H. W. and J. Loscalzo (2004). "Pulmonary arterial hypertension." N Engl J Med **351**(16): 1655-1665.

Feng, G. H., T. Bailin, J. Oh and R. A. Spritz (1997). "Mouse pale ear (ep) is homologous to human Hermansky-Pudlak syndrome and contains a rare 'AT-AC' intron." Hum Mol Genet **6**(5): 793-797.

Feng, L., E. K. Novak, L. M. Hartnell, J. S. Bonifacino, L. M. Collinson and R. T. Swank (2002). "The Hermansky-Pudlak syndrome 1 (HPS1) and HPS2 genes independently contribute to the production and function of platelet dense granules, melanosomes, and lysosomes." Blood **99**(5): 1651-1658.

Feng, L., A. B. Seymour, S. Jiang, A. To, A. A. Peden, E. K. Novak, L. Zhen, M. E. Rusiniak, E. M. Eicher, M. S. Robinson, M. B. Gorin and R. T. Swank (1999). "The beta3A subunit gene (Ap3b1) of the AP-3 adaptor complex is altered in the mouse hypopigmentation mutant pearl, a model for Hermansky-Pudlak syndrome and night blindness." Hum Mol Genet **8**(2): 323-330.

Fernandez, I. E. and O. Eickelberg (2012). "The impact of TGF-beta on lung fibrosis: from targeting to biomarkers." Proc Am Thorac Soc **9**(3): 111-116.

Fernandez Perez, E. R., C. E. Daniels, D. R. Schroeder, J. St Sauver, T. E. Hartman, B. J. Bartholmai, E. S. Yi and J. H. Ryu (2010). "Incidence, prevalence, and clinical course of idiopathic pulmonary fibrosis: a population-based study." Chest **137**(1): 129-137.

Fidzianska, A., E. Walczak and M. Walski (2007). "Abnormal chaperone-mediated autophagy (CMA) in cardiomyocytes of a boy with Danon disease." Folia Neuropathol **45**(3): 133-139.

Fujita, N., M. Hayashi-Nishino, H. Fukumoto, H. Omori, A. Yamamoto, T. Noda and T. Yoshimori (2008). "An Atg4B mutant hampers the lipidation of LC3 paralogues and causes defects in autophagosome closure." Mol Biol Cell **19**(11): 4651-4659.

Gahl, W. A., M. Brantly, M. I. Kaiser-Kupfer, F. Iwata, S. Hazelwood, V. Shotelersuk, L. F. Duffy, E. M. Kuehl, J. Troendle and I. Bernardini (1998). "Genetic defects and clinical characteristics of patients with a form of oculocutaneous albinism (Hermansky-Pudlak syndrome)." N Engl J Med **338**(18): 1258-1264.

Gahl, W. A., M. Brantly, J. Troendle, N. A. Avila, A. Padua, C. Montalvo, H. Cardona, K. A. Calis and B. Gochuico (2002). "Effect of pirfenidone on the pulmonary fibrosis of Hermansky-Pudlak syndrome." Mol Genet Metab **76**(3): 234-242.

Gao, F., V. L. Kinnula, M. Myllarniemi and T. D. Oury (2008). "Extracellular superoxide dismutase in pulmonary fibrosis." Antioxid Redox Signal **10**(2): 343-354.

Gardner, J. M., S. C. Wildenberg, N. M. Keiper, E. K. Novak, M. E. Rusiniak, R. T. Swank, N. Puri, J. N. Finger, N. Hagiwara, A. L. Lehman, T. L. Gales, M. E. Bayer, R. A. King and M. H. Brilliant (1997). "The mouse pale ear (ep) mutation is the homologue of human Hermansky-Pudlak syndrome." Proc Natl Acad Sci U S A **94**(17): 9238-9243.

Gochuico, B. R., M. Huizing, G. A. Golas, C. D. Scher, M. Tsokos, S. D. Denver, M. J. Frei-Jones and W. A. Gahl (2012). "Interstitial lung disease and pulmonary fibrosis in Hermansky-Pudlak syndrome type 2, an adaptor protein-3 complex disease." Mol Med **18**: 56-64.

Gribbin, J., R. B. Hubbard, I. Le Jeune, C. J. Smith, J. West and L. J. Tata (2006). "Incidence and mortality of idiopathic pulmonary fibrosis and sarcoidosis in the UK." Thorax **61**(11): 980-985.

Gross, T. J. and G. W. Hunninghake (2001). "Idiopathic pulmonary fibrosis." N Engl J Med **345**(7): 517-525.

Guillot, L., R. Epaud, G. Thouvenin, L. Jonard, A. Mohsni, R. Couderc, F. Counil, J. de Blic, R. A. Taam, M. Le Bourgeois, P. Reix, F. Flamein, A. Clement and D. Feldmann (2009). "New surfactant protein C gene mutations associated with diffuse lung disease." J Med Genet **46**(7): 490-494.

Guttentag, S. H., A. Akhtar, J. Q. Tao, E. Atochina, M. E. Rusiniak, R. T. Swank and S. R. Bates (2005). "Defective surfactant secretion in a mouse model of Hermansky-Pudlak syndrome." Am J Respir Cell Mol Biol **33**(1): 14-21.

Hardie, W. D., S. W. Glasser and J. S. Hagood (2009). "Emerging concepts in the pathogenesis of lung fibrosis." Am J Pathol **175**(1): 3-16.

Hermansky, F. and P. Pudlak (1959). "Albinism associated with hemorrhagic diathesis and unusual pigmented reticular cells in the bone marrow: report of two cases with histochemical studies." Blood **14**(2): 162-169.

Hsia, C. C., D. M. Hyde, M. Ochs and E. R. Weibel (2010). "An official research policy statement of the American Thoracic Society/European Respiratory Society: standards for quantitative assessment of lung structure." Am J Respir Crit Care Med **181**(4): 394-418.

Huang, L., Y. M. Kuo and J. Gitschier (1999). "The pallid gene encodes a novel, syntaxin 13-interacting protein involved in platelet storage pool deficiency." Nat Genet **23**(3): 329-332.

Huang, R., Y. Xu, W. Wan, X. Shou, J. Qian, Z. You, B. Liu, C. Chang, T. Zhou, J. Lippincott-Schwartz and W. Liu (2015). "Deacetylation of nuclear LC3 drives autophagy initiation under starvation." Mol Cell **57**(3): 456-466.

Huizing, M., Y. Anikster and W. A. Gahl (2000). "Hermansky-Pudlak syndrome and related disorders of organelle formation." Traffic **1**(11): 823-835.

Huizing, M., C. D. Scher, E. Strovel, D. L. Fitzpatrick, L. M. Hartnell, Y. Anikster and W. A. Gahl (2002). "Nonsense mutations in ADTB3A cause complete deficiency of the

beta3A subunit of adaptor complex-3 and severe Hermansky-Pudlak syndrome type 2." Pediatr Res **51**(2): 150-158.

Ichimura, Y., T. Kirisako, T. Takao, Y. Satomi, Y. Shimonishi, N. Ishihara, N. Mizushima, I. Tanida, E. Kominami, M. Ohsumi, T. Noda and Y. Ohsumi (2000). "A ubiquitin-like system mediates protein lipidation." Nature **408**(6811): 488-492.

Ihrke, G., A. Kyttala, M. R. Russell, B. A. Rous and J. P. Luzio (2004). "Differential use of two AP-3-mediated pathways by lysosomal membrane proteins." Traffic **5**(12): 946-962.

Inoue, D., H. Kubo, K. Taguchi, T. Suzuki, M. Komatsu, H. Motohashi and M. Yamamoto (2011). "Inducible disruption of autophagy in the lung causes airway hyper-responsiveness." Biochem Biophys Res Commun **405**(1): 13-18.

Iwai, K., T. Mori, N. Yamada, M. Yamaguchi and Y. Hosoda (1994). "Idiopathic pulmonary fibrosis. Epidemiologic approaches to occupational exposure." Am J Respir Crit Care Med **150**(3): 670-675.

Kantheti, P., X. Qiao, M. E. Diaz, A. A. Peden, G. E. Meyer, S. L. Carskadon, D. Kapfhamer, D. Sufalko, M. S. Robinson, J. L. Noebels and M. Burmeister (1998). "Mutation in AP-3 delta in the mocha mouse links endosomal transport to storage deficiency in platelets, melanosomes, and synaptic vesicles." Neuron **21**(1): 111-122.

Karim, M. R., T. Kanazawa, Y. Daigaku, S. Fujimura, G. Miotto and M. Kadowaki (2007). "Cytosolic LC3 ratio as a sensitive index of macroautophagy in isolated rat hepatocytes and H4-II-E cells." Autophagy **3**(6): 553-560.

Katzenstein, A. L. and J. L. Myers (1998). "Idiopathic pulmonary fibrosis: clinical relevance of pathologic classification." Am J Respir Crit Care Med **157**(4 Pt 1): 1301-1315.

Kelekar, A. (2005). "Autophagy." Ann N Y Acad Sci **1066**: 259-271.

Kim, H. P., X. Wang, Z. H. Chen, S. J. Lee, M. H. Huang, Y. Wang, S. W. Ryter and A. M. Choi (2008). "Autophagic proteins regulate cigarette smoke-induced apoptosis: protective role of heme oxygenase-1." Autophagy **4**(7): 887-895.

Kimura, S., T. Noda and T. Yoshimori (2007). "Dissection of the autophagosome maturation process by a novel reporter protein, tandem fluorescent-tagged LC3." Autophagy **3**(5): 452-460.

Kishimoto, T., K. Kato, H. Arakawa, K. Ashizawa, K. Inai and Y. Takeshima (2011). "Clinical, radiological, and pathological investigation of asbestosis." Int J Environ Res Public Health **8**(3): 899-912.

Klionsky, D. J. et al.(2016). "Guidelines for the use and interpretation of assays for monitoring autophagy (3rd edition)." Autophagy **12**(1): 1-222.

Klionsky, D. J. et al.(2008). "Guidelines for the use and interpretation of assays for monitoring autophagy in higher eukaryotes." Autophagy **4**(2): 151-175.

Klionsky, D. J. and S. D. Emr (2000). "Autophagy as a regulated pathway of cellular degradation." Science **290**(5497): 1717-1721.

Kloer, D. P., R. Rojas, V. Ivan, K. Moriyama, T. van Vlijmen, N. Murthy, R. Ghirlando, P. van der Sluijs, J. H. Hurley and J. S. Bonifacino (2010). "Assembly of the biogenesis of lysosome-related organelles complex-3 (BLOC-3) and its interaction with Rab9." J Biol Chem **285**(10): 7794-7804.

Koike, M., M. Shibata, S. Waguri, K. Yoshimura, I. Tanida, E. Kominami, T. Gotow, C. Peters, K. von Figura, N. Mizushima, P. Saftig and Y. Uchiyama (2005). "Participation of

autophagy in storage of lysosomes in neurons from mouse models of neuronal ceroid-lipofuscinoses (Batten disease)." Am J Pathol **167**(6): 1713-1728.

Komatsu, M., S. Waguri, M. Koike, Y. S. Sou, T. Ueno, T. Hara, N. Mizushima, J. Iwata, J. Ezaki, S. Murata, J. Hamazaki, Y. Nishito, S. Iemura, T. Natsume, T. Yanagawa, J. Uwayama, E. Warabi, H. Yoshida, T. Ishii, A. Kobayashi, M. Yamamoto, Z. Yue, Y. Uchiyama, E. Kominami and K. Tanaka (2007). "Homeostatic levels of p62 control cytoplasmic inclusion body formation in autophagy-deficient mice." Cell **131**(6): 1149-1163.

Konings, A. W. and J. J. Rasker (1978). "Subcellular localization of 57Co-bleomycin in normal and tumor tissues." Strahlentherapie **154**(1): 63-70.

Kook, S., P. Wang, L. R. Young, M. Schwake, P. Saftig, X. Weng, Y. Meng, D. Neculai, M. S. Marks, L. Gonzales, M. F. Beers and S. Guttentag (2016). "Impaired Lysosomal Integral Membrane Protein 2-dependent Peroxiredoxin 6 Delivery to Lamellar Bodies Accounts for Altered Alveolar Phospholipid Content in Adaptor Protein-3-deficient pearl Mice." J Biol Chem **291**(16): 8414-8427.

Korfei, M., C. Ruppert, P. Mahavadi, I. Henneke, P. Markart, M. Koch, G. Lang, L. Fink, R. M. Bohle, W. Seeger, T. E. Weaver and A. Guenther (2008). "Epithelial endoplasmic reticulum stress and apoptosis in sporadic idiopathic pulmonary fibrosis." Am J Respir Crit Care Med **178**(8): 838-846.

Korfei, M., D. von der Beck, I. Henneke, P. Markart, C. Ruppert, P. Mahavadi, B. Ghanim, W. Klepetko, L. Fink, S. Meiners, O. H. Kramer, W. Seeger, C. Vancheri and A. Guenther (2013). "Comparative proteome analysis of lung tissue from patients with idiopathic pulmonary fibrosis (IPF), non-specific interstitial pneumonia (NSIP) and organ donors." J Proteomics **85**: 109-128.

Lagares, D., O. Busnadiego, R. A. Garcia-Fernandez, M. Kapoor, S. Liu, D. E. Carter, D. Abraham, X. Shi-Wen, P. Carreira, B. A. Fontaine, B. S. Shea, A. M. Tager, A. Leask, S. Lamas and F. Rodriguez-Pascual (2012). "Inhibition of focal adhesion kinase prevents experimental lung fibrosis and myofibroblast formation." Arthritis Rheum **64**(5): 1653-1664.

Lamark, T., V. Kirkin, I. Dikic and T. Johansen (2009). "NBR1 and p62 as cargo receptors for selective autophagy of ubiquitinated targets." Cell Cycle **8**(13): 1986-1990.

Lappi-Blanco, E., S. T. Lehtonen, R. Sormunen, H. M. Merikallio, Y. Soini and R. L. Kaarteenaho (2013). "Divergence of tight and adherens junction factors in alveolar epithelium in pulmonary fibrosis." Hum Pathol **44**(5): 895-907.

Lawson, W. E., P. F. Crossno, V. V. Polosukhin, J. Roldan, D. S. Cheng, K. B. Lane, T. R. Blackwell, C. Xu, C. Markin, L. B. Ware, G. G. Miller, J. E. Loyd and T. S. Blackwell (2008). "Endoplasmic reticulum stress in alveolar epithelial cells is prominent in IPF: association with altered surfactant protein processing and herpesvirus infection." Am J Physiol Lung Cell Mol Physiol **294**(6): L1119-1126.

Lawson, W. E., V. V. Polosukhin, G. T. Stathopoulos, O. Zoia, W. Han, K. B. Lane, B. Li, E. F. Donnelly, G. E. Holburn, K. G. Lewis, R. D. Collins, W. M. Hull, S. W. Glasser, J. A. Whitsett and T. S. Blackwell (2005). "Increased and prolonged pulmonary fibrosis in surfactant protein C-deficient mice following intratracheal bleomycin." Am J Pathol **167**(5): 1267-1277.

Le Borgne, R., A. Alconada, U. Bauer and B. Hoflack (1998). "The mammalian AP-3 adaptor-like complex mediates the intracellular transport of lysosomal membrane glycoproteins." J Biol Chem **273**(45): 29451-29461.

Lee, C. G., S. J. Cho, M. J. Kang, S. P. Chapoval, P. J. Lee, P. W. Noble, T. Yehualaeshet, B. Lu, R. A. Flavell, J. Milbrandt, R. J. Homer and J. A. Elias (2004). "Early

growth response gene 1-mediated apoptosis is essential for transforming growth factor beta1-induced pulmonary fibrosis." J Exp Med **200**(3): 377-389.

Lee, S. J., A. Smith, L. Guo, T. P. Alastalo, M. Li, H. Sawada, X. Liu, Z. H. Chen, E. Ifedigbo, Y. Jin, C. Feghali-Bostwick, S. W. Ryter, H. P. Kim, M. Rabinovitch and A. M. Choi (2011). "Autophagic protein LC3B confers resistance against hypoxia-induced pulmonary hypertension." Am J Respir Crit Care Med **183**(5): 649-658.

Li, W., M. E. Rusiniak, S. Chintala, R. Gautam, E. K. Novak and R. T. Swank (2004). "Murine Hermansky-Pudlak syndrome genes: regulators of lysosome-related organelles." Bioessays **26**(6): 616-628.

Li, W., Q. Zhang, N. Oiso, E. K. Novak, R. Gautam, E. P. O'Brien, C. L. Tinsley, D. J. Blake, R. A. Spritz, N. G. Copeland, N. A. Jenkins, D. Amato, B. A. Roe, M. Starcevic, E. C. Dell'Angelica, R. W. Elliott, V. Mishra, S. F. Kingsmore, R. E. Paylor and R. T. Swank (2003). "Hermansky-Pudlak syndrome type 7 (HPS-7) results from mutant dysbindin, a member of the biogenesis of lysosome-related organelles complex 1 (BLOC-1)." Nat Genet **35**(1): 84-89.

Liang, X. H., L. K. Kleeman, H. H. Jiang, G. Gordon, J. E. Goldman, G. Berry, B. Herman and B. Levine (1998). "Protection against fatal Sindbis virus encephalitis by beclin, a novel Bcl-2-interacting protein." J Virol **72**(11): 8586-8596.

Liao, G., Y. Yao, J. Liu, Z. Yu, S. Cheung, A. Xie, X. Liang and X. Bi (2007). "Cholesterol accumulation is associated with lysosomal dysfunction and autophagic stress in Npc1 -/- mouse brain." Am J Pathol **171**(3): 962-975.

Liebau, M. C., F. Braun, K. Hopker, C. Weitbrecht, V. Bartels, R. U. Muller, S. Brodesser, M. A. Saleem, T. Benzing, B. Schermer, M. Cybulla and C. E. Kurschat (2013). "Dysregulated autophagy contributes to podocyte damage in Fabry's disease." PLoS One **8**(5): e63506.

Lieberman, A. P., R. Puertollano, N. Raben, S. Slaugenhaupt, S. U. Walkley and A. Ballabio (2012). "Autophagy in lysosomal storage disorders." Autophagy **8**(5): 719-730.

Lin, H. H., X. Li, J. L. Chen, X. Sun, F. N. Cooper, Y. R. Chen, W. Zhang, Y. Chung, A. Li, C. T. Cheng, L. Yang, X. Deng, X. Liu, Y. Yen, D. L. Johnson, H. M. Shih, A. Yang and D. K. Ann (2012). "Identification of an AAA ATPase VPS4B-dependent pathway that modulates epidermal growth factor receptor abundance and signaling during hypoxia." Mol Cell Biol **32**(6): 1124-1138.

Liu, J., Y. Lin, H. Yang, Q. Deng, G. Chen and J. He (2011). "The expression of p33(ING1), p53, and autophagy-related gene Beclin1 in patients with non-small cell lung cancer." Tumour Biol **32**(6): 1113-1121.

Lloyd, V., M. Ramaswami and H. Kramer (1998). "Not just pretty eyes: Drosophila eye-colour mutations and lysosomal delivery." Trends Cell Biol **8**(7): 257-259.

Luciani, A., V. R. Villella, S. Esposito, N. Brunetti-Pierri, D. Medina, C. Settembre, M. Gavina, L. Pulze, I. Giardino, M. Pettoello-Mantovani, M. D'Apolito, S. Guido, E. Masliah, B. Spencer, S. Quaratino, V. Raia, A. Ballabio and L. Maiuri (2010). "Defective CFTR induces aggresome formation and lung inflammation in cystic fibrosis through ROS-mediated autophagy inhibition." Nat Cell Biol **12**(9): 863-875.

Lyerla, T. A., M. E. Rusiniak, M. Borchers, G. Jahreis, J. Tan, P. Ohtake, E. K. Novak and R. T. Swank (2003). "Aberrant lung structure, composition, and function in a murine model of Hermansky-Pudlak syndrome." Am J Physiol Lung Cell Mol Physiol **285**(3): L643-653.

Mahavadi, P., M. Korfei, I. Henneke, G. Liebisch, G. Schmitz, B. R. Gochuico, P. Markart, S. Bellusci, W. Seeger, C. Ruppert and A. Guenther (2010). "Epithelial stress and

apoptosis underlie Hermansky-Pudlak syndrome-associated interstitial pneumonia." Am J Respir Crit Care Med **182**(2): 207-219.

Maher, T. M. (2010). "Pirfenidone in idiopathic pulmonary fibrosis." Drugs Today (Barc) **46**(7): 473-482.

Mai, S., B. Muster, J. Bereiter-Hahn and M. Jendrach (2012). "Autophagy proteins LC3B, ATG5 and ATG12 participate in quality control after mitochondrial damage and influence lifespan." Autophagy **8**(1): 47-62.

Maiuri, M. C., E. Zalckvar, A. Kimchi and G. Kroemer (2007). "Self-eating and self-killing: crosstalk between autophagy and apoptosis." Nat Rev Mol Cell Biol **8**(9): 741-752.

Marino, G., M. Niso-Santano, E. H. Baehrecke and G. Kroemer (2014). "Self-consumption: the interplay of autophagy and apoptosis." Nat Rev Mol Cell Biol **15**(2): 81-94.

Martina, J. A., K. Moriyama and J. S. Bonifacino (2003). "BLOC-3, a protein complex containing the Hermansky-Pudlak syndrome gene products HPS1 and HPS4." J Biol Chem **278**(31): 29376-29384.

Martinez-Lopez, N., D. Athonvarangkul, P. Mishall, S. Sahu and R. Singh (2013). "Autophagy proteins regulate ERK phosphorylation." Nat Commun **4**: 2799.

Mastorci, K., B. Montico, D. A. Fae, L. Sigalotti, M. Ponzoni, G. Inghirami, R. Dolcetti and J. Dal Col (2016). "Phospholipid scramblase 1 as a critical node at the crossroad between autophagy and apoptosis in mantle cell lymphoma." Oncotarget **7**(27): 41913-41928.

Mayhew, T. M. and J. M. Lucocq (2008). "Quantifying immunogold labelling patterns of cellular compartments when they comprise mixtures of membranes (surface-occupying) and organelles (volume-occupying)." Histochem Cell Biol **129**(3): 367-378.

McGarry, M. P., M. Reddington, E. K. Novak and R. T. Swank (1999). "Survival and lung pathology of mouse models of Hermansky-Pudlak syndrome and Chediak-Higashi syndrome." Proc Soc Exp Biol Med **220**(3): 162-168.

Menzies, F. M., A. Fleming and D. C. Rubinsztein (2015). "Compromised autophagy and neurodegenerative diseases." Nat Rev Neurosci **16**(6): 345-357.

Miller, C. L., M. Burmeister and K. E. Stevens (1999). "Hippocampal auditory gating in the hyperactive mocha mouse." Neurosci Lett **276**(1): 57-60.

Miyake, Y., S. Sasaki, T. Yokoyama, K. Chida, A. Azuma, T. Suda, S. Kudoh, N. Sakamoto, K. Okamoto, G. Kobashi, M. Washio, Y. Inaba and H. Tanaka (2005). "Occupational and environmental factors and idiopathic pulmonary fibrosis in Japan." Ann Occup Hyg **49**(3): 259-265.

Moeller, A., K. Ask, D. Warburton, J. Gauldie and M. Kolb (2008). "The bleomycin animal model: a useful tool to investigate treatment options for idiopathic pulmonary fibrosis?" Int J Biochem Cell Biol **40**(3): 362-382.

Moore, B. B. and C. M. Hogaboam (2008). "Murine models of pulmonary fibrosis." Am J Physiol Lung Cell Mol Physiol **294**(2): L152-160.

Moore, B. B., R. Paine, 3rd, P. J. Christensen, T. A. Moore, S. Sitterding, R. Ngan, C. A. Wilke, W. A. Kuziel and G. B. Toews (2001). "Protection from pulmonary fibrosis in the absence of CCR2 signaling." J Immunol **167**(8): 4368-4377.

Morgan, N. V., S. Pasha, C. A. Johnson, J. R. Ainsworth, R. A. Eady, B. Dawood, C. McKeown, R. C. Trembath, J. Wilde, S. P. Watson and E. R. Maher (2006). "A germline mutation in BLOC1S3/reduced pigmentation causes a novel variant of Hermansky-Pudlak syndrome (HPS8)." Am J Hum Genet **78**(1): 160-166.

Mortensen, M., D. J. Ferguson, M. Edelmann, B. Kessler, K. J. Morten, M. Komatsu and A. K. Simon (2010). "Loss of autophagy in erythroid cells leads to defective removal of mitochondria and severe anemia in vivo." Proc Natl Acad Sci U S A **107**(2): 832-837.

Muggia, F. M., A. C. Louie and B. I. Sikic (1983). "Pulmonary toxicity of antitumor agents." Cancer Treat Rev **10**(4): 221-243.

Mulugeta, S., V. Nguyen, S. J. Russo, M. Muniswamy and M. F. Beers (2005). "A surfactant protein C precursor protein BRICHOS domain mutation causes endoplasmic reticulum stress, proteasome dysfunction, and caspase 3 activation." Am J Respir Cell Mol Biol **32**(6): 521-530.

Nakagawa, I., A. Amano, N. Mizushima, A. Yamamoto, H. Yamaguchi, T. Kamimoto, A. Nara, J. Funao, M. Nakata, K. Tsuda, S. Hamada and T. Yoshimori (2004). "Autophagy defends cells against invading group A Streptococcus." Science **306**(5698): 1037-1040.

Nathan, S. D., O. A. Shlobin, N. Weir, S. Ahmad, J. M. Kaldjob, E. Battle, M. J. Sheridan and R. M. du Bois (2011). "Long-term course and prognosis of idiopathic pulmonary fibrosis in the new millennium." Chest **140**(1): 221-229.

Natsuga, K., M. Akiyama, T. Shimizu, T. Suzuki, S. Ito, Y. Tomita, J. Tanaka and H. Shimizu (2005). "Ultrastructural features of trafficking defects are pronounced in melanocytic nevus in Hermansky-Pudlak syndrome type 1." J Invest Dermatol **125**(1): 154-158.

Navaratnam, V., K. M. Fleming, J. West, C. J. Smith, R. G. Jenkins, A. Fogarty and R. B. Hubbard (2011). "The rising incidence of idiopathic pulmonary fibrosis in the U.K." Thorax **66**(6): 462-467.

Nazarian, R., J. M. Falcon-Perez and E. C. Dell'Angelica (2003). "Biogenesis of lysosome-related organelles complex 3 (BLOC-3): a complex containing the Hermansky-Pudlak syndrome (HPS) proteins HPS1 and HPS4." Proc Natl Acad Sci U S A **100**(15): 8770-8775.

Nightingale, J. A., R. Maggs, P. Cullinan, L. E. Donnelly, D. F. Rogers, R. Kinnersley, K. F. Chung, P. J. Barnes, M. Ashmore and A. Newman-Taylor (2000). "Airway inflammation after controlled exposure to diesel exhaust particulates." Am J Respir Crit Care Med **162**(1): 161-166.

Nixon, R. A. (2013). "The role of autophagy in neurodegenerative disease." Nat Med **19**(8): 983-997.

Nogee, L. M., A. E. Dunbar, 3rd, S. E. Wert, F. Askin, A. Hamvas and J. A. Whitsett (2001). "A mutation in the surfactant protein C gene associated with familial interstitial lung disease." N Engl J Med **344**(8): 573-579.

Noth, I., S. M. Zangan, R. V. Soares, A. Forsythe, C. Demchuk, S. M. Takahashi, S. B. Patel, M. E. Strek, J. A. Krishnan, M. G. Patti and H. Macmahon (2012). "Prevalence of hiatal hernia by blinded multidetector CT in patients with idiopathic pulmonary fibrosis." Eur Respir J **39**(2): 344-351.

Novak, E. K., S. W. Hui and R. T. Swank (1981). "The mouse pale ear pigment mutant as a possible animal model for human platelet storage pool deficiency." Blood **57**(1): 38-43.

Novak, E. K., S. W. Hui and R. T. Swank (1984). "Platelet storage pool deficiency in mouse pigment mutations associated with seven distinct genetic loci." Blood **63**(3): 536-544.

Odorizzi, G., C. R. Cowles and S. D. Emr (1998). "The AP-3 complex: a coat of many colours." Trends Cell Biol **8**(7): 282-288.

Oh, J., T. Bailin, K. Fukai, G. H. Feng, L. Ho, J. I. Mao, E. Frenk, N. Tamura and R. A. Spritz (1996). "Positional cloning of a gene for Hermansky-Pudlak syndrome, a disorder of cytoplasmic organelles." Nat Genet **14**(3): 300-306.

Oh, J., L. Ho, S. Ala-Mello, D. Amato, L. Armstrong, S. Bellucci, G. Carakushansky, J. P. Ellis, C. T. Fong, J. S. Green, E. Heon, E. Legius, A. V. Levin, H. K. Nieuwenhuis, A. Pinckers, N. Tamura, M. L. Whiteford, H. Yamasaki and R. A. Spritz (1998). "Mutation analysis of patients with Hermansky-Pudlak syndrome: a frameshift hot spot in the HPS gene and apparent locus heterogeneity." Am J Hum Genet **62**(3): 593-598.

Oldham, J. M. and I. Noth (2014). "Idiopathic pulmonary fibrosis: early detection and referral." Respir Med **108**(6): 819-829.

Oral, O., D. Oz-Arslan, Z. Itah, A. Naghavi, R. Deveci, S. Karacali and D. Gozuacik (2012). "Cleavage of Atg3 protein by caspase-8 regulates autophagy during receptor-activated cell death." Apoptosis **17**(8): 810-820.

Osellame, L. D. and M. R. Duchen (2013). "Defective quality control mechanisms and accumulation of damaged mitochondria link Gaucher and Parkinson diseases." Autophagy **9**(10): 1633-1635.

Pacheco, C. D., R. Kunkel and A. P. Lieberman (2007). "Autophagy in Niemann-Pick C disease is dependent upon Beclin-1 and responsive to lipid trafficking defects." Hum Mol Genet **16**(12): 1495-1503.

Pankiv, S., T. H. Clausen, T. Lamark, A. Brech, J. A. Bruun, H. Outzen, A. Overvatn, G. Bjorkoy and T. Johansen (2007). "p62/SQSTM1 binds directly to Atg8/LC3 to facilitate degradation of ubiquitinated protein aggregates by autophagy." J Biol Chem **282**(33): 24131-24145.

Patel, A. S., L. Lin, A. Geyer, J. A. Haspel, C. H. An, J. Cao, I. O. Rosas and D. Morse (2012). "Autophagy in idiopathic pulmonary fibrosis." PLoS One **7**(7): e41394.

Peden, A. A., V. Oorschot, B. A. Hesser, C. D. Austin, R. H. Scheller and J. Klumperman (2004). "Localization of the AP-3 adaptor complex defines a novel endosomal exit site for lysosomal membrane proteins." J Cell Biol **164**(7): 1065-1076.

Peden, A. A., R. E. Rudge, W. W. Lui and M. S. Robinson (2002). "Assembly and function of AP-3 complexes in cells expressing mutant subunits." J Cell Biol **156**(2): 327-336.

Pfeffer, S. R. (1999). "Transport-vesicle targeting: tethers before SNAREs." Nat Cell Biol **1**(1): E17-22.

Pierson, D. M., D. Ionescu, G. Qing, A. M. Yonan, K. Parkinson, T. C. Colby and K. Leslie (2006). "Pulmonary fibrosis in hermansky-pudlak syndrome. a case report and review." Respiration **73**(3): 382-395.

Poornima Mahavadi, L. K., Shalini Venkatesan, Ingrid Henneke, Jan Hegermann, Christoph Wrede, Matthias Ochs, Saket Ahuja, Shashi Chillappagari, Clemens Ruppert, Werner Seeger, Martina Korfei and Andreas Guenther (2015). "Regulation of macroautophagy in amiodarone-induced pulmonary fibrosis." The Journal of Pathology: Clinical Research **1**(4): 252-263.

Pron, G., N. Mahrour, S. Orlowski, O. Tounekti, B. Poddevin, J. Belehradek, Jr. and L. M. Mir (1999). "Internalisation of the bleomycin molecules responsible for bleomycin toxicity: a receptor-mediated endocytosis mechanism." Biochem Pharmacol **57**(1): 45-56.

Puissant, A., N. Fenouille and P. Auberger (2012). "When autophagy meets cancer through p62/SQSTM1." Am J Cancer Res **2**(4): 397-413.

Pulkkinen, V., S. Bruce, J. Rintahaka, U. Hodgson, T. Laitinen, H. Alenius, V. L. Kinnula, M. Myllarniemi, S. Matikainen and J. Kere (2010). "ELMOD2, a candidate gene for idiopathic pulmonary fibrosis, regulates antiviral responses." FASEB J **24**(4): 1167-1177.

Pyo, J. O., S. M. Yoo, H. H. Ahn, J. Nah, S. H. Hong, T. I. Kam, S. Jung and Y. K. Jung (2013). "Overexpression of Atg5 in mice activates autophagy and extends lifespan." Nat Commun **4**: 2300.

Qu, X., J. Yu, G. Bhagat, N. Furuya, H. Hibshoosh, A. Troxel, J. Rosen, E. L. Eskelinen, N. Mizushima, Y. Ohsumi, G. Cattoretti and B. Levine (2003). "Promotion of tumorigenesis by heterozygous disruption of the beclin 1 autophagy gene." J Clin Invest **112**(12): 1809-1820.

Raben, N., R. Baum, C. Schreiner, S. Takikita, N. Mizushima, E. Ralston and P. Plotz (2009). "When more is less: excess and deficiency of autophagy coexist in skeletal muscle in Pompe disease." Autophagy **5**(1): 111-113.

Raben, N., V. Hill, L. Shea, S. Takikita, R. Baum, N. Mizushima, E. Ralston and P. Plotz (2008). "Suppression of autophagy in skeletal muscle uncovers the accumulation of ubiquitinated proteins and their potential role in muscle damage in Pompe disease." Hum Mol Genet **17**(24): 3897-3908.

Raghu, G., H. R. Collard, J. J. Egan, F. J. Martinez, J. Behr, K. K. Brown, T. V. Colby, J. F. Cordier, K. R. Flaherty, J. A. Lasky, D. A. Lynch, J. H. Ryu, J. J. Swigris, A. U. Wells, J. Ancochea, D. Bouros, C. Carvalho, U. Costabel, M. Ebina, D. M. Hansell, T. Johkoh, D. S. Kim, T. E. King, Jr., Y. Kondoh, J. Myers, N. L. Muller, A. G. Nicholson, L. Richeldi, M. Selman, R. F. Dudden, B. S. Griss, S. L. Protzko and H. J. Schunemann (2011). "An official ATS/ERS/JRS/ALAT statement: idiopathic pulmonary fibrosis: evidence-based guidelines for diagnosis and management." Am J Respir Crit Care Med **183**(6): 788-824.

Raghu, G., T. D. Freudenberger, S. Yang, J. R. Curtis, C. Spada, J. Hayes, J. K. Sillery, C. E. Pope, 2nd and C. A. Pellegrini (2006). "High prevalence of abnormal acid gastro-oesophageal reflux in idiopathic pulmonary fibrosis." Eur Respir J **27**(1): 136-142.

Raghu, G., D. Weycker, J. Edelsberg, W. Z. Bradford and G. Oster (2006). "Incidence and prevalence of idiopathic pulmonary fibrosis." Am J Respir Crit Care Med **174**(7): 810-816.

Redente, E. F., K. M. Jacobsen, J. J. Solomon, A. R. Lara, S. Faubel, R. C. Keith, P. M. Henson, G. P. Downey and D. W. Riches (2011). "Age and sex dimorphisms contribute to the severity of bleomycin-induced lung injury and fibrosis." Am J Physiol Lung Cell Mol Physiol **301**(4): L510-518.

Ricci, A., E. Cherubini, D. Scozzi, V. Pietrangeli, L. Tabbi, S. Raffa, L. Leone, V. Visco, M. R. Torrisi, P. Bruno, R. Mancini, G. Ciliberto, C. Terzano and S. Mariotta (2013). "Decreased expression of autophagic beclin 1 protein in idiopathic pulmonary fibrosis fibroblasts." J Cell Physiol **228**(7): 1516-1524.

Richmond, B., M. Huizing, J. Knapp, A. Koshoffer, Y. Zhao, W. A. Gahl and R. E. Boissy (2005). "Melanocytes derived from patients with Hermansky-Pudlak Syndrome types 1, 2, and 3 have distinct defects in cargo trafficking." J Invest Dermatol **124**(2): 420-427.

Roberts, S. N., S. E. Howie, W. A. Wallace, D. M. Brown, D. Lamb, E. A. Ramage and K. Donaldson (1995). "A novel model for human interstitial lung disease: hapten-driven lung fibrosis in rodents." J Pathol **176**(3): 309-318.

Roggli, V. L., A. R. Gibbs, R. Attanoos, A. Churg, H. Popper, P. Cagle, B. Corrin, T. J. Franks, F. Galateau-Salle, J. Galvin, P. S. Hasleton, D. W. Henderson and K. Honma (2010). "Pathology of asbestosis- An update of the diagnostic criteria: Report of the asbestosis committee of the college of american pathologists and pulmonary pathology society." Arch Pathol Lab Med **134**(3): 462-480.

Rommens, J. M., M. C. Iannuzzi, B. Kerem, M. L. Drumm, G. Melmer, M. Dean, R. Rozmahel, J. L. Cole, D. Kennedy, N. Hidaka and et al. (1989). "Identification of the cystic fibrosis gene: chromosome walking and jumping." Science **245**(4922): 1059-1065.

Ryu, J. H., T. Moua, C. E. Daniels, T. E. Hartman, E. S. Yi, J. P. Utz and A. H. Limper (2014). "Idiopathic pulmonary fibrosis: evolving concepts." Mayo Clin Proc **89**(8): 1130-1142.

Samuel, C. S., C. Zhao, R. A. Bathgate, C. P. Bond, M. D. Burton, L. J. Parry, R. J. Summers, M. L. Tang, E. P. Amento and G. W. Tregear (2003). "Relaxin deficiency in mice is associated with an age-related progression of pulmonary fibrosis." FASEB J **17**(1): 121-123.

Sanchez, V. C., J. R. Pietruska, N. R. Miselis, R. H. Hurt and A. B. Kane (2009). "Biopersistence and potential adverse health impacts of fibrous nanomaterials: what have we learned from asbestos?" Wiley Interdiscip Rev Nanomed Nanobiotechnol **1**(5): 511-529.

Sardiello, M., M. Palmieri, A. di Ronza, D. L. Medina, M. Valenza, V. A. Gennarino, C. Di Malta, F. Donaudy, V. Embrione, R. S. Polishchuk, S. Banfi, G. Parenti, E. Cattaneo and A. Ballabio (2009). "A gene network regulating lysosomal biogenesis and function." Science **325**(5939): 473-477.

Sato, Y., R. Tsuboi, R. Lyons, H. Moses and D. B. Rifkin (1990). "Characterization of the activation of latent TGF-beta by co-cultures of endothelial cells and pericytes or smooth muscle cells: a self-regulating system." J Cell Biol **111**(2): 757-763.

Scotton, C. J. and R. C. Chambers (2007). "Molecular targets in pulmonary fibrosis: the myofibroblast in focus." Chest **132**(4): 1311-1321.

Seibold, M. A., A. L. Wise, M. C. Speer, M. P. Steele, K. K. Brown, J. E. Loyd, T. E. Fingerlin, W. Zhang, G. Gudmundsson, S. D. Groshong, C. M. Evans, S. Garantziotis, K. B. Adler, B. F. Dickey, R. M. du Bois, I. V. Yang, A. Herron, D. Kervitsky, J. L. Talbert, C. Markin, J. Park, A. L. Crews, S. H. Slifer, S. Auerbach, M. G. Roy, J. Lin, C. E. Hennessy, M. I. Schwarz and D. A. Schwartz (2011). "A common MUC5B promoter polymorphism and pulmonary fibrosis." N Engl J Med **364**(16): 1503-1512.

Seixas, E., M. Barros, M. C. Seabra and D. C. Barral (2013). "Rab and Arf proteins in genetic diseases." Traffic **14**(8): 871-885.

Selman, M., T. E. King and A. Pardo (2001). "Idiopathic pulmonary fibrosis: prevailing and evolving hypotheses about its pathogenesis and implications for therapy." Ann Intern Med **134**(2): 136-151.

Selman, M. and A. Pardo (2006). "Role of epithelial cells in idiopathic pulmonary fibrosis: from innocent targets to serial killers." Proc Am Thorac Soc **3**(4): 364-372.

Semenza, G. L. (2011). "Oxygen sensing, homeostasis, and disease." N Engl J Med **365**(6): 537-547.

Settembre, C., A. Fraldi, L. Jahreiss, C. Spampanato, C. Venturi, D. Medina, R. de Pablo, C. Tacchetti, D. C. Rubinsztein and A. Ballabio (2008). "A block of autophagy in lysosomal storage disorders." Hum Mol Genet **17**(1): 119-129.

Settembre, C., R. Zoncu, D. L. Medina, F. Vetrini, S. Erdin, T. Huynh, M. Ferron, G. Karsenty, M. C. Vellard, V. Facchinetti, D. M. Sabatini and A. Ballabio (2012). "A lysosome-to-nucleus signalling mechanism senses and regulates the lysosome via mTOR and TFEB." EMBO J **31**(5): 1095-1108.

Sheppard, D. (2006). "Transforming growth factor beta: a central modulator of pulmonary and airway inflammation and fibrosis." Proc Am Thorac Soc **3**(5): 413-417.

Shotelersuk, V., E. C. Dell'Angelica, L. Hartnell, J. S. Bonifacino and W. A. Gahl (2000). "A new variant of Hermansky-Pudlak syndrome due to mutations in a gene responsible for vesicle formation." Am J Med **108**(5): 423-427.

Shotelersuk, V. and W. A. Gahl (1998). "Hermansky-Pudlak syndrome: models for intracellular vesicle formation." Mol Genet Metab **65**(2): 85-96.

Sime, P. J., Z. Xing, F. L. Graham, K. G. Csaky and J. Gauldie (1997). "Adenovector-mediated gene transfer of active transforming growth factor-beta1 induces prolonged severe fibrosis in rat lung." J Clin Invest **100**(4): 768-776.

Sisson, T. H., M. Mendez, K. Choi, N. Subbotina, A. Courey, A. Cunningham, A. Dave, J. F. Engelhardt, X. Liu, E. S. White, V. J. Thannickal, B. B. Moore, P. J. Christensen and R. H. Simon (2010). "Targeted injury of type II alveolar epithelial cells induces pulmonary fibrosis." Am J Respir Crit Care Med **181**(3): 254-263.

Spampanato, C., E. Feeney, L. Li, M. Cardone, J. A. Lim, F. Annunziata, H. Zare, R. Polishchuk, R. Puertollano, G. Parenti, A. Ballabio and N. Raben (2013). "Transcription factor EB (TFEB) is a new therapeutic target for Pompe disease." EMBO Mol Med **5**(5): 691-706.

Starcher, B. C., C. Kuhn and J. E. Overton (1978). "Increased elastin and collagen content in the lungs of hamsters receiving an intratracheal injection of bleomycin." Am Rev Respir Dis **117**(2): 299-305.

Stewart, J. P., J. J. Egan, A. J. Ross, B. G. Kelly, S. S. Lok, P. S. Hasleton and A. A. Woodcock (1999). "The detection of Epstein-Barr virus DNA in lung tissue from patients with idiopathic pulmonary fibrosis." Am J Respir Crit Care Med **159**(4 Pt 1): 1336-1341.

Sueblinvong, V., D. C. Neujahr, S. T. Mills, S. Roser-Page, J. D. Ritzenthaler, D. Guidot, M. Rojas and J. Roman (2012). "Predisposition for disrepair in the aged lung." Am J Med Sci **344**(1): 41-51.

Sugita, M., X. Cao, G. F. Watts, R. A. Rogers, J. S. Bonifacino and M. B. Brenner (2002). "Failure of trafficking and antigen presentation by CD1 in AP-3-deficient cells." Immunity **16**(5): 697-706.

Sun, Y., B. Liou, H. Ran, M. R. Skelton, M. T. Williams, C. V. Vorhees, K. Kitatani, Y. A. Hannun, D. P. Witte, Y. H. Xu and G. A. Grabowski (2010). "Neuronopathic Gaucher disease in the mouse: viable combined selective saposin C deficiency and mutant glucocerebrosidase (V394L) mice with glucosylsphingosine and glucosylceramide accumulation and progressive neurological deficits." Hum Mol Genet **19**(6): 1088-1097.

Suzuki, T., W. Li, Q. Zhang, A. Karim, E. K. Novak, E. V. Sviderskaya, S. P. Hill, D. C. Bennett, A. V. Levin, H. K. Nieuwenhuis, C. T. Fong, C. Castellan, B. Miterski, R. T. Swank and R. A. Spritz (2002). "Hermansky-Pudlak syndrome is caused by mutations in HPS4, the human homolog of the mouse light-ear gene." Nat Genet **30**(3): 321-324.

Suzuki, T., N. Oiso, R. Gautam, E. K. Novak, J. J. Panthier, P. G. Suprabha, T. Vida, R. T. Swank and R. A. Spritz (2003). "The mouse organellar biogenesis mutant buff results from a mutation in Vps33a, a homologue of yeast vps33 and Drosophila carnation." Proc Natl Acad Sci U S A **100**(3): 1146-1150.

Swank, R. T., E. K. Novak, M. P. McGarry, M. E. Rusiniak and L. Feng (1998). "Mouse models of Hermansky Pudlak syndrome: a review." Pigment Cell Res **11**(2): 60-80.

Swank, R. T., E. K. Novak, M. P. McGarry, Y. Zhang, W. Li, Q. Zhang and L. Feng (2000). "Abnormal vesicular trafficking in mouse models of Hermansky-Pudlak syndrome." Pigment Cell Res **13 Suppl 8**: 59-67.

Takacs-Vellai, K., T. Vellai, A. Puoti, M. Passannante, C. Wicky, A. Streit, A. L. Kovacs and F. Muller (2005). "Inactivation of the autophagy gene bec-1 triggers apoptotic cell death in C. elegans." Curr Biol **15**(16): 1513-1517.

Tanaka, Y., G. Guhde, A. Suter, E. L. Eskelinen, D. Hartmann, R. Lullmann-Rauch, P. M. Janssen, J. Blanz, K. von Figura and P. Saftig (2000). "Accumulation of autophagic vacuoles and cardiomyopathy in LAMP-2-deficient mice." Nature **406**(6798): 902-906.

Tang, Y. W., J. E. Johnson, P. J. Browning, R. A. Cruz-Gervis, A. Davis, B. S. Graham, K. L. Brigham, J. A. Oates, Jr., J. E. Loyd and A. A. Stecenko (2003). "Herpesvirus DNA is consistently detected in lungs of patients with idiopathic pulmonary fibrosis." J Clin Microbiol **41**(6): 2633-2640.

Tanjore, H., T. S. Blackwell and W. E. Lawson (2012). "Emerging evidence for endoplasmic reticulum stress in the pathogenesis of idiopathic pulmonary fibrosis." Am J Physiol Lung Cell Mol Physiol **302**(8): L721-729.

Taskar, V. S. and D. B. Coultas (2006). "Is idiopathic pulmonary fibrosis an environmental disease?" Proc Am Thorac Soc **3**(4): 293-298.

Teng, R. J., J. Du, S. Welak, T. Guan, A. Eis, Y. Shi and G. G. Konduri (2012). "Cross talk between NADPH oxidase and autophagy in pulmonary artery endothelial cells with intrauterine persistent pulmonary hypertension." Am J Physiol Lung Cell Mol Physiol **302**(7): L651-663.

Thrall, R. S., J. R. McCormick, R. M. Jack, R. A. McReynolds and P. A. Ward (1979). "Bleomycin-induced pulmonary fibrosis in the rat: inhibition by indomethacin." Am J Pathol **95**(1): 117-130.

Tierney, D. F. (1989). "Lung surfactant: some historical perspectives leading to its cellular and molecular biology." Am J Physiol **257**(2 Pt 1): L1-12.

Tomashefski, J. F., Jr. (2000). "Pulmonary pathology of acute respiratory distress syndrome." Clin Chest Med **21**(3): 435-466.

Toth, M. L., T. Sigmond, E. Borsos, J. Barna, P. Erdelyi, K. Takacs-Vellai, L. Orosz, A. L. Kovacs, G. Csikos, M. Sass and T. Vellai (2008). "Longevity pathways converge on autophagy genes to regulate life span in Caenorhabditis elegans." Autophagy **4**(3): 330-338.

Varga, J. and S. A. Jimenez (1986). "Stimulation of normal human fibroblast collagen production and processing by transforming growth factor-beta." Biochem Biophys Res Commun **138**(2): 974-980.

Vasilescu, D. M., Z. Gao, P. K. Saha, L. Yin, G. Wang, B. Haefeli-Bleuer, M. Ochs, E. R. Weibel and E. A. Hoffman (2012). "Assessment of morphometry of pulmonary acini in mouse lungs by nondestructive imaging using multiscale microcomputed tomography." Proc Natl Acad Sci U S A **109**(42): 17105-17110.

Venugopal, B., N. T. Mesires, J. C. Kennedy, C. Curcio-Morelli, J. M. Laplante, J. F. Dice and S. A. Slaugenhaupt (2009). "Chaperone-mediated autophagy is defective in mucolipidosis type IV." J Cell Physiol **219**(2): 344-353.

Vergarajauregui, S., P. S. Connelly, M. P. Daniels and R. Puertollano (2008). "Autophagic dysfunction in mucolipidosis type IV patients." Hum Mol Genet **17**(17): 2723-2737.

Vestbo, J., S. S. Hurd, A. G. Agusti, P. W. Jones, C. Vogelmeier, A. Anzueto, P. J. Barnes, L. M. Fabbri, F. J. Martinez, M. Nishimura, R. A. Stockley, D. D. Sin and R. Rodriguez-Roisin (2013). "Global strategy for the diagnosis, management, and prevention of chronic obstructive pulmonary disease: GOLD executive summary." Am J Respir Crit Care Med **187**(4): 347-365.

Wang, L., J. Yu, J. Ni, X. M. Xu, J. Wang, H. Ning, X. F. Pei, J. Chen, S. Yang, C. B. Underhill, L. Liu, J. Liekens, J. Merregaert and L. Zhang (2003). "Extracellular matrix protein 1 (ECM1) is over-expressed in malignant epithelial tumors." Cancer Lett **200**(1): 57-67.

Weaver, T. E., C. L. Na and M. Stahlman (2002). "Biogenesis of lamellar bodies, lysosome-related organelles involved in storage and secretion of pulmonary surfactant." Semin Cell Dev Biol **13**(4): 263-270.

Wei, M. L. (2006). "Hermansky-Pudlak syndrome: a disease of protein trafficking and organelle function." Pigment Cell Res **19**(1): 19-42.

Wijnen, J., P. M. Khan, H. Vasen, F. Menko, H. van der Klift, M. van den Broek, I. van Leeuwen-Cornelisse, F. Nagengast, E. J. Meijers-Heijboer, D. Lindhout, G. Griffioen, A. Cats, J. Kleibeuker, L. Varesco, L. Bertario, M. L. Bisgaard, J. Mohr, R. Kolodner and R. Fodde (1996). "Majority of hMLH1 mutations responsible for hereditary nonpolyposis colorectal cancer cluster at the exonic region 15-16." Am J Hum Genet **58**(2): 300-307.

Witkop, C. J., M. Nunez Babcock, G. H. Rao, F. Gaudier, C. G. Summers, F. Shanahan, K. R. Harmon, D. Townsend, H. O. Sedano, R. A. King and et al. (1990). "Albinism and Hermansky-Pudlak syndrome in Puerto Rico." Bol Asoc Med P R **82**(8): 333-339.

Wolters, P. J., H. R. Collard and K. D. Jones (2014). "Pathogenesis of idiopathic pulmonary fibrosis." Annu Rev Pathol **9**: 157-179.

Won, K. Y., G. Y. Kim, S. J. Lim and Y. W. Kim (2012). "Decreased Beclin-1 expression is correlated with the growth of the primary tumor in patients with squamous cell carcinoma and adenocarcinoma of the lung." Hum Pathol **43**(1): 62-68.

Wuyts, W. A., C. Agostini, K. M. Antoniou, D. Bouros, R. C. Chambers, V. Cottin, J. J. Egan, B. N. Lambrecht, R. Lories, H. Parfrey, A. Prasse, C. Robalo-Cordeiro, E. Verbeken, J. A. Verschakelen, A. U. Wells and G. M. Verleden (2013). "The pathogenesis of pulmonary fibrosis: a moving target." Eur Respir J **41**(5): 1207-1218.

Xu, J., E. T. Gonzalez, S. S. Iyer, V. Mac, A. L. Mora, R. L. Sutliff, A. Reed, K. L. Brigham, P. Kelly and M. Rojas (2009). "Use of senescence-accelerated mouse model in bleomycin-induced lung injury suggests that bone marrow-derived cells can alter the outcome of lung injury in aged mice." J Gerontol A Biol Sci Med Sci **64**(7): 731-739.

Yang, Z. and D. J. Klionsky (2007). "Permeases recycle amino acids resulting from autophagy." Autophagy **3**(2): 149-150.

Yousefi, S., R. Perozzo, I. Schmid, A. Ziemiecki, T. Schaffner, L. Scapozza, T. Brunner and H. U. Simon (2006). "Calpain-mediated cleavage of Atg5 switches autophagy to apoptosis." Nat Cell Biol **8**(10): 1124-1132.

Yuan, K., C. Huang, J. Fox, D. Laturnus, E. Carlson, B. Zhang, Q. Yin, H. Gao and M. Wu (2012). "Autophagy plays an essential role in the clearance of Pseudomonas aeruginosa by alveolar macrophages." J Cell Sci **125**(Pt 2): 507-515.

Yue, Z., S. Jin, C. Yang, A. J. Levine and N. Heintz (2003). "Beclin 1, an autophagy gene essential for early embryonic development, is a haploinsufficient tumor suppressor." Proc Natl Acad Sci U S A **100**(25): 15077-15082.

Zada, S., H. S. Noh, S. M. Baek, J. H. Ha, J. R. Hahm and D. R. Kim (2015). "Depletion of p18/LAMTOR1 promotes cell survival via activation of p27(kip1) -dependent autophagy under starvation." Cell Biol Int **39**(11): 1242-1250.

Zhao, E. and M. J. Czaja (2012). "Transcription factor EB: a central regulator of both the autophagosome and lysosome." Hepatology **55**(5): 1632-1634.

Zhen, L., S. Jiang, L. Feng, N. A. Bright, A. A. Peden, A. B. Seymour, E. K. Novak, R. Elliott, M. B. Gorin, M. S. Robinson and R. T. Swank (1999). "Abnormal expression and

subcellular distribution of subunit proteins of the AP-3 adaptor complex lead to platelet storage pool deficiency in the pearl mouse." Blood **94**(1): 146-155.

10. APPENDIX

10.1 List of primary antibodies

Name	Source	Dilution	Purpose	Company
atg5	Rabbit	1:1000	WB	Abcam
atg5-atg12	Rabbit	1:1000	WB	Abcam
atg7	Rabbit	1:1000	WB	Sigma
b-actin	Rabbit	1:30000	WB	Abcam
Beclin1	Sheep	1:1000	WB	R&D systems
Caspase 8	Rabbit	1:100	IF	Abcam
Cl. caspase 3	Rabbit	1:50	IF	Cellsignalling
Cl. caspase 3	Rabbit	1:1000	WB	Cellsignalling
GAPDH	Rabbit	1:10000	WB	Abcam
GFP	Goat	1:2000	WB	Abcam
HPS1	Mouse	1:1000	WB	Santacruz
LC3B	Rabbit	1:5000	WB	Abcam
LC3B	Rabbit	1:200	IHC	Abcam
LC3B	Rabbit	1:100	IF	Abcam
LAMP1	Rat	1:25	IF	Santacruz
LAMP2	Rat	1:1000	WB	Millipore
myc	Rabbit	1:1000	WB	Abcam
p62	Rabbit	1:3000	WB	Sigma
p62	Rabbit	1:100	IF	Sigma
p62	Rabbit	1:200	IHC	Sigma
pro SP-C	Rabbit	1:500	IHC	Millipore
TFEB	Goat	1:1000	WB	Novus Biologicals

10.2 List of secondary antibodies

Name	Source	Dilution	Company
Anti-rabbit	Swine	1:2000	Dako
Anti-goat	Rabbit	1:2000	Dako
Anti-rat	Rabbit	1:2000	Dako
Anti-sheep	Rabbit	1:2000	Dako

10.3 List of fluorescent labelled secondary antibodies

Name	Dilution	Company
Donkey Anti-Rabbit IgG (H+L) secondary antibody, AlexaFluor® 488 conjugate	1:400	Life Technologies
Donkey Anti-Rabbit IgG (H+L) secondary antibody, AlexaFluor® 555 conjugate	1:400	Life Technologies
Donkey Anti-Rat IgG (H+L) secondary antibody, AlexaFluor® 488 conjugate	1:400	Life Technologies
Donkey Anti-Goat IgG (H+L) secondary antibody, AlexaFluor® 488 conjugate	1:400	Life Technologies

11. List of Publications:

1. **MAP1LC3B overexpression protects against Hermansky-Pudlak syndrome type-1 induced defective autophagy *in vitro*. Ahuja et al, American Journal of Physiology - Lung Cellular and Molecular Physiology 2016, 310(6), L519-L531.**
2. **Regulation of macroautophagy in amiodarone induced pulmonary fibrosis. Mahavadi et al, The Journal of Pathology: Clinical Research, 2015. 1(4): p. 252-263.**

12. DECLARATION

Hiermit erkläre ich, dass ich die vorliegende Arbeit selbständig und ohne unzulässige Hilfe oder Benutzung anderer als der angegebenen Hilfsmittel angefertigt habe. Alle Textstellen, die wörtlich oder sinngemäß aus veröffentlichten oder nichtveröffentlichten Schriften entnommen sind, und alle Angaben, die auf mündlichen Auskünften beruhen, sind als solche kenntlich gemacht. Bei den von mir durchgeführten und in der Dissertation erwähnten Untersuchungen habe ich die Grundsätze guter wissenschaftlicher Praxis, wie sie in der „Satzung der Justus-Liebig-Universität Gießen zur Sicherung guter wissenschaftlicher Praxis“ niedergelegt sind, eingehalten sowie ethische, datenschutzrechtliche und tierschutzrechtliche Grundsätze befolgt. Ich versichere, dass Dritte von mir weder unmittelbar noch mittelbar geldwerte Leistungen für Arbeiten erhalten haben, die im Zusammenhang mit dem Inhalt der vorgelegten Dissertation stehen, oder habe diese nachstehend spezifiziert. Die vorgelegte Arbeit wurde weder im Inland noch im Ausland in gleicher oder ähnlicher Form einer anderen Prüfungsbehörde zum Zweck einer Promotion oder eines anderen Prüfungsverfahrens vorgelegt. Alles aus anderen Quellen und von anderen Personen übernommene Material, das in der Arbeit verwendet wurde oder auf das direkt Bezug genommen wird, wurde als solches kenntlich gemacht. Insbesondere wurden alle Personen genannt, die direkt und indirekt an der Entstehung der vorliegenden Arbeit beteiligt waren. Mit der Überprüfung meiner Arbeit durch eine Plagiatserkennungssoftware bzw. ein internetbasiertes Softwareprogramm erkläre ich mich einverstanden.

_____ _____

Ort, Datum Unterschrift

13. ACKNOWLEDGEMENT

First and foremost, I would like to thank Prof. Dr. Andreas Günther for providing me the opportunity to work on my thesis in his workgroup, guidance and for being supportive in the times when the things did not go right professionally and personally.

My thesis supervisor Dr. Poornima Mahavadi, it has been a pleasure working with you over these years. You have been a teacher, a friend, and a family member at the same time. This work could not have been completed without your support, guidance, and encouragement especially in the trying times when the things did not go as planned. Nowords will ever be enough to tell how grateful I am for everything you have done to help me complete this work.

I would also like to thank our collaborators, Dr. Bernadette R. Gochuico, Dr. Matthias Ochs and Dr. Lars Knudsen. Without your support and contribution this work would never have been completed.

I would also like to thank Prof. Dr. Werner Seeger and Dr. Rory Morty for accepting me into “Molecular Biology and Medicine of the Lung” programme. A lot of knowledge and good memories have been made while being part of the programme and will always be cherished.

A big shoutout to the other members of the lab, Dr. Martina Korfei, Dr. Clemens Ruppert, Dr. Ingrid Henneke, other PhD students as well as technical assistants, especially Silke Handel. Things would have been hard without support from all of you.

And the last but not the least, I would like to thank my family for being supportive of me in every possible way. Without you all, there would have been nothing. Thanks for being there for me even when I was not there with you!